PPPL--2863

DE93 005724

CHARACTERISTICS OF THE TFTR LIMITER H-MODE: THE TRANSITION, ELMs, TRANSPORT AND CONFINEMENT

C.E. Bush,[1] N. Bretz, R. Nazikian, B.C. Stratton, E. Synakowski, G. Taylor, R. Budny, A.T. Ramsey, S.D. Scott, M. Bell, R. Bell, H. Biglari, M. Bitter, D.S. Darrow, P.Efthimion, R. Fonck,[2] E.D.Fredrickson, K. Hill, H. Hsuan, S. Kilpatrick, K.M. McGuire, D. Manos, D. Mansfield, S.S. Medley, D. Mueller, Y. Nagayama,[3] H. Park, S. Paul, S. Sabbagh, J. Schivell, M. Thompson, H.H. Towner, R.M. Wieland, M.C. Zarnstorff, and S. Zweben

Princeton Plasma Physics Laboratory
Princeton University, P.O. Box 451
Princeton, NJ, 08543

ABSTRACT

H-Modes obtained through transitions from the supershot regime have been studied on TFTR. The characteristics of these H-modes are similar to those found on other tokamaks with one main exception, the density profiles can be highly peaked. In the best cases the enhanced confinement in the core of the initial supershot is retained in the H-mode phase, while the confinement in a broad edge region is enhanced. Thus in TFTR, all of the important physics of H-modes such as transitions, enhanced edge confinement, ELMs and other phenomena are studied in a large circular limiter tokamak with the added feature of centrally peaked density profiles and the advantage of an extensive set of diagnostics. The threshold power for the transition is found to be a linear function of plasma current. Transitions and ELMs are affected by the mix of co-and counter-neutral beam injection (NBI) and by perturbations introduced by pellet injection, gas puffing, and current ramping before and during NBI. Fluctuations near both transition and ELM events have been characterized. High frequency magnetic fluctuations in the range $\geq$ 100-250 kHz usually decrease during the transition. Microwave scattering spectra of density fluctuations in the plasma edge show a feature at high frequency (> 1.5 MHz at $k_\perp = 5.5\ cm^{-1}$) during the H-mode, which is not observed in the plasma core and which is consistent with an edge poloidal rotation velocity, V_θ, of ~ 10^4 m/s. The fluctuations begin at the transition, propagate in the direction of electron diamagnetic drift, and have modulation correlated with ELMs. Several TFTR H-modes showed a modest improvement in confinement over that of the supershots from which they originated, and an understanding of these may eventually lead to a plasma with the combined advantages of both the supershot and the H-mode. The characteristics and physics of the TFTR H-modes are considered relative to other tokamaks and in light of various theoretical studies.

---

[1] Oak Ridge National Laboratory, Oak Ridge, Tennessee, USA.

[2] University of Wisconsin, Madison, Wisconsin, USA.

[3] University of Tokyo, Tokyo, Japan.

I. INTRODUCTION

The TFTR supershot to limiter H-mode transition [1-3] is of interest to advanced tokamaks including burning plasma scenarios and the International Thermonuclear Experimental Reactor (ITER) [4]. The main reason for this interest is that the resulting H-mode has a density profile which is peaked at the center, while the enhanced confinement of the initial supershot is retained. In addition, access to this regime on TFTR allows the study of transport and confinement in several regimes on a common tokamak. These include the H-mode [5], supershot [6], L-mode and high beta poloidal [7] regimes. The details of the conditions for the transition, the physics of the transition and ELMs and the transport and confinement of the TFTR limiter H-mode are described in this report. In Sec. II, the technique and operational parameter range are discussed and Sec. III contains a brief discussion of the characteristics of the TFTR H-mode. A detailed discussion of the supershot to H-mode transition is given in Sec. IV including characteristics of the fluctuations observed. A similar discussion for ELM characteristics is given in Sec. V. Experimental results showing the transport and confinement for these H-modes are presented in Sec. VI. Data which show modest increases in confinement, for several H-modes, over that of the pre-transition supershot are presented in a subsection of Sec. VI. These data are important since they demonstrate the possibility of combining the "good" characteristics of both the supershot and the H-mode, and this could result in a net advancement in plasma confinement. The experimental results and their implications are discussed in Sec. VII. In this section, characteristics and scalings are compared with those of other tokamaks and the implications of the data relative to current H-mode theories are also discussed. A summary of results and a discussion are presented in Sec. VIII.

II. TECHNIQUE AND OPERATING PARAMETERS

The vast majority of H-modes obtained on TFTR have come about through supershot to H-mode rather than L- to H-mode transitions. A few L- to H-mode transitions have been observed; however, more favorable results (such as retention of significantly enhanced confinement) were obtained using supershot base plasmas. Supershots are obtained on TFTR by degassing the graphite limiters [8] in order to achieve a significant reduction in the recycling coefficient (R = 0.60). The main limiter is a toroidally symmetric inner belt of graphite tiles which extends $\pm$ 60° poloidally from the midplane. The target densities for the vast majority (> 85%) of shots which result in limiter H-modes range from 5×10^{18} m^{-3} to 1.25×10^{19} m^{-3}.

The range of operating parameters over which H-modes have been obtained is relatively wide. This includes plasma currents, I_p = 0.7 - 1.7 MA, toroidal fields, B_ϕ =

3.0-5.2 T, major radii, R_p = 2.45-2.60 m, minor radii, a_p = 0.79-0.95 m (circular minor cross section) and neutral beam injection heating (NBI) powers, $P_b \sim$ 11-28 MW. Beam heating pulses range from 0.5-2.0 sec duration. For the supershot to H-mode transition, where recycling is low, the line averaged density, $\bar{n}_e$ is usually $\geq 2 \times 10^{19} m^{-3}$ at the transition. All of the H-modes to date on TFTR have been obtained during high power neutral beam injection; no attempt has been made at obtaining an H-mode transition using ICRH. Also, bi-directional (co- plus counter-NBI) injection is necessary. The H-mode transitions occurred either "spontaneously", i.e., seemingly on their own accord, or were stimulated or "induced" by intentional perturbations such as gas puffs, pellet injection, or I_p ramps.

TFTR has an extensive set of profile and fluctuation diagnostics for effective study of H-modes [3]. These include three different ECE diagnostics for $T_e(r,t)$, the multichannel infrared interferometer for $n_e(r,t)$, Thomson scattering for $T_e(r)$ and $n_e(r)$ at a single time during the discharge, a charge exchange recombination spectroscopy (CHERS) system for $V_\phi(r,t)$, $T_i(r,t)$ and carbon density, $n_c(r,t)$, measurements, and vertical, horizontal, and tangential bolometer and soft X-ray cameras. Fluctuation diagnostics include poloidal and toroidal Mirnov coil arrays for $\tilde{B}_\theta$ measurements, microwave scattering for $\tilde{n}^2$ spectra, beam emission spectroscopy (BES), and reflectometry.

III. GENERAL CHARACTERISTICS OF CIRCULAR LIMITER H-MODES

A. General results

Transitions from the supershot regime to the limiter H-mode regime on TFTR are identified operationally by the presence of edge localized MHD modes or ELMs [9], by decreases in D_α and CII emission, and by increases in edge density and temperature. Detailed studies show that these and other features such as changes in V_ϕ and V_θ (as inferred from microwave scattering data [10]) are qualitatively similar to those of divertor H-modes. In addition, at the H-mode transition decreases in high frequency (> 100 kHz) magnetic fluctuations and increases in energetic ion efflux from the plasma edge are also observed in TFTR

Generally, the observation of ELMs is the clearest and most reliable indicator of the H-mode; only about 10 of the more than 300 TFTR H-modes have been ELM free. The decreases in D_α and CII emission are also fairly reliable indicators, however, they are relatively slow, decreasing over a few to 10's of msec rather than the 1 to 2 msec observed for divertor L- to H-mode transitions. In some cases on TFTR, there is no obvious drop in D_α emission before the onset of ELMs and the increase in edge n_e and T_e. Modest drops in

D_α light during the supershot to H-mode transition may be due to the inherently low recycling level of the initial supershot plasma. This is different from divertor H-modes, however, such behavior has been observed for limiter H-modes on other tokamaks [11, 12]. Distinct broad edge pedestals of n_e and T_e form following the supershot to H-mode transition, clearly reflecting a reduction in edge heat and particle transport. To date the magnitude of these pedestals have been considerably smaller than those obtained in the best divertor H-modes [13-16], thereby yielding only a modest pedestal in energy density and at most a small increase in total stored energy. However, it should be kept in mind that the supershot itself is an enhanced confinement regime. In contrast, for divertors, the transition is from the L-mode and thus the resulting edge pedestal contributes substantially to the total stored energy. Therefore, the TFTR H-modes to date essentially represent a modest edge transport barrier imposed on a regime with already favorable core confinement.

Despite the quantitative differences between H-modes on TFTR and those on divertor tokamaks, the details of the H-mode phenomena for the two cases are strikingly similar. Thus a reasonable presumption is that the same physical mechanisms underlie the H-mode in both geometries, with detailed evolution affected by the differing edge conditions, including differences in particle recycling. A robust theoretical model of phenomena involved must allow for H-modes in a limiter configuration. It should account for the observed differences in the size of the edge pedestals and in the transition time-constant between limiter and divertor H-modes. This paper describes results of detailed studies of limiter H-mode plasmas in TFTR, which must be accounted for in any theoretical model. A potential benefit of understanding the H-mode on TFTR would be identification of a plasma regime that could superimpose a large H-mode edge pedestal in stored energy on top of the peaked profiles and favorable core confinement of supershots.

Some of the usual characteristics found for TFTR H-modes are illustrated in Fig. 1, which shows the time variation of several signals; the D_α, edge n_el (r/a ~ 0.8), edge T_e(r/a ~0.8), the density profile peakedness parameter, $F_{ne} = n_e(0)/\langle n_e \rangle$, and the energy confinement time (from magnetics), τ_E. At the transition (beginning at ~ 4.42 sec) the D_α and CII (not shown) signals decrease and n_e and T_e near the edge begin to increase. For the discharge shown in Fig. 1 there is a short (~ 100 ms) quiescent period after the D_α signal begins to decrease, during which the edge values of n_e and T_e increase. ELMs begin at 4.5 sec, after which the edge values of n_e and T_e remain constant or slowly decrease. (Note: For the remainder of the paper, "edge" will generally refer to the region r/a $\geq$ 0.8).

The energy confinement time is usually significantly higher in the limiter H-mode than in L-mode scaling [17]. Often but not always, there is a small to modest (a few to >

10%) transient increase in τ_E above that of the initial supershot, as in Fig. 1 (a small increase), which takes place before ELMs begin, but there is a decrease in τ_E during ELMs. The fact that the increase in τ_E is often transient may be due to confinement improvement in the edge plasma causing a decrease in F_{ne} and thus a subsequent decrease in τ_E in accordance with supershot scaling.

B. Response of the density profile

The peakedness (F_{ne}) of the n_e profile can be relatively high in TFTR H-modes, ranging from 1.4 to 2.7. F_{ne} often begins to slowly decrease at the start of the transition and continues to do so during the quiescent period before the beginning of ELMs. However, there were several cases where F_{ne} actually increased following the transition. Confinement is, in general, slightly improved across the profile during the quiescent period with the most significant improvement taking place in a broad region at the plasma edge. The improved edge confinement causes an initial broadening in the n_e profile. Although F_{ne} usually remains significantly above L-mode values ($F_{ne}^{L\text{-mode}} < 1.5$), there are a variety of n_e profile responses observed during and after the H-mode transition on TFTR. A few of these are illustrated in Figs. 2-4. Figure 2 also illustrates the differences in time evolution of various parameters for two different discharges, one in which a spontaneous H-mode transition takes place and the other which remains a supershot. I_p for the case with the H-mode transition was set at a value 5% lower than for the plasma in which a transition did not take place. Figure 2(a) - 2(d) show $n_e l$, F_{ne}, D_α, and τ_E respectively to be essentially the same for the two plasmas up to t ~4.55 sec at which time the transition to the H-mode takes place. After the transition, plasma parameters for the two cases diverge. The time evolutions of the n_e profiles for the two plasmas (up to the time of the first ELM in the H-mode case) are shown in Figs. 2(e) and (f). For the non-H-mode case the profile becomes more peaked and reaches and remains at a constant value of F_{ne} for the remainder of the beam pulse. The H-mode plasma of Fig. 2(e) is an example where the peak value at the center of the density profile remained relatively constant, while the value in a broad edge region increased. This resulted in a decrease in F_{ne} from 2.4 at the beginning of the D_α drop (at 4.5 sec) to ~ 2.0 at t = 4.7 sec.

The main purpose of Fig. 3 is to further illustrate the variety of responses observed for the TFTR limiter H-mode. In contrast to the H-mode of Fig. 2, Fig. 3(a) shows $n_e(R)$ data for five different times of a plasma where the profile of the core retained its peaked shape while rising on a broad edge pedestal. A transient increase of ~ 10% in τ_E resulted during the quiescent period after the transition and before the first ELM for the plasma of Fig. 3(a). A similar plasma in which a 15-20% increase in τ_E was realized is discussed in

more detail in Sec. VI.C. The plasma of Fig. 3(b) is an example in which the profile became more peaked at the center (F_{ne} increased from 1.6 to 2.0) following the transition and continued to do so for ~180 msec following the first ELM. In this case deuterium gas puffing, at a slow rate, was started (at t = 3 sec) during the OH phase and maintained to the end of the beam phase (NBI from 3.5 to 4.5 sec). This example illustrates the fact that the enhanced confinement at the edge does not necessarily retard the peaking at the center of the n_e profile in all TFTR H-modes. The H-mode transition occurred ~ 280 msec (at t ~ 3.78 sec) after beam turn on and ELMs began shortly after, at t ~ 3.82 sec. The ELMs were "grassy" (i.e., of small to modest amplitude and high frequency) throughout the H-mode phase. Also, q_{Lim} was significantly higher for the plasma of Fig. 3(b) than for 3(a), 7.5 and 4.9, respectively.

Parameters and profiles for a plasma in which an H-mode transition followed, essentially instantaneously, upon injection of a small (3 mm diameter) deuterium pellet at t = 4.5 sec is shown in Fig. 4. The outer limiter radius was at R = 3.25 m and the pellet penetrated to R = 2.95 m or 30 cm into the plasma column. The time evolution of D_α light, $\tilde{B}_\theta$, $n_e l$, and τ_E are plotted in Figs. 4(a) - (d), respectively. Density profiles for four different times are plotted in Fig. 4(e). The D_α signal from a detector viewing on the midplane radially toward the inner wall drops sharply early after (at 4.504 sec) pellet injection at 4.5 sec while the edge n_e is elevated dramatically. ELMs began ~ 50 msec after the initial drop in the midplane D_α signal. At the same time signals for D_α detectors angled off the midplane show an initial fast spike. Also, the $\tilde{B}_\theta$ signal shows the high frequency magnetic fluctuations decrease sharply. Two scenarios (there are probably others) which could explain the transitions induced by pellets are as follows: (1) As the pellets move inward they may skim off fast ions, leading to a charge up of the plasma and thus a sheared E_rxB flow and (2) The pellet fueling could steepen the n_e and T_e gradients at the edge thereby inducing a transition. Additional experiments will have to be done to determine whether either of these scenarios apply. Similar to the result with pellet injection, H-mode transitions have been triggered using short modest to high flow rate deuterium and helium gas puffs. The n_e profiles for transitions following gas puffs were similar to those of Fig. 4(e).

IV. H-MODE TRANSITION

A. Requirements for the supershot to H-mode transition

The transition to the H-mode on TFTR depends on or may be affected by (1) plasma current I_p, (2) edge T_e, (3) the amount and mix of co- and counter-NBI power, (4) the conditioning or recycling level of the graphite limiters, (5) pellet injection, (6) deuterium and impurity gas puffing, and (7) plasma current ramping. Once the H-mode is obtained it

can apparently be maintained in steady state. Figure 1 illustrates an H-mode which occurred during a 2 sec beam pulse. The H-mode switched on spontaneously at ~ 4.42 sec and remained until NBI was turned off at t = 6 sec. The H-mode phase lasted 1.6 sec, the longest duration H-mode for TFTR (~ 13 energy confinement times). The duration was limited by the available 2 sec NBI pulse.

Bidirectional neutral beam injection was required to obtain all H-modes studied on TFTR. Balanced-NBI was not necessary, but H-modes were not obtained when either co- only or counter- only NBI heating was used. In fact the co- / counter- mix could be significantly imbalanced and still result in H-modes. In one study with P_b = 11 MW, I_p = 0.8 MA, and B_T = 4 T and basically the same OH target plasma, three cases were considered: (1) all co-NBI, (2) all counter-NBI, and (3) balanced-NBI. An H-mode was obtained only for the balanced-NBI case and the transition began ~ 400 msec after beam turn on. The edge T_e, measured at 400 msec after beam turn on in all three cases, was found to be significantly higher in the balanced-NBI or H-mode case. The values of T_e(edge) measured near the inside belt limiter were 700, 480 and 380 eV for the balanced-NBI (H-mode), counter-NBI, and co-NBI cases, respectively. Therefore, the possibility of a critical edge T_e for the supershot to H-mode transitions was investigated. A consistent and quantitative demonstration of a critical edge T_e requirement for the transition, valid for the full TFTR H-mode database, was not found. However, for certain limited groupings of discharges, there were hints of an edge T_e dependence. For example, at the transition the edge T_e value can be nearly equal for plasmas with fairly different limiter conditioning and operating parameters. This is illustrated in Fig. 5 where the D_α and edge T_e(r/a = 0.8) data for two somewhat different H-mode plasmas are compared. Both discharges had B_ϕ = 4 T, but one had higher I_p and P_b (1.05 MA and 15 MW compared to 0.9 MA and 13 MW) and probably higher recycling. The H-mode was triggered earlier in the high D_α (higher recycling) case, at ~ 3.92 sec compared to ~ 4.1 sec for the other case. However, the transitions for the two cases occurred at the same edge T_e value of ~ 0.8 keV and ELMs began at T_e (edge) ~ 1.2 keV in both cases. For a given magnetic field, the edge T_e is typically higher for a supershot in which an H-mode transition occurs, than for a supershot in which a transition is not realized. In addition, the value of T_e (edge) at which ELMs begin is usually higher than the value at the beginning of the transition. Some of the main features and dynamic behavior of T_e(edge), n_e(r), V_ϕ(r), and T_i (r) at or near the transition are clearly illustrated in Figs. 2 and 6, both of which include data for the same discharge.

In general for a wide range of parameters, the threshold power, P_{th}, for transitions to the limiter H-mode on TFTR depends on plasma current. Figures 2 and 6(b) illustrate the effect of a small change in I_p, when B_ϕ and P_b are held constant (B_ϕ = 4 T and P_b = 14

MW). A transition was obtained for I_p = 1.0 MA but was suppressed when I_p was raised by ~ 5% to I_p = 1.05 MA. The edge T_e was slightly higher by ~ 200 eV (at 4.56 sec) for the H-mode plasma as can be seen from Fig. 6(b). In Fig. 6, the D_α light and T_e near the outer edges (at R = 3.15 cm, when R_{Lim} = 3.25 cm) of the plasmas are plotted for the two cases of Fig. 2. The large spikes on the T_e signal beginning at about 4.8 sec are due to non-thermal bursts of ECE associated with each ELM and do not represent real oscillations in the edge temperature (the spikes are discussed in more detail in a later section). Values of V_ϕ (R,t) and T_i(R,t), determined using the CHERS system, for a broad region at the plasma edge are also plotted for the H-mode plasma. Carbon line emission from C^{5+}(n = 8 -7, 5292 Angstroms) was used for all CHERS measurements (spatial resolution of $\pm$ 2.5 cm) of V_ϕ, T_i, and carbon concentration. In addition to the hint of a possible edge temperature requirement, the two cases of Figs. 2 and 6 also indicate a plasma current dependence of the power required for the H-mode transition in that higher beam power was necessary for the higher current (I_p ~ 1.05 MA) case. This dependence of the threshold power on I_p is illustrated in Fig. 7, which is a plot of beam power versus plasma current for nearly all H-mode plasmas obtained on TFTR. The minimum beam power at which H-modes have been obtained for 0.9 MA discharges is ~ 10 MW. At the higher I_p of 1.6 MA, the minimum is ~ 18 MW. Thus, the threshold power for transitions may be roughly characterized by the simple linear relation

$$P_{th}\,(\mathrm{MW}) = 11(\mathrm{MW/MA})\cdot I_p\,(\mathrm{MA}) \quad . \qquad (1)$$

A wide range of plasma parameters and wall conditioning are represented in Fig. 7. No investigations have been carried out beyond the conditions and parameter ranges represented in Fig.7 or included in preceding discussions. Comparisons of the power threshold scaling of Fig. 7 with those of other tokamaks are presented in Sec. VII.

B. Fluctuations and poloidal and toroidal rotation

B.1 Magnetic fluctuations

Recent attempts to explain the H-mode transition have emphasized shear stabilization of turbulence [18, 19] which, in turn, is postulated to lead to a bifurcation in plasma confinement and transport. In order to understand the physics of these transitions, it is important to have time resolved measurements of the magnetic and density fluctuations and velocity, temperature, and density profiles. Magnetic and density fluctuations provide information as to the degree to which turbulence may be playing a part in determining the transport and confinement properties of a plasma. On TFTR, high frequency magnetic

fluctuations in the range 150-250 kHz often decrease at the transition and remain at reduced levels well into the H-mode. Magnetic fluctuations in the range 250-350 kHz often decrease slightly later than those in the 150-250 kHz range, and also often remain at reduced levels well into the H-mode. Low frequency fluctuations in the range 15-25 kHz (not shown) sometimes increase at the transition, however, this response is not observed nearly as often as the trend at high frequencies. In the majority of cases the high frequency magnetic fluctuation levels begin to increase with the onset of ELMs or during periods of intense coherent (m = 2) MHD activity but decrease again during extended ELM free periods. Figure 8 shows fluctuation levels for high frequency oscillations in the range of 150-350 kHz for the same discharge shown in Fig. 1. The initial decrease in fluctuations appears to be simultaneous with the slight decrease in D_α light. The fluctuation levels also decrease during the ELM free periods such as those between 4.67-4.72 sec and 4.75 - 4.80 sec. In fact, the amplitudes of the $\tilde{B}_\theta$ signals begin to decrease as the size of the D_α bursts decrease. The slow oscillations in τ_E [Fig. 1(e)] from t = 4.57 to 5.2 sec are in phase with the quiet periods, with peaks in τ_E occurring just before the next burst of ELMs begin.

The frequencies over which decreases in magnetic fluctuations are observed vary significantly from one discharge to another. A few have shown decreases over the entire spectrum from 25 up to 350 kHz, while others have shown decreases only in the range 100-350 kHz. Although there is a wide variation in the frequency range and level of decrease of magnetic fluctuations, the occurrence of some observable decrease is frequent enough that it is often used as an indicator of the supershot to H-mode transition. However, it is clear from the results presented that the picture of the magnetic fluctuations is complex and that the observation of a significant decrease in $\tilde{B}_\theta$ for the TFTR Mirnov coil set does not necessarily occur for all TFTR H-modes. Figure 9 shows results of two studies in which the change in $\tilde{B}_\theta$ was more evident than the D_α drop and thus was helpful in determining the times at which the H-modes began. Also, when the portions of the D_α signals before ELMs are magnified the onset of the D_α drops are obvious. The results show qualitatively the effect of the level of beam power and deuterium gas puffing on the H-mode transition. Plotted in Fig. 9 are the D_α and $\tilde{B}_\theta$ signals for two power levels (17 and 19.5 MW, at B_ϕ = 3.9 T and I_p = 1 MA) and three gas puff flow rates (0, 5, and 20 T1/s). The data in Fig. 9 show that the transition occurs earlier (i.e., closer to beam turn on) as the flow rate is increased or as NBI power is increased for the same B_ϕ and I_p. The power threshold for a transition may depend on T and ∇T at the plasma edge and a gas puff may change both of these parameters. In general, there is usually a time delay after beam turn on for the transition to occur and this varies from ~ 100 msec to greater than 500 msec.

In the gas puff study of Fig. 9, the transition begins at ~ 250 msec after beam turn on for the 20 T1/s puff and is delayed by nearly 450 msec for the 17 MW (no gas puff) case.

B.2. Density fluctuations and poloidal and toroidal rotation

There is strong evidence of changes in the poloidal velocity profile, $V_\theta(R)$, at the supershot to H-mode transition in TFTR, which are correlated with the changes in $V_\phi(R)$ from CHERS measurements which are shown in Fig. 6(c). Features in the microwave scattering spectrum are consistent with a poloidal spin up of the edge plasma beginning slightly before or at the transition. These observations may support several theoretical models of the H-mode which are based on stabilization of turbulence by shear in the velocity profiles. Experimental observation of sudden changes in V_θ and V_ϕ at the transition have also been made on several other tokamaks [20-22].

Studies of the effects of shear flow on turbulence and confinement in H-modes require detailed measurements of the temporal behavior of the amplitude and spectral and spatial distributions of density fluctuations. The microwave scattering diagnostic has a broad frequency range and it has time resolution which may allow determination of cause and effect relative to changes in shear and fluctuation amplitude. However, the spatial information is limited. Density fluctuation and toroidal velocity data are provided in Figs. 10-12 which illustrate the behavior of the edge plasma flow for fairly typical TFTR H-modes. It is clear from Figs. 10(a), 11(a), and 12(a) that the scattering data has a strongly shifted or asymmetric high frequency feature (shift can be > 1 MHz) which begins at the transition and lasts for the duration of the H-mode. Figure 10(a) shows a contour plot of the scattered power from the edge plasma (at $r \sim 0.7 \pm 0.15$ m) as a function of time and frequency. The D_α signal and the toroidal velocity, $V_\phi(R)$, from CHERS for four outer radial positions are shown in Figs. 10(b) and 10(c), respectively. For Fig. 10(a), $k_\theta = 5.4$ cm^{-1} and the scattering signal is from a 30 cm long volume, which includes the region between r = 50 or 60 cm and the plasma surface at r = 80 cm. The limited spatial resolution does not allow precise determination of the minor radius of the volume of plasma responsible for the shifted feature, however, the feature is not observed for the plasma core ($r = 30 \pm 15$ cm). In fact, the scattered spectrum consists of two distinct components; (1) a large amplitude broadband feature with $\langle\omega\rangle \sim 0$ and half width at half maximum of ~ 150 kHz, and (2) the lower amplitude strongly shifted high frequency asymmetric feature. A shifted feature has been observed in all TFTR H-modes. The existence of this shifted component of the scattered spectrum is consistent with a poloidal rotation of a portion of the scattering volume of $V_\theta \simeq 10^4$ m/s in the electron diamagnetic drift direction regardless of the sign of the average beam induced central toroidal rotation (i.e., whether or not the

injection is co- or counter- dominated). This poloidal flow is also consistent with the establishment of a radially inward pointing electric field and has magnitude given by $-E_r \times B_\phi$. The magnitude of the shift is inconsistent with the magnitude and uncorrelated with the sign of the edge toroidal rotation as measured by CHERS.

The magnitude of the shift of the asymmetric feature of the microwave scattering spectra begins to increase with time just before or at the beginning of the transition. This would infer a steady increase in poloidal rotation. This is illustrated explicitly in Fig. 11 which shows microwave scattering spectra $S_k(\omega)$, for a plasma similar to that of Fig. 10(a) but with faster time resolution. The D_α signal is shown in Fig. 11(b) where six different times during the discharge are indicated. The scattered spectra for these times are overlaid in Fig. 11(a), where $t_1 \sim 4.06$ sec is the time just before the transition, $t_2 \sim 4.08$ sec is the time of the D_α drop, and t_3 to t_6 are successive times during the evolution of the H-mode after the transition. The peak of the shifted part of the spectrum at t_6 is ~ 1 MHz greater than that at t_2. This difference is equivalent to an increase of ~ 15 km/s in the poloidal drift velocity within the 80 msec between times t_2 and t_6. The first ELM occurs at ~ 4.25 sec, well past the transition.

The inferred poloidal rotation is modulated by ELM activity, which begins at ~ 4.1 sec for the discharge of Fig. 10. The ELMs were relatively large and persisted until beam turn off at 4.5 sec. τ_E remained at a nearly constant value of 0.11 sec or 2.25 times $\tau_{L\text{-mode}}$ throughout the ELM phase. However, the edge T_e decreased from ~ 1.3 keV at the time of the first ELM to 1 keV at beam turn off. The time resolution of the data of Fig. 10(a) is not good enough to study the effect of individual ELMs. The asymmetric component of the spectra of Figs. 10-12, indicative of fluctuations in the shear layer, is modulated by each individual ELM. Evidence for this modulation is provided by fast time resolved microwave scattering data which are presented in a later section on ELMs.

ELMs are not the only phenomena which can be correlated with degraded confinement and changes in plasma rotation during H-modes. For a large number of plasmas, coherent MHD activity (m = 2), not necessarily exclusively associated with ELMs, has been correlated with degradation in τ_E. Figure 12 shows a case for which such activity was coincidental with a decrease in the inferred poloidal spin up and a relaxation of the edge V_ϕ and T_i values obtained during the transition. The main difference between the two plasmas of Figs. 10 and 12 is that m=2 activity of much higher amplitude occurs in the plasma of Fig. 12, beginning ~ 200 msec before the end of the beam pulse. The microwave scattering spectrum, D_α, $\tilde{B}_\theta$ (m = 2), V_ϕ (edge), and T_i (edge) are plotted in Figs. 12(a)-(e), respectively. The H-mode transition begins at ~ 4.05 sec, and a burst of large amplitude ELMs beginning at t ~ 4.17 sec is correlated with a decrease in the inferred

V_θ. During the latter half of the H-mode phase, the growth of the m = 2 mode takes place at the same time as a dramatic drop in the inferred $-E_r \times B_\phi$ poloidal rotation. By the end of the beam pulse, τ_E has been reduced to a value significantly below the value just before beam turnoff for the plasma of Fig. 10.

The behavior of the toroidal velocity profile has been found to be a reliable indicator of the supershot-to-H-mode transition on TFTR. Also, details of the V_ϕ profile may reflect the dynamics of the transition and the spatial extent of the bifurcation region, although shear in poloidal flow is expected to be much more effective than shear in toroidal flow in suppressing plasma turbulence. Recent theoretical studies [23], however, indicate that there are regimes in which V_ϕ should be important relative to effects of sheared flow. Usually during TFTR supershot to H-mode transitions, the toroidal velocity in the outer 25 cm layer of plasma becomes less positive (+ or positive sign implies rotation in direction of I_p). This means that if for example at R = 3.14 m, $V_\phi = 0$ just before the transition, then the rotation becomes counter, i.e., $V_\phi < 0$, just after the transition. At the beginning of the H-mode transition the toroidal velocity abruptly shifts toward the counter direction and T_i begins to increase within a broad edge region. Typical behavior of V_ϕ and T_i in the outer ~ 1/3 of the plasma minor cross-section is illustrated in Figs. 6, 13, and 14. Because of the finite radial resolution of the CHERS channel which views the plasma edge (at R = 3.24 m), V_ϕ measured with this diagnostic is actually an average of the velocity shear within the outer 4 cm shell of plasma. This may explain why V_ϕ (R = 3.24 m) is ~ 2.5 x 10^4 m/s rather than negligibly small just before the transition for the H-mode plasma of Fig. 6. In general, the value of V_ϕ at R = 3.24 m ± 2.5 cm as provided by CHERS is non-zero. The main quantitative use of the CHERS chord at R = 3.24 m is the determination of the difference in V_ϕ, i.e., ΔV_ϕ (R), at the very edge of the plasma before and after the H-mode transition.

This characteristic trend in V_ϕ can also be seen in the data of Fig. 13(a), which shows the V_ϕ profile for four times; just before (t = 4.0 sec) and during (t = 4.05 sec, 4.07, and 4.10 sec) the transition. V_ϕ at R = 3.14 m goes from ~ 0 at 4.0 sec to ~ -5 × 10^4 m/s at t = 4.10 sec, where (-) means the counter-direction. $V_\phi \sim 6 \times 10^4$ m/s for the outermost position (R = 3.24 m) just before the transition and decreases sharply to a value of ~ 3.5×10^4 m/s; concurrently, there is a small decrease in D_α light. Within the core, at R = 2.74 m, V_ϕ goes from - 10 x 10^4 m/s to -8 × 10^4 m/s or a change of ~ 2 × 10^4 m/s in counter toroidal velocity. The change in the value of V_ϕ at the Shafranov shifted plasma center at R = 2.64 m was smaller than that at R = 2.74 m. Both the T_i and n_e profiles [Figs. 13(b) and 13(c), respectively] broadened during the transition due to decreases in these parameters in the core region and increases in the edge plasmas. The usual decrease

in the high frequency magnetic oscillations in the range 150 - 350 kHz was observed at the transition for this discharge, however, there was also a burst of oscillations in the low frequency range of 5 - 25 kHz. In all cases studied in detail, the trend of V_ϕ is to become more counter going (or less co- going) in the outer plasma layer, however, for the core region the result is more complex.

In general the trends in the V_ϕ data for many plasmas with H-mode transitions are similar to those in Fig. 13(a). However, there are variations and this is clear from Fig. 14 which shows V_ϕ profiles for four different plasmas, with four different time slices for each plasma. In all four cases, beam heating is from 3.5 to 4.5 sec. Figure 14(a) is for a plasma in which the transition took place late in the NBI phase (transition at ~ 4.25 sec or 750 msec after beam turn on); Fig. 14(c) is a case in which there was no transition and no H-mode; Figs. 14(b) and (d) are cases in which the transition occurred early or ~ 400 msec after beam turn on (the majority of transitions occur < 600 msec after beam turn on). Although the transition is late for Fig. 14(a), the profile at an early time of ~3.85 sec is shown for comparison and is similar to the profile in Fig. 13(a) which is just before the transition (3.95 sec) for that plasma. However, the profiles at the early times of Figs. 13(a) and 14(a) (t = 3.85 sec) are significantly different from that just before the transition (t ~ 4.25 sec) in Fig. 14(a). Thus, even though I_p, B_ϕ, P_b and the co-/counter- mix of the beams are the same for the two cases, the toroidal velocity in the plasma core (R ~ 2.3 - 2.9 m) is negative for the plasma of Fig. 13(a) and positive for Fig. 14(a) at the time of the respective transitions.

In all five cases (Figs. 13 and 14) the V_ϕ profiles from R = 2.94 m out to R = 3.24 m are similar in that the velocity at the plasma edge (3.24 m) is more positive than that at 2.94 m. At the transition, the outer portion of the velocity profile (R > 2.9 m) retains this shape, becoming less positive, or if initially counter-going, becoming more negative. In Fig. 14(a) the core velocity has evolved for a longer time and is at a quasi-equilibrium just before the transition. For this H-mode, the net change in the V_ϕ profile at the plasma core is smaller than the net change at the edge. This may be an indication that the evolution in the core region for transitions occurring early after beam turn-on may be related more to the evolution resulting from the initial dynamics of beam heating itself rather than the H-mode transition. In contrast it is clear that the evolution of V_ϕ at the plasma edge is correlated with the transition. Data such as that of Figs. 13(a) and 14 have been used to determine the net change in V_ϕ at R = 3.24 m, and the results are plotted in Fig. 15 as ΔV_ϕ(R=3.24 m) versus P_b for a variety of TFTR limiter H-modes. For most of these plasmas ΔV_ϕ(R=3.24 m) ranged from - 1 x 10^4 to -4 x 10^4 m/s .

On TFTR the cross product of a counter toroidal velocity and the poloidal field, i.e., $V_\phi \times B_\theta$, would be in the direction consistent with a radially inward pointing electric field ($-E_r$). In this way the change, ΔV_ϕ, as seen in Fig. 15, contributes to a change in the $-E_r \times B_\theta$ flow. At the L- to H- transition on DIII-D [21] a shift in V_ϕ to the counter direction of about 20 km/s (similar to values for TFTR) is usually observed for the outer most channel of the charge exchange recombination spectroscopy system.

C. Energetic Ions and Particles

Preferential loss of energetic ions, especially counter injected particles at the injected beam voltage (usually 90 - 110 keV), could lead to radial electric fields of magnitudes which are expected to be sufficient to cause shear flow effects on turbulence. Also energetic fusion product ions such as the 3 MeV proton and 800 keV He-3 ion from the D-D reaction have large banana orbits which intersect the limiters. Such losses would also contribute to formation of a radial electric field. On TFTR, fusion product probes [24] at the plasma edge, usually at the outer limiter radius, are used to monitor trapped energetic beam and fusion product ions directly. The position of the probe in the magnetic field and the probe aperture geometry determine the particle energies and species detected. The ion detector element of the probe is a scintillator and additional energy and species discrimination is obtained by recording the position at which particles strike the scintillator surface. An array of charge exchange analyzers viewing along chords perpendicular to the plasma column is used to monitor the beam injected and plasma thermal particles indirectly.

At the transition, the signal of a fast ion probe near the midplane shows a prompt increase. The probe signal is a measure of the energetic ion flux (EIF) and is plotted in Fig. 16(a) along with the (b) D_α, (c) charge exchange flux, and (d) V_ϕ signals. The charge exchange fluxes of 70, 80, and 90 keV particles plotted in Fig. 16(c) increase more slowly than the EIF at the transition. The prompt increase in the energetic ion flux (EIF) to the probe just before 4.0 sec is clearly correlated with the beginning of the decrease in the D_α signal. In fact the rate of rise of the EIF signal appears to be greater than the rate of decrease of the D_α signal. There is a second decrease in D_α light 25 msec later at $t \sim 4.02$ sec and a corresponding second prompt increase in EIF. ELMS begin just after 4.04 sec and there are corresponding oscillations in EIF. The initial changes in EIF and D_α light appear to be simultaneous. Quantitative determination of whether or not one signal leads the other would have implications as to whether or not the EIF rise is a precursor to or a consequence of the transition. Such a determination was not possible for the discharge of Fig. 16.

There were two prominent features in the scintillator light pattern of the EIF probe for the plasma of Fig. 16. These features were observed during NBI before and after the H-mode transition, however, they become more intense at the transition. Detailed fast ion orbit calculations indicate that these features are most likely due to 800 keV He-3 and 3 MeV proton fusion product ions. Contributions to the probe signal due to fast beam injected ions are also possible.

V. ELM CHARACTERISTICS AND BEHAVIOR ON TFTR

A. Importance of Studying ELMs

ELM studies are important from at least two perspectives; the deleterious effects of ELMs on particle and energy transport and confinement on the one hand, and the beneficial use of ELMs for controlling impurities and, thus, obtaining a steady state H-mode for reactor applications on the other. In fact, ELMs have been proposed as a means for controlling impurity concentration and for expelling helium ash in ITER and other advanced tokamaks. Thus, studies on TFTR are aimed at understanding the physics of, and the spatial origin of ELMs. Indirect evidence of the nature of ELMs is provided by observing the effects of operating parameters such as I_p, T, n and B_ϕ on the size and frequency of ELMs. On the other hand, effects of ELMs on the plasma, i.e., on confinement and transport, also provide information as to their origin and physics. Effects on ELMs due to the influx of neutrals are determined by varying the conditioning of the graphite limiters or/and by gas puffing. The ultimate aim is to understand the conditions leading to an ELM (precursor activity) and what happens during and after an ELM, i.e., the relaxation and recovery of the plasma between ELMs.

Gross effects of ELMs on transport and confinement are evident from changes in global confinement τ_E and inferred $E_r \times B_\phi$ rotation. In a number of cases, there were decreases in confinement to the extent that τ_E during the ELM phase was significantly below that of the initial supershot. Modulation of H-modes associated with ELM activity is seen in Fig. 1, where bursts of ELMs are correlated with decreases in τ_E, with recovery in confinement occurring during ELM free periods. The longer the time between ELMs, the more the confinement improves. In general, for many discharges, the larger size ELMs occur after long ELM free periods.

B. Precursors to and Spatial Origin of ELMs

Apparent precursor activity to ELMs has been observed using magnetic, soft X-ray and electron cyclotron emission (ECE) diagnostics for some TFTR H-mode plasmas. The dynamics associated with an individual ELM appears to be as follows: a burst of magnetic

fluctuations, $\tilde{B}_\theta$, begins just before (or concurrently with) the rise in D_α; at the same time there is a drop in soft X-ray emission from the edge plasma, and for some discharges intense spikes in ECE are observed to occur at the beginning of the burst of magnetic fluctuations. The correlation of the $\tilde{B}_\theta$ signal and ECE spikes at the beginning of the D_α rise is shown in Fig. 17. The $\tilde{B}_\theta$ signal is from one of a system of Mirnov coils, the D_α signal is from a detector looking along the midplane at the inner wall, and the ECE signal is from a grating polychromator which measured extraordinary mode second harmonic ECE on the midplane.

The Mirnov coil system was used to characterize the MHD mode numbers associated with the burst of precursor magnetic fluctuations to the ELM. The data were digitized at 2 MHz both during ELM activity and during an ELM free period. An increase in the intensity of high frequency magnetic fluctuations in the range of 50-500 kHz is seen during ELMs. These fluctuations are in phase toroidally for all Mirnov coils mounted in the upper half of the torus and 180° out of phase with the signals from coils in the lower half of the torus. Thus, the ELM precursor was found to be a dominant m = 1, n = 0 MHD mode, [25] or an up down motion of the plasma, with an amplitude of 0.01 to 0.05 gauss. This is unlike the ELM precursor seen on ASDEX [26], which had an outwardly ballooning structure with m = 3 or 4 and n = 1. High frequency ELM precursor oscillations have also been observed on PBX-M [27] but, unlike the TFTR precursors, those on PBX-M are not axisymmetric.

In addition to temporal information, ECE data also provide information on the spatial origin of ELMs (and possibly of the bifurcation region). In some cases where the ECE spikes can be localized spatially, they appear to originate in the bifurcation layer at the edge of the plasma. The ECE measurement of Fig. 17 corresponds to a major radius R = 3.2 m, or 5 to 10 cm inside from the plasma edge. These spikes may have their source deeper in the plasma but are not always observed, due to significant reabsorption of the ECE by the local thermal electron distribution. Between the intense spikes of ECE which occur immediately before the rise in the D_α signal, there is also a small but measurable rise in local electron temperature (~50-100 eV) in the region 0.1-0.2 m from the plasma edge, followed by a sudden drop at the start of the ELM. This is clear from Fig. 18 which shows T_e near the very edge of the plasma. At the plasma surface [Fig. 18(c), r/a ~1 or R = 3.25 m], there is a gradual decrease in T_e between the ELMs and a sudden rise at the start of an ELM. This is in contrast to the behavior at r/a ~ 0.9 m [Fig. 18(b) where R = 3.18 m] and the difference implies that between the ELMs there is a small increase in the T_e gradient near the plasma edge. This behavior has also been observed on ASDEX [28] at r/a ~ 0.5. Since the pressure profiles in TFTR H-modes are peaked on center, a significant effect of

ELMs on the T_e profile does not extend as deeply into the plasma column as in broader pressure profiles of divertor plasmas.

The ECE spikes preceding ELMs have a spectral width ranging from 10-50 GHz at the second ECE harmonic, corresponding to $5\% < \Delta f/f < 20\%$. If this frequency spread is due entirely to relativistic broadening, it implies an electron energy of 10-100 keV. It is fairly certain that the spikes are non-thermal, the main question has to do with the mechanism which creates them and their source within the plasma profile. Possibilities are a pre-existing population of energetic electrons which are thrown out by some stochastic process, or their creation and expulsion by phenomena active at the instant of the ELM.

The minimum spectral width ($\Delta f \sim 15$ GHz) and spatial location of the ECE spike for a typical TFTR H-mode are shown in Fig. 19. In plasmas where $\Delta f/f$ of the spike is < 10%, the emission appears to be localized within at least 0.2 m of the plasma edge. Figure 19 shows a comparison of two profiles of ECE radiation temperature versus frequency [Fig. 19(a)] and major radius [Fig. 19(b)] immediately before and during an ELM spike. The emission profile appears to be thermal between ELMs. In general, spikes last 20-50 μsec and in the case of Fig. 19 have a frequency spread of 10-20 GHz corresponding to an electron energy < 20 keV. Figure 20 shows a contour plot of the ECE radiation temperature versus major radius and time for the plasma of Fig. 19. The local peak corresponding to the ECE burst indicates that the origin of the ELM disturbance was near R ~ 3.15 m. The peak of the ECE intensity occurs at later times at successively larger major radii. This delay can be interpreted as corresponding to an outwardly directed propagation with radial velocity $\sim 2 \times 10^3$ m/s. Velocities as high as 3×10^3 m/s have been observed during ELMs on TFTR.

C. Density Fluctuations During ELMs: modulation of poloidal rotation

Similar to effects on τ_E, the microwave scattering signals are affected by ELMs, and this implies modulation of the poloidal rotation gained during the initial quiescent period (before the first ELM) as shown in Fig. 12. The correlation of the ELMs with the modulation of the contours of the spectrum plotted in Fig. 12(a) is clear. In all H-modes where microwave scattering data from the edge plasma exists, the maximum frequency of the shifted component of the spectrum has been attained during the initial quiescent period before ELMs. The maximum frequency is ~ 1.9 MHz at ~4.15 sec for Fig. 10(b) and about 1.75 MHz at ~4.25 sec for Fig. 12. The maximum poloidal phase velocity is reached just before the first ELM in each case. On the other hand as discussed earlier, it should be kept in mind that strong coherent MHD fluctuations, not necessarily associated with ELMs, can also cause decreases in τ_E, V_θ and V_ϕ.

The narrow band (< 200 kHz, FWHM) central component of the microwave scattering spectrum appears to increase in intensity during an ELM as shown in Fig. 21. Also, there is a time correlation between bursts in the D_α light and bursts in the microwave scattering raw data as seen in Fig. 22. The ELM bursts were ~ 5 ms apart. Modulation of the frequency shifted component of the spectrum during and in the recovery after ELMs is clearly evident in fast time resolved microwave scattering data [29]. The average poloidal velocity between ELMs is estimated to be $\langle V_\theta \rangle \sim 10^4$ m/s.

The beam emission spectroscopy (BES) [30] system shows density fluctuations during the ELM phase which are more coherent than those observed using the microwave scattering technique. A low frequency, 20-30 kHz, feature has been observed during ELM activity using BES with $k \leq 1.5$ cm^{-1}. In contrast to microwave scattering which shows high frequency fluctuations propagating in the electron diamagnetic drift direction, the BES system shows low frequency (20-30kHz) fluctuations which propagate in the ion diamagnetic direction. From Fig. 23, we see that this coherent activity occurs as bursts between, rather than during, ELMs. These fluctuations have been observed, in a region 4-10 cm from the plasma edge and have a highly coherent poloidal structure with m = 15 to 20. The poloidal coherence length is greater than 15 cm and the phase velocity is 6×10^3 m/s. These features were not observed when the viewing geometry of the BES system was set for studies of the core of TFTR limiter H-mode plasmas.

D. Other Observations about ELMs: fast ion flux

High frequency or grassy ELMs or low frequency ELMs of constant magnitude are usually associated with a linear decrease in edge T_e with time. This trend is clearly seen in the T_e(edge) data of Fig. 5(b). Grassy ELMs often result when the intrinsic recycling at the limiter is high or with gas puffing. This effect is illustrated in Fig. 9 which shows data for plasmas with two different levels of gas puffing. The "grassiest" ELMs of the four shots of Fig. 9, are those for the plasma of Fig. 9(a) in which the strongest gas puff (20 Tl/s) was used. Grassy ELMs similar to those of the high D_α plasma (I_p = 1.05 MA) of Fig. 5 and the plasma of Fig. 9(a) also occurred for several H-mode plasmas which followed discharges which ended in disruptions. Disruptions lead to coating of the limiter surface with impurities and neutral gas and thus temporarily (for several subsequent discharges) increase the recycling coefficient. A number of discharges were studied in order to understand the dependence of ELM amplitude and frequency on various parameters. Figure 24 shows a plot of the amplitude of the D_α spikes, ΔD_α, during ELMs versus frequency for a single but fairly typical discharge; the ELM amplitude is seen to be inversely dependent on the frequency of the ELM spikes. A possible explanation for this

trend is that the longer time between ELMs allows the plasma more time to recover stored energy at the edge. As a result, more energy is involved in the instability associated with the ELM. These features were observed for a number of H-modes.

Variations in the energetic ion and the charge exchange effluxes are also correlated with ELM activity just as there are correlations with the supershot to H-mode transition phase (discussed earlier). Figure 25 shows the D_α and energetic ion flux (EIF) signals during ELM activity for the H-mode of Fig. 16. The maxima of the two signals appear to be 180° out of phase. Often, the EIF signal begins to slowly decrease before the D_α spike begins to rise. The shapes of the two signals appear to be independent of each other and this may imply that two different sets of phenomena may be dominating these two signals during ELMs. The fact that the EIF signal "leads" the D_α signal could be indicative of ELM precursor activity involving a decrease in the radial ion current required to maintain the inferred E_r associated with the enhanced confinement at the edge of the plasma. In Fig. 26 during ELMs, the D_α signal also appears to be anti-correlated with the perpendicular charge exchange signal for a viewing chord through the outer edge (R = 3.23 m or r/a ~ 0.97) of the plasma and correlated with the chord through the inner (R = 1.94 m or r/a ~ 0.64) or high field side of the minor cross section. The vertical dashed lines in Fig. 26 indicate four different times of interest (~ 4.288, 4.304, 4.336, and 4.362 sec), all of which are at the beginning of the increase in the D_α signal for four different ELMs. In all cases, the spikes of the CX flux signal at R = 1.94 m are correlated with or peak just slightly later than the D_α signal. At the same time the CX flux for the chord at R = 3.23 m drops sharply after the peak in the D_α spikes, and this can be by > 50% of the CX flux signal just before the ELM.

VI. TRANSPORT AND CONFINEMENT

A. Transport: TRANSP analysis

There is clear evidence for changes in transport within the edge plasma starting at the transition. Changes are observed in T_e and n_e at the edge, in magnetic and density fluctuations and in edge toroidal and poloidal rotation. Figure 27 shows the time variation of D_α, $n_e l$, T_e (edge) and τ_E^{mag} for a 1 MA H-mode. The phases of this shot are the supershot phase which ends at ~ 3.88 sec, the transition plus ELM free period of ~ 3.88-3.97 sec, and the ELM phase which lasts for the remainder of the beam pulse (3.97-4.50 sec). Time dependent transport calculations, using the TRANSP code [31], were carried out for the plasma of Fig. 27 and the resulting χ_i and χ_e profiles are shown in Fig. 28 for the supershot phase (t = 3.85 sec) and the H-mode phase (t = 3.96 sec). TRANSP calculations show little difference in the χ_i and χ_e profiles for the supershot and H-mode

phases of the plasma. In general, the main difference between the H-mode and supershot is in the outer layer of plasma where χ_e is lower for the H-mode than for the supershot. During the transition and short ELM free period, the thermal energy confinement time remains nearly constant. Stored energies, W_e and W_i in the outer quarter of the plasma increase until the onset of ELMs. Z_{eff} begins to rise from a value of ~ 3.2 at the transition, and plateaus at a value of ~ 3.5 (9% increase) at 4.1 sec or about 120 msec into the ELM phase. In this case, the maximum value of τ_E during NBI is 0.145 sec and is reached at the time (t = 3.95 sec) of the minimum in the D_α signal. At ~ 4.02 sec or ~ 50 msec into ELM activity, τ_E has decreased to ~ 0.115 sec, for a decrease of ~ 20% from what it was before the onset of ELMs.

B. Energy and Particle Confinement:

The values of τ_E (obtained from magnetics) for TFTR limiter H-modes resulting from supershot to H-mode transitions varied from ~ 1.4 to 3.0 times the values for L-mode scaling [17]. Plots of τ_E versus I_p and $\tau_E/\tau_{L\text{-mode}}$ versus F_{ne} are given in Figs. 29 and 30, respectively, which include all of the shots with transitions from supershot to H-mode. The lack of I_p scaling of τ_E is as observed for supershots [32]. The values of τ_E for the limiter H-mode range from 0.08 to 0.15 sec, while the range realized for supershots is 0.06 to 0.18 sec. The average value is essentially constant with I_p. Figures 29 and 30 demonstrate that τ_E and the ratio $\tau_E/\tau_{L\text{-mode}}$ increase with F_{ne} for limiter H-modes similar to the trend observed for supershots. There appears to be a small shift in τ_E down from values obtained for supershots with similar F_{ne}. Values of τ_E for supershots are usually reported for the time of peak stored energy, while for the H-modes the data is taken at t ~ τ_E (one confinement time) from the beginning of the transition. In many cases, this is several 10's of milliseconds into the ELM phase and also strong m = 2 and other MHD activity not necessarily associated exclusively with the H-mode have had time to become prominent. From Fig. 30 it is clear that the value of $\tau_E/\tau_{L\text{-mode}}$ is > 2 for the vast majority of H-modes, and for $F_{ne} > 2$ the average value of the ratio is ~ 2.5.

Most of the data of Fig. 30 are for cases for which I_p was held constant for the duration of the discharge. The shaded points, however, at $\tau_E/\tau_{L\text{-mode}} \geq 3$ represent four shots for which current ramp down was completed just at the instant NBI was turned on. This was about 300 msec before the H-mode transition and about 430 msec before the data shown in Fig. 30 for these four discharges were recorded. In general, the I_p ramp cases are rather transient with the increase in τ_E usually lasting for a period less than the instantaneously inferred τ_E itself. The decrease in τ_E following the peak for the I_p ramp shots, just as for constant I_p cases, appears to be correlated with the ELM phase. Thus,

much higher values of τ_E may be possible if a technique is found to extend the ELM free phase of these I_p ramp discharges.

C. Limiter H-modes with Modest Improvement in τ_E

Improvement in confinement over the supershot base plasma has been realized in a few cases. These gains are modest and transient in nature. However, knowledge of the characteristics of these discharges and operational techniques for obtaining them may allow further improvements in τ_E. Figure 31 shows parameters for a discharge in which τ_E improved by ~ 17% after the supershot to H-mode transition. Also, shown in Fig. 32(a) and (b) are D_α and τ_E data for a similar discharge in which τ_E increased by 10%, but remained constant at the elevated value for a longer and quasi-equilibrium time of ~ 150 msec. These discharges fall into a group with the following characteristics: usually there is a small to modest increase in confinement; the density profile within 10 cm of the edge steepens; the core portion of the n_e profile retains or gains in peakedness while rising slightly on a broad edge pedestal; the decrease in the D_α signal is much clearer than usual; and the neutron level remains relatively constant, often through a significant portion of the ELM phase. Also, the I_p ramp down H-modes appear to be more resistant to degradation due to MHD activity; with neutron levels, stored energy, and τ_E often remaining relatively constant during strong bursts of MHD fluctuations. All of these characteristics were not always realized in each discharge of this group, and in addition, they were obtained more consistently in plasmas where I_p was ramped down and reached its flattop around the time of beam turn on. The I_p ramp can be completed up to 500 msec before the transition. I_p was ramped down from 1.4 to 0.85 MA for the plasma of Fig. 31 and from 1.6 to 0.85 MA for that of Fig. 32. In both cases $\tilde{B}_\theta$ in the range 100-350 kHz [Fig. 31(b)] decreased sharply at the transition. Confinement was already significantly enhanced in the pre transition plasma of Fig. 31, with $\tau_E \sim 2.5 \times \tau_{L\text{-mode}}$. At the transition τ_E increased sharply in Case 1 beginning at t = 3.66 sec and peaked about 50 msec later, but began to decrease before the start of ELMs. The value of $\tau_E/\tau_{L\text{-mode}}$ was 3.2 at the peak in τ_E at t ~ 3.7 sec.

In Figs. 33(a) and (b) calculated current density profiles, J(r), for the discharge of Fig.32 are compared to those for the constant I_p plasma of Fig. 1. The J(r) calculations are results from TRANSP analysis of the two cases. Full J(r) profiles for the two cases are plotted in Fig. 33(a) at times just before the transition. The I_p ramp causes narrowing of the J(r) profile at the plasma edge and actually a reversal of sign at r = 55 cm = $(2/3)a_p$. Time evolutions of the J(r) profiles for the two cases are indicated in Fig. 33(b), where profiles before and 300 msec after the H-mode transition are plotted for the outer half of the

plasma. The local peaking in J(r) at the plasma edge, r = 0.72 m, during the H-mode in both cases, is attributed to the bootstrap current. The increase in J(r) at the plasma edge causes increased magnetic shear. In a similar fashion, current ramps are used to trigger H-modes on the JIPP T-IIU tokamak [33].

VII. DISCUSSION: COMPARISON WITH OTHER TOKAMAKS AND WITH CURRENT THEORETICAL MODELS.

A. Similarities and Differences

It has been shown that TFTR limiter H-modes have characteristics similar to those of H-modes on other tokamaks. As seen in Sec. III and IV there are also some differences, the main one being that the TFTR H-mode density profile is peaked on axis. Even in cases where there is a decrease in peakedness in going from the supershot to the H-mode, the change in F_{ne} is often due to the gain in n_e at the plasma edge while the shape of the core portion (inner 30 cm radius) remains essentially unchanged. In addition to illustrating the dependence of $\tau_{E/\tau_{L\text{-mode}}}$ on F_{ne}, Fig. 30 also shows the range of F_{ne} for the TFTR H-mode to be 1.2-2.7. For supershots, the range is ~ 1.2-3.2. There may be a small decrease in τ_E from supershots to H-modes due to the loss in F_{ne}.

However, as illustrated earlier there is a variety of responses of the n_e profile with time through the transition, from basically no change to a slight gain in F_{ne}, to broadening across the entire profile. On the other hand, a significant observation is that the peaked profile can be retained after the transition and during ELMs. In several H-mode plasmas of ~ 1.6 sec duration, τ_E and F_{ne} remained relatively constant for ~ 1.4 sec of ELM activity. This indicates that it may be possible to obtain steady-state centrally-peaked n_e profiles. Such a profile is important since some reactor design studies indicate that the degree of enhanced confinement required for ignition is lowered as the temperature and density and thus pressure profiles become more peaked at the center [34-36].

In general, the D_α response is similar to other tokamaks, especially for limiter H-modes. However, the apparent slow decrease of the D_α signal has not been mentioned in reports for other tokamaks. It is possible that the transition in TFTR does take place within 1 or 2 msec, and that the slow decrease is actually an indication of a period of improving confinement following the transition. On the other hand, biased limiter experiments on CCT [37] indicate that a sharp, sudden, "bifurcation" may not be necessary for a transition to the H-mode. As pointed out in Sec. III.A, the lack of a large fast change in D_α light at the transition has also been reported for limiter H-modes on other tokamaks. On TFTR for the supershot to H-mode transition, this may be due to the fact that the graphite limiter is degassed in order to obtain supershots and thus the recycling is already low prior to the

transition. Yet, in the presence of high recycling and strong gas puffing, large decreases in D_α were still not observed. However, in most cases, the puffing experiments were performed when the limiter was degassed to the extent that it behaved as an efficient pump for deuterium. For high recycling, the confinement enhancement over L-mode was small and this was probably reflected in the D_α signal. An argument against the degassed limiter conjecture is that nearly all transitions which resulted in at least a small initial gain in τ_E (usually transient) or a small loss during ELMs also showed clear D_α drops. This increase in τ_E and the drop in D_α light were especially obvious for the I_p ramp down experiments, even though the ramp was completed at the time NBI was turned on and the H-mode transition took place after several hundred milliseconds into the beam heating phase.

B. Thresholds

Knowledge of the scaling of thresholds for the transition and for the onset of ELMs and other H-mode phenomena should lead to a better understanding of the underlying physics. Such knowledge should also allow H-modes to be obtained efficiently and with better control over their confinement properties. The threshold results also help in the design of future research and power reactors since they allow extrapolations in order to determine power and edge plasma requirements. Some observations relative to thresholds for other tokamaks [13, 38, 39] are stated briefly in Table I. The scaling of P_{th} with I_p found for limiter H-modes on TFTR (see Fig. 7 and Eq. 1) has been extremely useful from an operational standpoint; with the proper P_b set above the threshold for a given I_p, H-modes were obtained within one or two shots. As is clear from Table I, however, there is no universal scaling for the threshold power for obtaining transitions to H-modes. For DIII-D with divertor, the threshold power for L- to H-mode transitions with H^o beams injected into D^+ plasmas scales as [38]:

$$P_{th}(MW) \sim 6.24 \times 10^{-20}\, \bar{n}_e\, B_\phi \qquad (2)$$

where $\bar{n}_e$ is in particles/m^3 and B_ϕ is in Tesla. Figure 34 is a plot of P_b versus $\bar{n}_e\, B_\phi$ for TFTR , where the values of $\bar{n}_e$ and B_ϕ are taken just before the transition. A straight line along the minima of this plot gives a threshold power scaling of

$$P_{th}(MW) \sim 9.2 \times 10^{-20}\, \bar{n}_e\, B_\phi \qquad (3)$$

Thus, the threshold power required to obtain limiter H-modes on TFTR is about 1.5 times the power indicated by Eq. (2) for DIII-D divertor H-modes [38]. However, P_{th} predicted

by Eq. (3) is somewhat lower than the values for limiter H-modes on DIII-D [38]. On the other hand on TFTR for supershots, $\bar{n}_e$ depends on P_b and I_p. $\bar{n}_e$ of ohmic target plasmas depends on I_p, and since the target density for supershots is very low due to degassing of the graphite limiter, the core of a supershot is essentially beam fuelled, so that $\bar{n}_e$ is a function of the heating beam power. The TFTR data did not fit the scaling indicated by that for JFT-2M.

Current ramp down was used on the JIPP T-IIU tokamak [33] to lower the threshold power for L- to H-mode transitions by 30 to 50%. This result was felt to be due to the skin effect, such that the I_p ramp caused increased magnetic shear at the plasma edge which reduced the "outward flow of heat and particles," thus triggering the H-mode transition. On TFTR, H-mode transitions appear to be easier to obtain using I_p ramp downs, although detailed studies to determine the difference in P_{th} with and without I_p ramps have not been done. The increase in magnetic shear may also explain the clearer D_α signature and larger increases in τ_E observed for the H-mode transitions obtained following I_p ramp down.

C. Comparisons with Theory: Fluctuations and Poloidal and Toroidal Flows

The TFTR limiter H-mode results may support several theoretical models. Comparisons of these results to various models [18, 19, 40-42] are summarized in Table II. Poloidal and toroidal rotation play a part in all of these, however, the rotations or flows differ as to origin. Mechanisms proposed for driving the flows range from formation of an E_r field due to electron accumulation or ion orbit losses to spontaneous generation of flows by turbulence which in turn suppresses the turbulence itself. Several results are in agreement with the neoclassical model of Shaing and Crume [41]. These are the observations that (1) the H-modes have only been observed for NBI heated plasmas and (2) there is no x-point within the TFTR plasma. The transition, according to the neoclassical model, is triggered by preferable loss of fast counter-injected ions. The prompt increase in the fast ion flux shown in Fig. 16 may be experimental evidence in support of this mechanism as the origin of a radial electric field. H-modes have not yet been observed in the presence of ohmic or ICRF heating in TFTR. On the other hand, the NBI results support the neoclassical theories in that energetic ions are inherent to beam heating and are expected to be a readily available source of fast ions (for orbit loss).

TFTR results show decreases in $\tilde{B}_\theta$ at the transition, and this may support theories [18, 19] based on the stabilization of turbulence as the trigger for the bifurcation in confinement. Scattering data from small scale fluctuations do not show a corresponding drop in $\tilde{n}^2$. The spatial resolution of the microwave scattering measurement is rather poor and the measurement is an average over a large volume which probably includes plasma

within and away from the suppression zone. As presented earlier in Figs. 8, 9 and 31, the magnetic fluctuations in the range of 100-250 kHz decrease at and during the transition and increase again during ELMs.

Even though a reduction in $\tilde{n}^2$ is not observed, scattering data clearly show a poloidal spinup of the plasma. This may be indicative of a change in the E × B flow, and shear in E × B flow is a leading candidate as a mechanism for turbulence stabilization. The main component of the E × B flow is due to the radial electric field, E_r, resulting from the zero order force balance equation given by:

$$E_r = \frac{1}{Z_i e}\left(\frac{T_i}{n_i}\frac{dn_i}{dr} + \frac{dT_i}{dr}\right) + V_\theta B_\phi - V_\phi B_\theta . \qquad (4)$$

The values of V_ϕ and T_i are measured using the CHERS diagnostic for the i^{th} impurity ion. For TFTR the C^{5+} (n = 8 - 7, 5792 Angstroms) line emission is used for the CHERS measurements. The microwave scattering data of Figs. 10-12 and 21 show an asymmetric feature which is consistent with a spin up in V_θ at the transition. The direction of the velocity is that of V_{De} and is the same for all H-mode transitions observed on TFTR to date. The direction of $V_\theta \times B_\phi$ is such as to yield a radially inward pointing (or negative) E_r. This is in agreement with the theories of Shaing and Crume [41], Biglari et al. [18, 19], and the revised theory of Itoh and Itoh [40]. This result is also in agreement with experimentally determined values of V_θ found on DIII-D and JFT2-M. Figures 6 and 12-15 show changes in V_ϕ and T_i at the transition which would lead to changes in E_r as given by Eq. (4). Changes in V_ϕ and T_i in the plasma edge at the L- to H-transition have also been observed on DIII-D.[21]

The model by Hassam, et al., predicts a spontaneous poloidal spin up by a mechanism which depends on having poloidal asymmetry in the particle flux. TFTR H-mode transitions which follow small pellet injection and gas puffs may support this mechanism since they are initially localized perturbations on the intrinsic particle flow. On the other hand such perturbations also change the edge T and ∇T; these changes may also trigger transitions.

VIII. Summary and Conclusions.

Circular limiter H-modes have been obtained on TFTR which have density profiles that are peaked at the center. Values of F_{ne} range from ~ 1.2 to > 2.7. The global energy confinement can be enhanced over Goldston L-mode scaling by a factor > 2.8. Usually in the absence of strong MHD activity, τ_E decreases slightly when F_{ne} decreases somewhat

due to the broadening in n_e as a result of the improved confinement in the edge plasma. There is usually (but not always) a decrease in τ_E at the onset of ELMs. Modest, but transient increases in τ_E, 15% or more, over that of the target supershot have been observed in some cases. The characteristics of the TFTR H-mode are similar to H-modes on other tokamaks, but there are a few differences in addition to the peaked density profile (which is attributable to the initial supershot regime). Drops in D_α and CII light are usually but not always observed and have time constants of a few msec to greater than 10's of msec. This is in contrast to divertor H-modes in which the D_α drops always occur and with a time constant of 1 or 2 msec. Increases in n_e, T_e, and T_i occur over a broad edge region. Also, the V_ϕ profile changes at the transition with the value over a broad outer region (outer 20-30 cm) becoming less positive ($|\Delta V_\phi(\text{edge})| \sim 1.5$ to 6.5×10^4 m/s) or more counter, while for V_ϕ in the core (inner 20-30 cm radius) there is no clear correlation with the transition.

Bi-directional NBI power is required for the supershot to H-mode transition. Confinement for H-modes obtained in the low recycling environment required for supershots is usually better than for H-modes obtained with high recycling. The threshold power required for the transition is $P_{th} \sim 11 \bullet I_p$, where the plasma current, I_p, is an operational parameter which is pre-set before the discharge. The threshold power scaling relative to the plasma parameter $\bar{n}_e$ is slightly lower for TFTR than for limiter H-modes on DIII-D and is $\sim 9 \times 10^{-20}\, \bar{n}_e\, B_\phi$. Qualitatively, there appear to be critical edge T_e's for obtaining H-modes and for the onset of ELMs, however, a quantitative dependence has yet to be determined.

TFTR results are consistent with a change in ExB flow and may be useful for testing theories which hypothesize turbulence stabilization by shear flow as the trigger for the transition to the H-mode. Increased fast ion efflux has been detected by probes located at the outer midplane edge of the plasma. This efflux may represent ion orbit losses, possibly contributing to establishment of a radial electric field, E_r, which could trigger an E_r x B rotation. High frequency magnetic fluctuations in the range of 100-250 kHz usually decrease at the transition. The hypothesis of turbulence stabilization is also being investigated using the spectra of density fluctuations obtained using the microwave scattering technique. The asymmetric portion of the spectra is indicative of poloidal flow and further study of this data may lead to understanding of shear flow effects on turbulence. The shift in frequency of the asymmetric feature is usually > 1 MHz and is in the direction consistent with a poloidal spin up in velocity at the plasma edge of $\sim 10^4$ m/s. In addition, the change in V_ϕ, as provided by CHERS measurements, could lead to a

change in the $V_\phi \times \tilde{B}_\theta$ contribution to E_r and thus to the possibility of increased shear in the $E_r \times B_\phi$ flow.

There are no strong low-m mode magnetic oscillations which precede ELMs on TFTR, however, high frequency (50-500 kHz) precursor magnetic oscillations have been observed for some ELMs and these were found to be m = 1, n = 0 standing waves which were not outward ballooning in structure. This is very similar to the quasi-coherent mode observed on PDX using infrared scattering [43]. TRANSP calculations show the transport to be similar for supershots and limiter H-modes, the main difference being reduced electron transport at the plasma edge of H-modes. The TFTR H-modes have been maintained with nearly constant peaking factors of ~2.3 and $\tau_E \sim 2.5\ \tau_{L\text{-mode}}$ for a duration of 1.6 sec, indicating the possibility of applications of these plasmas to future long pulse research devices such as ITER.

Acknowledgments

We wish to thank D. M. Meade, R. Hawryluk, and K. M. Young for their suggestions and continuing support. We also express our appreciation for the dedication and support of the TFTR physicists and staff. This work was supported by the U. S. Department of Energy Contract No. DE-AC02-76-CHO-3073.

TABLE I.

Dependence of the threshold power for the L- to H-mode transition on other tokamaks.

(Supershot to H-mode transition on TFTR.)

ASDEX	- P_{th} independent of device parameters
DIII-D	- $P_{th} \alpha B \cdot n$
JET	- $P_{th} \alpha B$
JFT-2M	- $P_{th} \alpha B/(I \cdot n)$

Dependence on local edge conditions

ASDEX	- Requires a critical T_e
DIII-D	- $T_e(crit) \alpha B$

TABLE 2.
H-mode Theoretical Models

Theoretical Model	Authors	Results from TFTR
Edge electric field	Itoh and Itoh	Mode propagation in electron direction $\Rightarrow E_r < 0$ **Model** $\Rightarrow$ $(dE_r/dr) < 0$ and $E_r < 0$.
Fast ion orbit effect	Shaing, Crume	Observed only with beams on TFTR. Prompt loss of fast beam and fusion product ions at transition. **Model** $\Rightarrow$ bifurcation in poloidal rotation.
Shear rotational stabilization of turbulence	Biglari et al.	$\tilde{B}_\theta \approx 200$ kHz decreases Supershot to H-mode. V_ϕ and V_θ (μ-wave scatt.) change. **Model** $\Rightarrow$ Fluctuations decrease, bifurcation in thermal confinement and hysteresis.
Spontaneous poloidal spin up	Hassam, et al.	Poloidally asymmetric particle flux (pellet and gas puff transitions on TFTR); $P_{th} \alpha n$. **Model** $\Rightarrow$ Spin up when magnetic pumping small; bifurcation.

FIGURE CAPTIONS

Fig. 1. Characteristics of a TFTR limiter H-mode. The transition was from supershot to H-mode and the duration of the H-mode phase was 1.6 sec. Shown are the following signals: the D_α, edge chord averaged density $n_e l$, T_e (edge), density peaking factor, F_{ne}, and τ_E from magnetics. Plasma radii were R = 2.45 m, a = 0.80 m.

Fig. 2. Comparison of parameters for a plasma with a supershot to H-mode transition and one without (I_p = 1.0 and 1.05 MA, respectively). (The solid curve is for the H-mode.) All plasma and operating parameters, except I_p, were essentially the same up to the time of the transition at ~ 4.56 sec. Shown are (a) $n_e l$ (edge), (b) density peaking factor, F_{ne}, (c) D_α signal, and (d) τ_E from magnetics. (e) and (f) are density profiles for four times. P_b = 14 MW, B_ϕ = 4.8 T.

Fig. 3. Density profiles for two different H-mode plasmas showing two different behaviors. (a) Core profile rises on edge pedestal; (b) a profile which continued to become more peaked after the transition and well into the ELMs (t = 4.0 sec is ~ 180 msec after first ELM).

Fig. 4. Characteristics of a plasma in which a supershot to H-mode transition resulted following injection of a small deuterium pellet. The time evolution of D_α, high frequency magnetic fluctuations, $\tilde{B}_\theta$, $n_e l$ (edge), τ_E, and $n_e(R)$ profiles are shown. B_ϕ = 4.8 T, I_p = 1.05 MA, and P_b = 14 MW (from 4-5 sec).

Fig. 5. Two H-modes for which the T_e's at the edge were equal at the transition and at the beginning of ELMs even though the parameters (P_b and I_p) and recycling were significantly different. B_ϕ = 4 T for both.

Fig. 6. Comparison of time evolutions of (a) D_α light and (b) T_e (edge) for the plasmas of Fig. 2, with and without a supershot to H-mode transition. Also shown are CHERS data (T_i and V_ϕ) for three outermost chord positions, 3.04, 3.14, and 3.24 m, for the H-mode plasma. Carbon line emission C^{5+} (n = 8 - 7, 5792 Angstroms) is used for the CHERS measurements.

Fig. 7. Plot of P_b vs Ip for the TFTR limiter H-mode. Data for a wide range of plasma parameters were included. A dependence of the threshold power, P_{th}, required for a transition to the H-mode on I_p is indicated.

Fig. 8. The intensity of high frequency magnetic fluctuations ($\tilde{B}_\theta$ in the range of 100 to 350 kHz) decreased during and just after the H-mode transition and during ELM free periods between "clumps" of ELMs for the plasma of Fig.1.

Fig. 9. Effect of deuterium gas puffing (recycling) and beam power on the triggering of H-modes. D_α and $\tilde{B}_\theta$ signals are shown for four different plasmas. Gas puffing (a) from 3.5 to 4.0 sec and (b) from 3.0 to 4.5 sec.

Fig. 10. (a) Contour plot of microwave scattering spectrum for a limiter H-mode. The transition is at ~ 4.02 sec (H-mode from ~ 4.02 - 4.52 sec) and ELMs begin at 4.1 sec. X-mode scattering was used with K_θ = 5.4 cm^{-1}, z = 0.57 m, R (receiver) = 2.86 m, I_p = 0.9 MA, B_ϕ = 4 T, R_p = 2.45 m, a_p = 0.8 m, P_b = 12.7 MW (from 3.5 to 4.5 sec). (b) D_α signal (c) Values of V_ϕ for four outer CHERS positions. Spatial resolution of V_ϕ data ~ $\pm$ 2.5 cm.

Fig. 11. Microwave scattering data showing details of the spectra during and after the transition. (a) Scattered signal vs frequency profiles for 6 times; (b) Time evolution of D_α light.

Fig. 12. (a) Microwave scattering spectrum for a plasma in which the H-mode characteristics appeared to be dissipated by growing intensity of coherent MHD activity. All parameters are the same as for Fig. 10. (b) D_α signal, (c) amplitude of MHD activity, (d) V_ϕ (edge) data and (e) T_i (edge) data.

Fig. 13. Toroidal velocity, $V_\phi(R)$, ion temperature, $T_i(R)$, and electron density, $n_e(R)$, profiles for the H-mode of Fig. 10, before the transition (4.37 sec), during the H-mode ELM free period (4.44 sec), and just at the first ELM (4.50 sec).

Fig. 14. Time evolution of the toroidal velocity profiles for four different plasmas. (a), (b), and (d) were H-modes and (c) was not an H-mode (P_b too low for I_p ~ 0.9 MA)

Fig. 15. The change in the edge toroidal velocity (r ~ 80 cm) ΔV_ϕ vs P_b across the supershot to H-mode transition period for I_p = 0.8, 0.9, and 1.0 MA. Data for the outermost CHERS chord at R = 3.24 m are shown.

Fig. 16. Time evolution of (a) the fast ion efflux, (b) D_α signal, (c) charge exchange flux, and (d) V_ϕ for an H-mode plasma. The fast ion signal increases promptly at the transition. Main contributions are probably the 800 keV He-3 and 3 MeV proton D-D fusion product ions.

Fig. 17. Time variation of D_α light, signal from Mirnov coil, and electron cyclotron emission (ECE) during a series of ELMs. The bursts in $\tilde{B}_\theta$ and the ECE spikes may be precursors to the ELMs.

Fig. 18. Signals from a midplane D_α monitor and from the grating polychromator for two positions near the plasma edge. The edge T_e gradient recovers (steepens) between ELMs. At time (1) just after the ELM, the edge T_e profile is broad and at time (2) just before the next ELM, the profile gradient is steep

Fig. 19. T_e profile showing the spectral and spatial location of a single ECE spike. The spectral width of the spike is equivalent to an energy range of 10-100 keV.

Fig. 20. Contour plot showing the disturbance in $T_e(R,t)$ during the ECE spike to propagate radially outward at a velocity ~ 2 x 10^3 m/s.

Fig. 21. Density fluctuation spectra during an ELM and at a time between ELMs. The component centered at $\omega = 0$ (symmetric component) is enhanced during ELMs. Between ELMs there is a clear peak in the shifted component at ~ 0.8 MHz.

Fig. 22. Microwave scattering and D_α signals during the ELM phase of a limiter H-mode.

Fig. 23. Beam emission spectroscopy (BES) and edge D_α signals during a series of ELMs. BES data shows a coherent mode in the outer 10 cm plasma region which propagates in the ion diamagnetic direction with a high-m (15-20) mode.

Fig. 24. Variation of the change in D_α (spike height) light intensity associated with an ELM as a function of the frequency of occurrence of ELMs during a single H-mode discharge. $B_\phi = 4$ T, $I_p = 0.9$ MA, $P_b = 13.2$ MW.

Fig. 25. The D_α and fast ion flux signals during several ELMs between times t = 4.085 and t = 4.11 sec of the discharge of Fig. 16.

Fig. 26. Charge exchange flux from an H-mode plasma measured using perpendicular CX analyzers. The signal for the viewing chord at the plasma edge (R = 3.23 m) shows a decrease after each D_α spike.

Fig. 27. Time variation of parameters D_α, $n_e l$, T_e and τ_E for an H-mode for which a TRANSP analysis of the transport and confinement was done. The solid vertical line marks the beginning of the transition. The vertical dashed lines are for times before (3.85) and during (3.97) the H-mode, at which the χ_i and χ_e results (Fig. 28) from the TRANSP analysis are compared.

Fig. 28. Comparison of transport between a supershot and a limiter H-mode. (a) χ_e, (b) χ_i. The times at which the supershot and H-mode phases are compared are indicated by the two vertical dashed lines of Fig. 27.

Fig. 29. Plot of the limiter H-mode confinement, τ_E, as a function of I_p. Data for a wide range in Ip, B_ϕ and P_b are included.

Fig. 30. Variation of $\tau_E/\tau_{L\text{-mode}}$ with n_e profile peakedness, F_{ne} for the data of Fig. 29.

Fig. 31. Variations of D_α, $\tilde{B}_\theta$ and τ_E for an H-mode which showed a transient improvement of 15-20% in confinement. Ip ramp down from 1.4 to 0.85 MA before beam turn on at 3.19 sec. H-mode transition at ~3.66 sec. Ip = 0.85 MA, $B_\phi = 4.8$ T, $P_b = 12$ MW at the transition.

Fig. 32 Time evolution of the D_α signal and τ_E for an H-mode with a 10% improvement in τ_E. The quiescent period before ELMs was longer than for the plasma of Fig.31. I_p ramp from 1.6 to 0.85 MA before beam turn on. Ip = 0.85 MA, B_ϕ = 4.8 T, $P_b = 12$ MW during H-mode.

Fig. 33 (a) Calculated current density profiles, J(r), resulting from a TRANSP analysis of two plasmas for times just before H-mode transitions; (1) a plasma with a pre-NBI current ramp down from 1.6 MA to 0.85 MA (P_b = 12 MW and B_ϕ = 4.8 T) and (2) a plasma with a constant I_p of 0.8 MA (P_b = 11.2 MW and B_ϕ = 4 T).
(b) Comparison of the time evolution of the J(r) profiles at r > a/2 for the two plasmas of Fig. 33(a). Profiles just before and at 300 msec after the H-mode transition are shown for each case.

Fig. 34 Plot of P_b vs $\bar{n}_e B_\phi$ for comparison of TFTR H-mode data with DIII-D scaling of P_{th} for H-mode transitions.

REFERENCES

[1] Bush, C. E., Goldston, R.J., Scott, S.D., et al., Phys. Rev. Lett. **65** (1990) 424.

[2] Bush, C. E., Bretz, N.L., Fredrickson, E.D., et al., in Plasma Physics and Controlled Nuclear Fusion Research 1990 (Proc. 13th Int. Conf. Washington, 1990), Vol. 1, IAEA, Vienna (1991) 309.

[3] Bush, C. E., Schivell, J., Taylor, G., et. al., Rev. Sci. Instrum. **61** (1990) 3532.

[4] Tomabechi, K., Gilleland, J.R., Sokolov, Yu.A., Toschi, R., and the ITER Team, Nucl. Fusion **31** (1991) 1135.

[5] Wagner, F., Becker, G., Behringer, K., et al., Phys. Rev. Lett. **49** (1982) 1408.

[6] Strachan, J. D., Bitter, M., Ramsey, A.T., et al., Phys. Rev. Lett. **58** (1987) 1004.

[7] Sabbagh, S. A., Gross, R.A., Mauel, M.E., et al., Phys. Fluids B **3** (1991) 2277.

[8] Dylla, H. F., LaMarche, P.H., Ulrickson, M., et al., Nucl. Fusion **27** (1987) 1221.

[9] Kaye, S. M., Bell, M.G., Bol, K., et al., J. Nucl. Mater. **121** (1984) 115.

[10] Bretz, N., Efthimion, P., Doane, J., and Kritz, A., Rev. Sci. Instrum. **59** (1988) 1538.

[11] Tubbing, B. J. D., Jacquinot, J.J., Stork, D., and Tanga, A., Nucl. Fusion **29** (1989) 1953.

[12] Sengoku, S., Funahashi, A., Hasegawa, M. et al., Phys. Rev. Lett. **59** (1987) 450.

[13] ASDEX Team, Nucl. Fusion **29** (1989) 1959.

[14] Sauthoff, N., Asakura, N., Bell, R., et al., in Plasma Physics and Controlled Nuclear Fusion Research 1990 (Proc. 13th Int. Conf. Washington, 1990), Vol. 1, IAEA, Vienna (1991) 709.

[15] Tubbing, B. J. D., Balet, B., Bartlett, D.V., et al., Nucl. Fusion 31 (1991) 839.

[16] Jackson, G. L., Winter, J., Taylor, T.S., et al., Phys. Rev. Lett. **67** (1991) 3098.

[17] Goldston, R. J., Plasma Phys. Controlled Fusion **26** (1984) 87.

[18] Biglari, H., Diamond, P.H., and Terry, P.W., Phys. Fluids **B2** (1990) 1.

[19] Biglari, H., Diamond, P.H., Kim, Y.-B., et al., in Plasma Physics and Controlled Nuclear Fusion Research 1990 (Proc. 13th Int. Conf. Washington, 1990), Vol. 2, IAEA, Vienna (1991) 191.

[20] Groebner, R. J., Gohil, P., Burrell, K.H., Osborne, T.H., Seraydarian, R.P., and St. John, H., in Controlled Fusion and Plasma Physics (Proc. 16th Eur. Conf. Venice, 1989), Vol. 13B, Part I, European Physical Society (1989) 245.

[21] Groebner, R. J., Burrell, K.H., and Seraydarian, R. P., Phys. Rev. Lett. **64** (1990) 3015.

[22] Ida, K., Hidekuma, S., Miura, Y., et al., Phys. Rev. Lett. **65** (1990) 1364.

[23] Kim, Y. B., Diamond, P.H., and Groebner, R.J., Phys. Fluids **B 3** (1991) 2050.

[24] Zweben, S. J., Nucl. Fusion **29** (1989) 825.

[25] McGuire, K. M., Fredrickson, E., Bush, C.E., et al., J. Nucl. Mater. **176 & 177** (1990) 711.

[26] Von Goeler, S., Kluber, O., Fussmann, G., Gernhardt, J., and Kornherr, M., Nucl. Fusion **30** (1990) 395.

[27] Kaye, S. M., Manickam, J., Asakura, N. et al., Nucl. Fusion **30** (1990) 2621.

[28] Keilhacker, M., Gierke, G. V., Muller, E. R. et al., Plasma Phys. Controlled Fusion **28** (1986) 29.

[29] Nazikian, N., Bush, C. E., Bretz, N., et al., (to be published)

[30] Paul, S. F. and Fonck, R. J., Rev. Sci. Instrum. **61** (1990) 3496.

[31] Hawryluk, R. J., in Physics of Plasmas Close to Thermonuclear Conditions **1** (1980) 19.

[32] Bell, M. G., Arunasalam, V., Barnes, C.W., et al., Plasma Phys. Controlled Nuclear Fusion Research 1988 (Proc. 12th Int. Conf. Nice, 1988), Vol. 1, IAEA, Vienna (1989) 27.

[33] Toi, K., Adati, K., Akiyama, R., et al., in Controlled Fusion and Plasma Physics (Proc. 16th Eur. Conf. Venice, 1989), Vol. 13B, Part I, European Physical Society (1989) 221.

[34] Redi, M. H., Zweben, S. J. and Bateman, G., Fusion Technol. **13** (1988) 57.

[35] Bateman, G., Princeton Plasma Physics Laboratory Report # PPPL-2373 (1986)

[36] Stotler, D. P. and Bateman, G., Fusion Technol. **15** (1989) 12.

[37] Taylor, R. J., Brown, M.L., Fried, B.D., et al., Phys. Rev. Lett. **63** (1989) 2365.

[38] Burrell, K. H., Allen, S.L., Bramson, G., et al., Plasma Phys. Controlled Fusion **31** (1989) 1649.

[39] Nardone, C., Bhatnagar, V.P., Campbell, D., et al., in Controlled Fusion and Plasma Physics (Proc. 18th Eur. Conf. Berlin, 1991), Vol. 15C, Part I, European Physical Society (1991) 377.

[40] Itoh, S. and Itoh, K., in Plasma Physics and Controlled Nuclear Fusion Research 1990 (Proc. 13th Int. Conf. Washington, 1990), Vol. 2, IAEA, Vienna (1991) 321.

[41] Shaing, K. C. and Crume, E.C., Jr., Phys. Rev. Lett. **63** (1989) 2369.

[42] Hassam, A. B., Antonsen, T.M., Jr., Drake, J.F. and Liu, C.S., Phys. Rev. Lett. **66** (1991) 309.

[43] Slusher, R., Surko, C. ,Valley, J., et al, Phys. Rev. Lett. **53** (1984) 667.

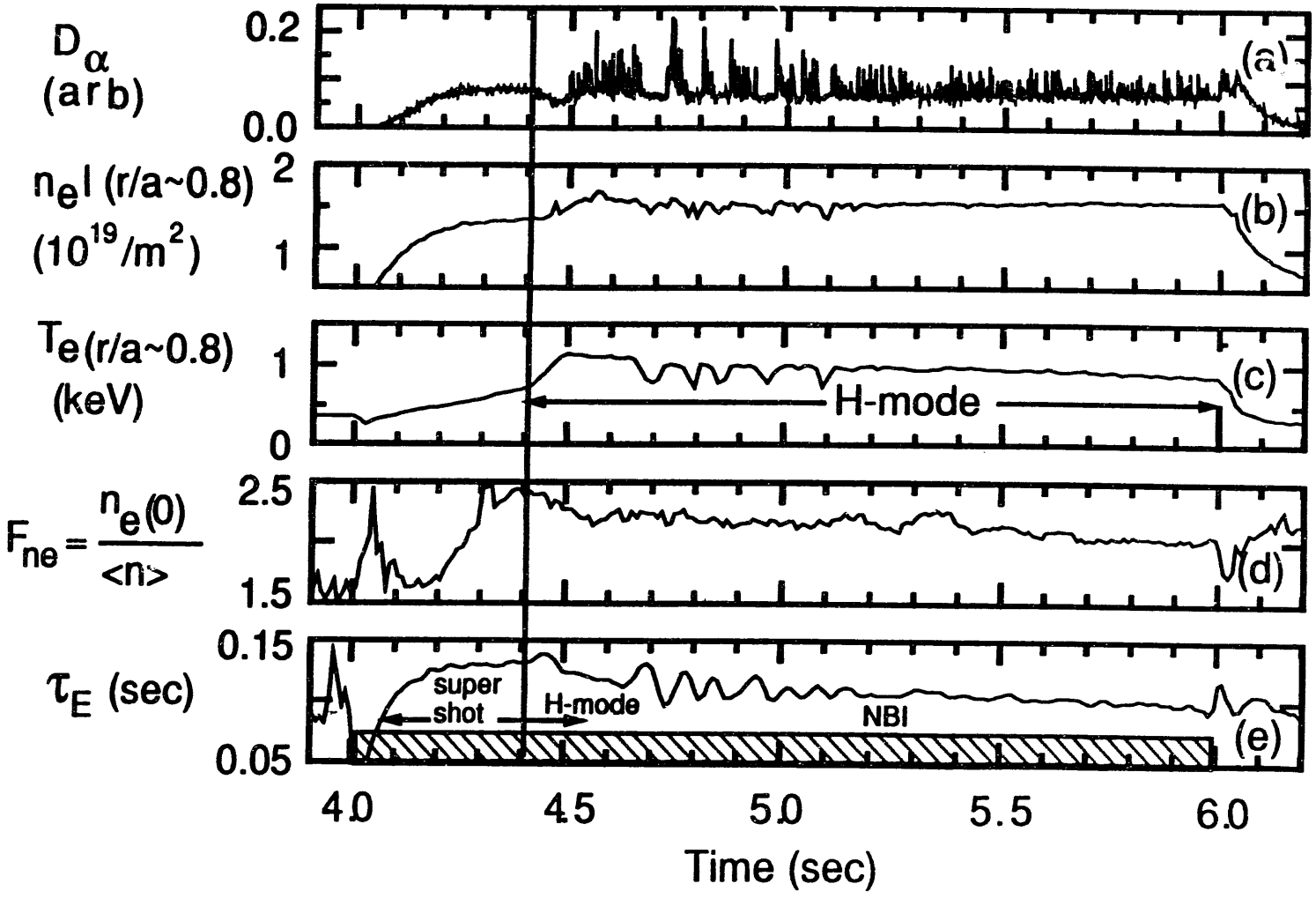
D_α (arb)
0.2
0.0
(a)
n_el (r/a~0.8) ($10^{19}/m^2$)
2
1
(b)
T_e(r/a~0.8) (keV)
1
0
(c)
H-mode
$F_{ne} = \frac{n_e(0)}{<n>}$
2.5
1.5
(d)
τ_E (sec)
0.15
0.05
super shot
H-mode
NBI
(e)
4.0
4.5
5.0
5.5
6.0
Time (sec)

Fig. 1

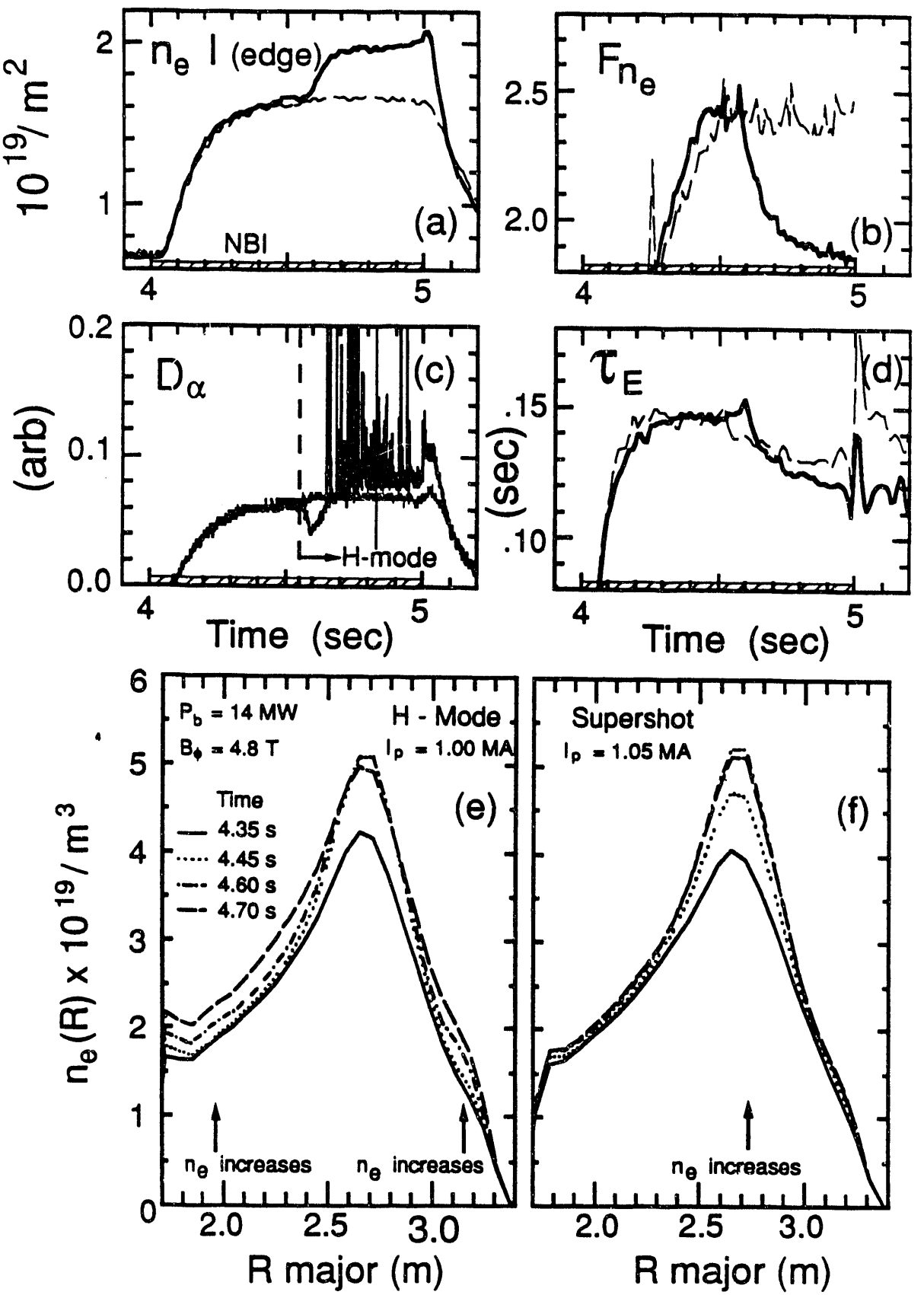
n_e l (edge)
$10^{19}/m^2$
NBI
(a)
F_{n_e}
(b)
D_α
(arb)
H-mode
(c)
τ_E
(sec)
(d)
Time (sec)
Time (sec)
P_b = 14 MW
H - Mode
B_ϕ = 4.8 T
I_p = 1.00 MA
Time
4.35 s
4.45 s
4.60 s
4.70 s
(e)
Supershot
I_p = 1.05 MA
(f)
$n_e(R) \times 10^{19}/m^3$
n_e increases
n_e increases
n_e increases
R major (m)
R major (m)

Fig. 2

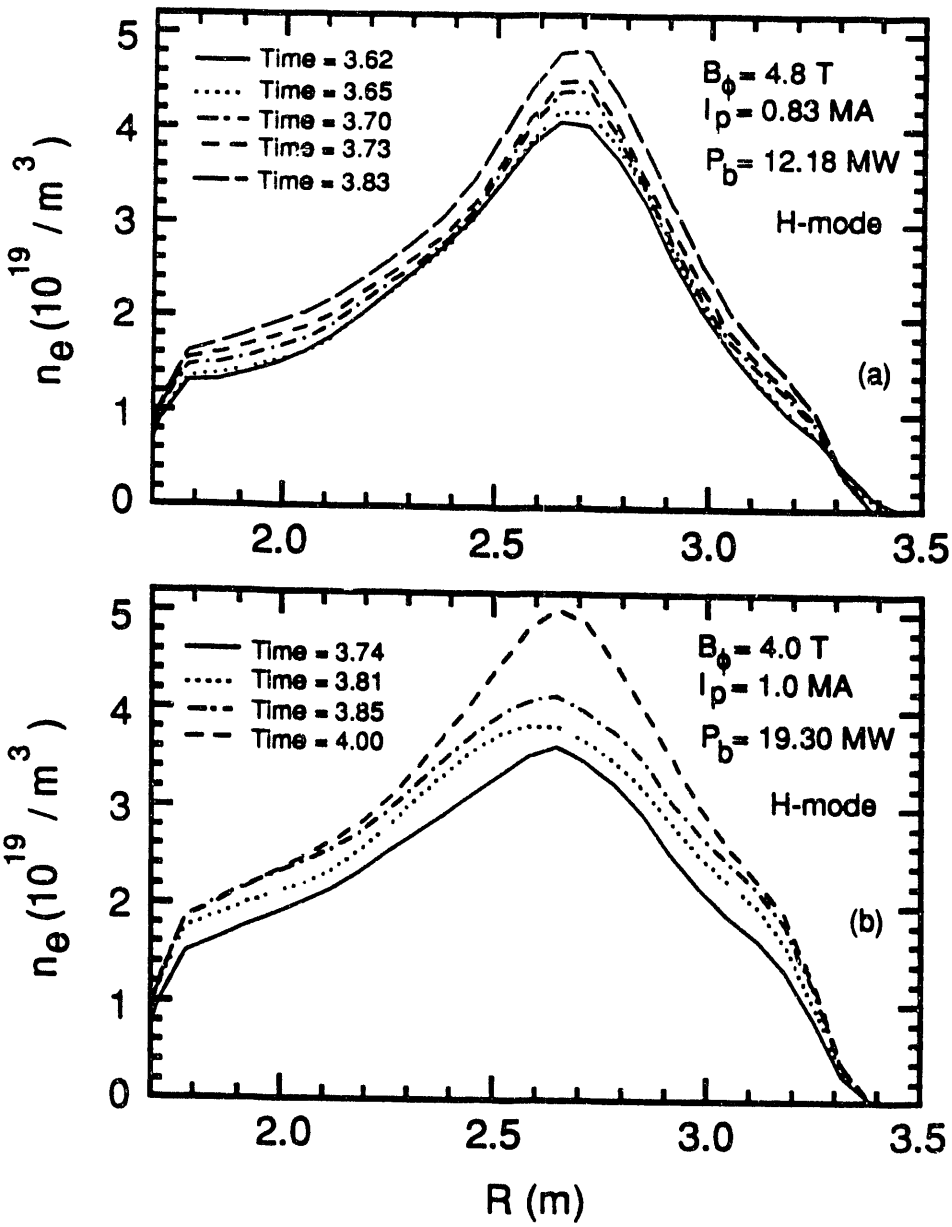
Time = 3.62
Time = 3.65
Time = 3.70
Time = 3.73
Time = 3.83
B_ϕ = 4.8 T
I_p = 0.83 MA
P_b = 12.18 MW
H-mode
(a)
$n_e (10^{19} / m^3)$
Time = 3.74
Time = 3.81
Time = 3.85
Time = 4.00
B_ϕ = 4.0 T
I_p = 1.0 MA
P_b = 19.30 MW
H-mode
(b)
$n_e (10^{19} / m^3)$
0
1
2
3
4
5
2.0
2.5
3.0
3.5
R (m)

Fig. 3

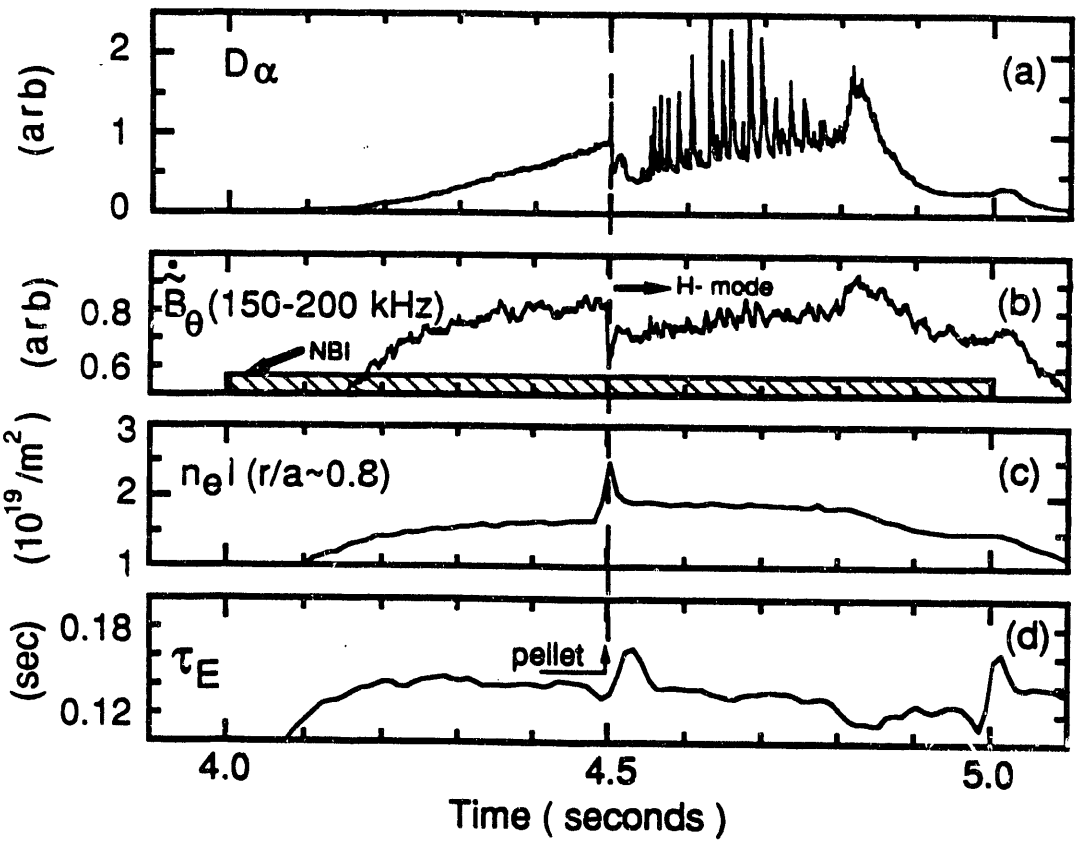
Dα
(arb)
(a)
$\tilde{B}_\theta$(150-200 kHz)
H- mode
NBI
(b)
$n_e l$ (r/a~0.8)
$(10^{19}/m^2)$
(c)
τ_E
pellet
(sec)
(d)
Time (seconds)

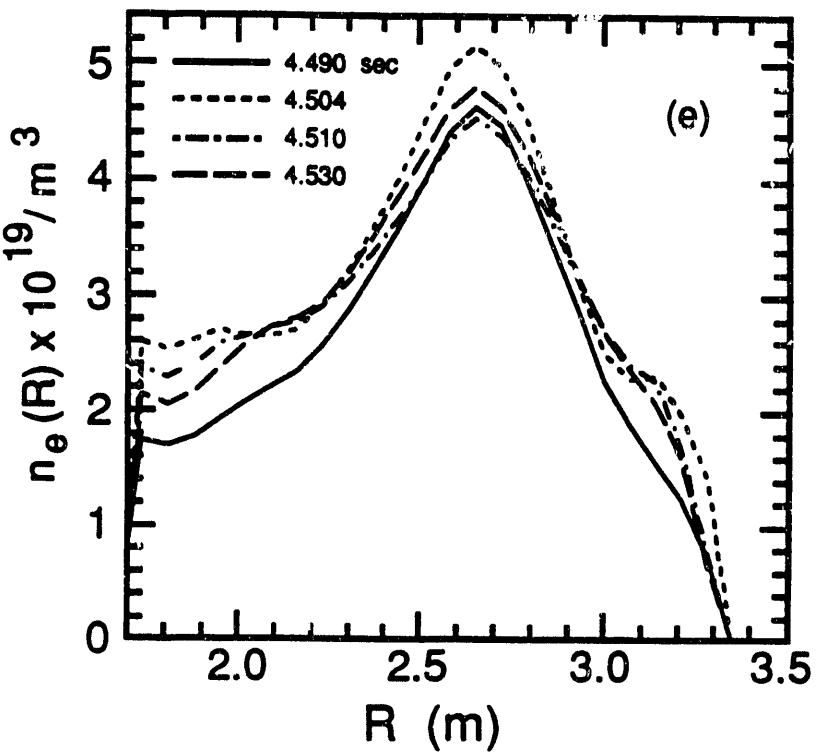
4.490 sec
4.504
4.510
4.530
(e)
$n_e(R) \times 10^{19}/m^3$
R (m)

Fig. 4

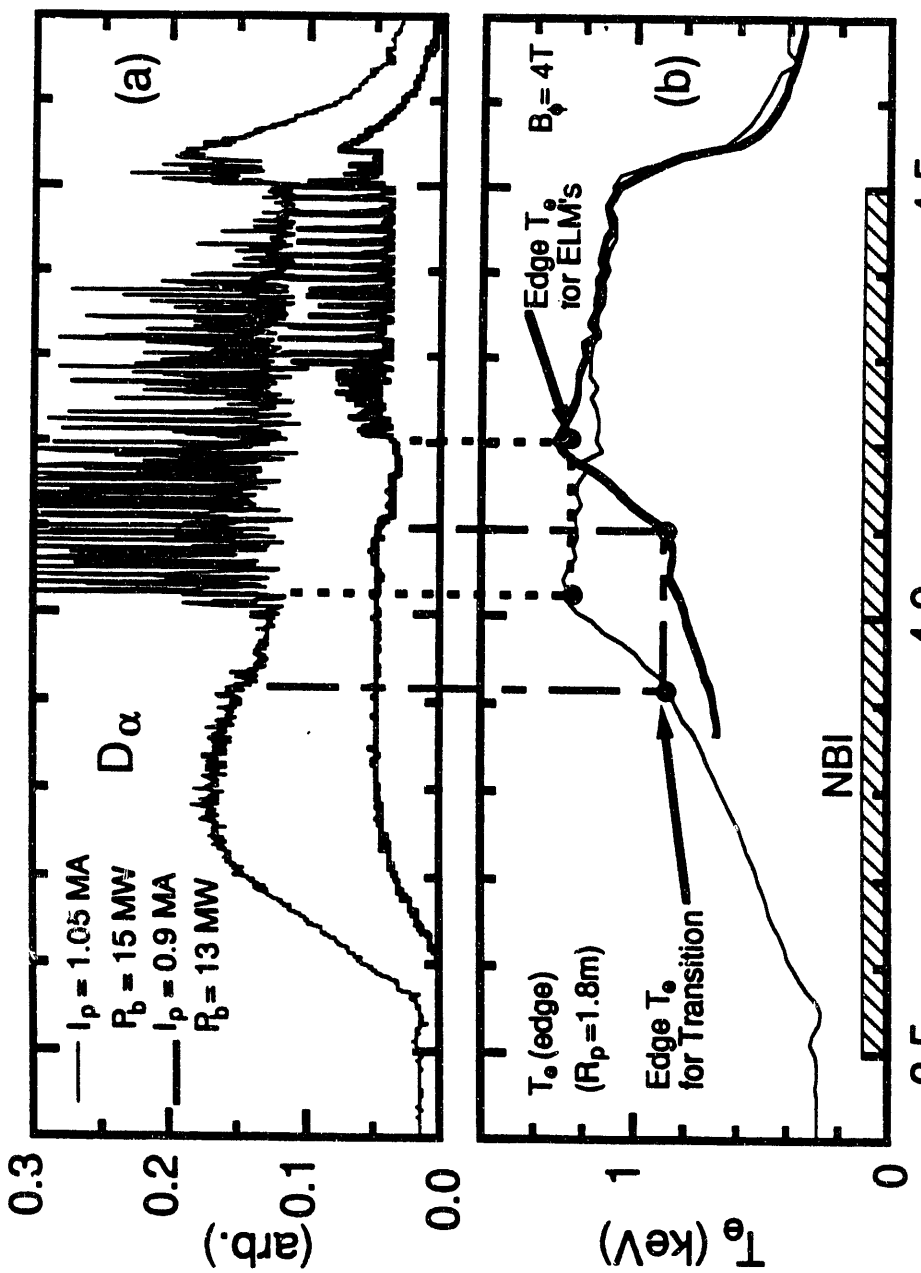
(a)
D_α
I_p = 1.05 MA
R_b = 15 MW
I_p = 0.9 MA
R_b = 13 MW
(arb.)
0.3
0.2
0.1
0.0
(b)
B_ϕ = 4T
Edge T_e for ELM's
T_e (edge)
(R_p=1.8m)
Edge T_e for Transition
NBI
T_e (keV)
1
0
3.5
4.0
4.5
TIME (sec)

Fig. 5

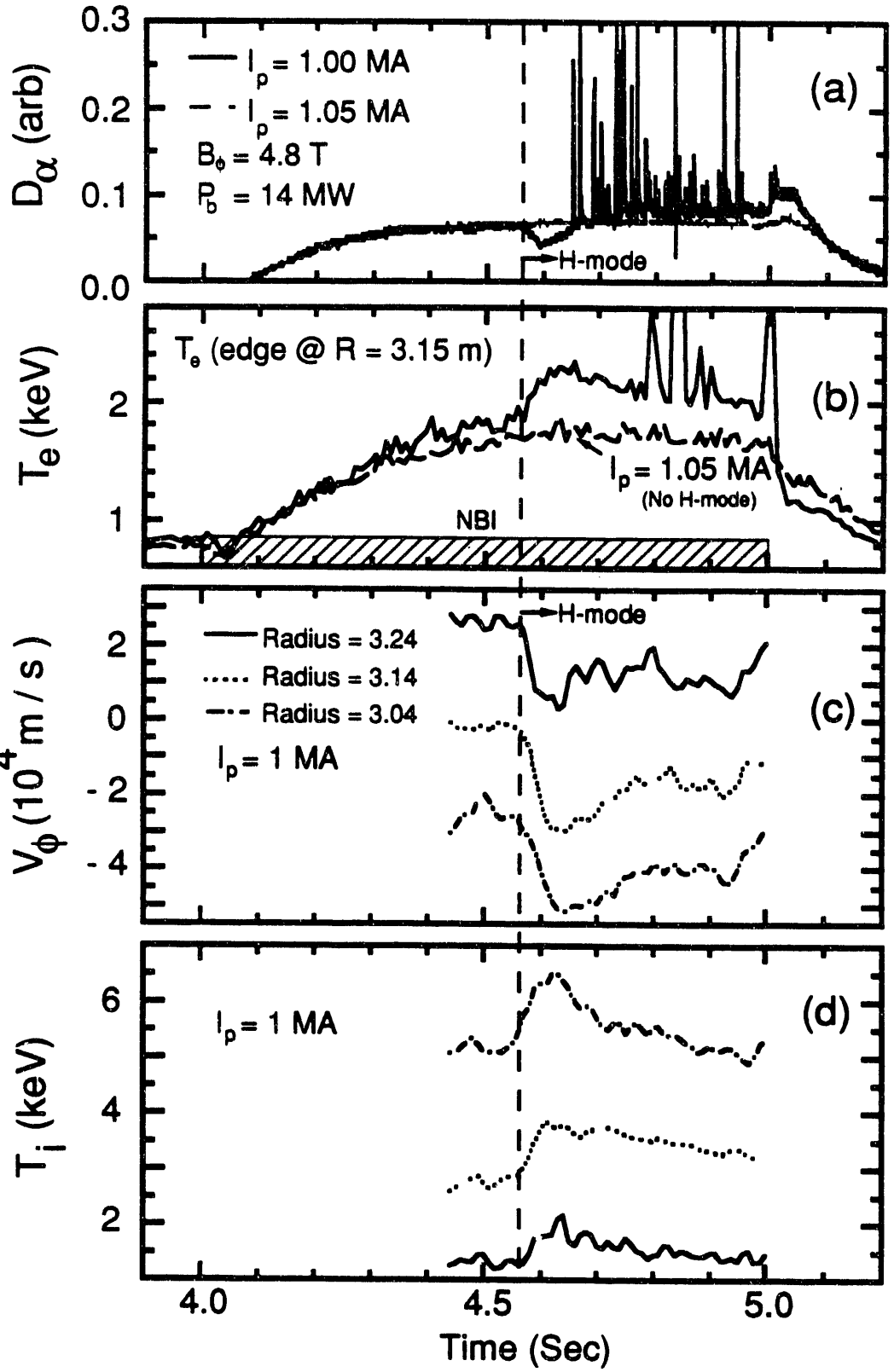
0.3
0.2
0.1
0.0
D_α (arb)
I_p = 1.00 MA
I_p = 1.05 MA
B_ϕ = 4.8 T
P_b = 14 MW
(a)
H-mode
T_e (keV)
T_e (edge @ R = 3.15 m)
(b)
I_p = 1.05 MA
(No H-mode)
NBI
V_ϕ (10^4 m / s)
Radius = 3.24
Radius = 3.14
Radius = 3.04
I_p = 1 MA
(c)
H-mode
T_i (keV)
I_p = 1 MA
(d)
4.0
4.5
5.0
Time (Sec)

Fig. 6

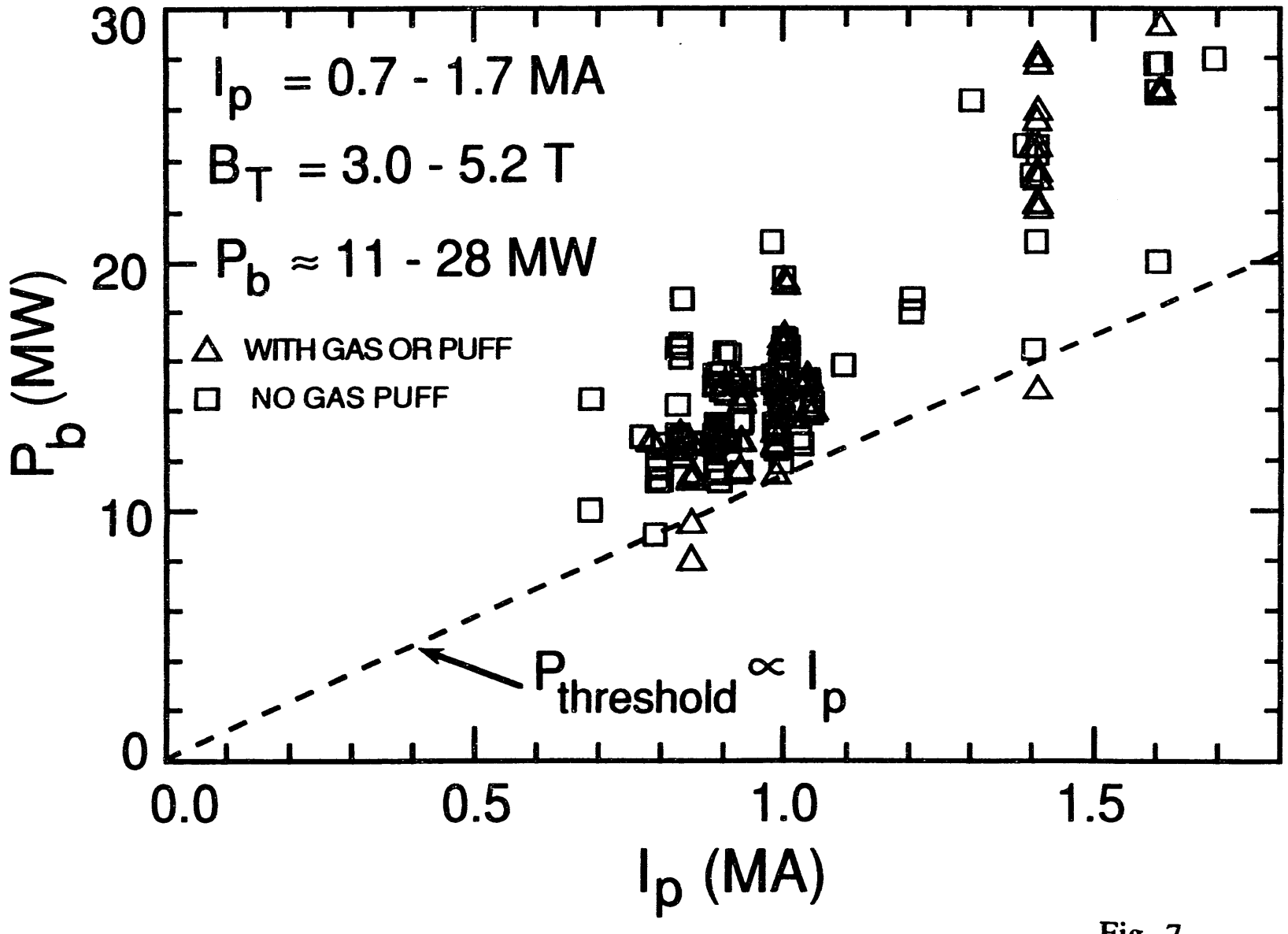
I_p = 0.7 - 1.7 MA
B_T = 3.0 - 5.2 T
$P_b \approx$ 11 - 28 MW
WITH GAS OR PUFF
NO GAS PUFF
$P_{threshold} \propto I_p$
P_b (MW)
I_p (MA)
0
10
20
30
0.0
0.5
1.0
1.5

Fig. 7

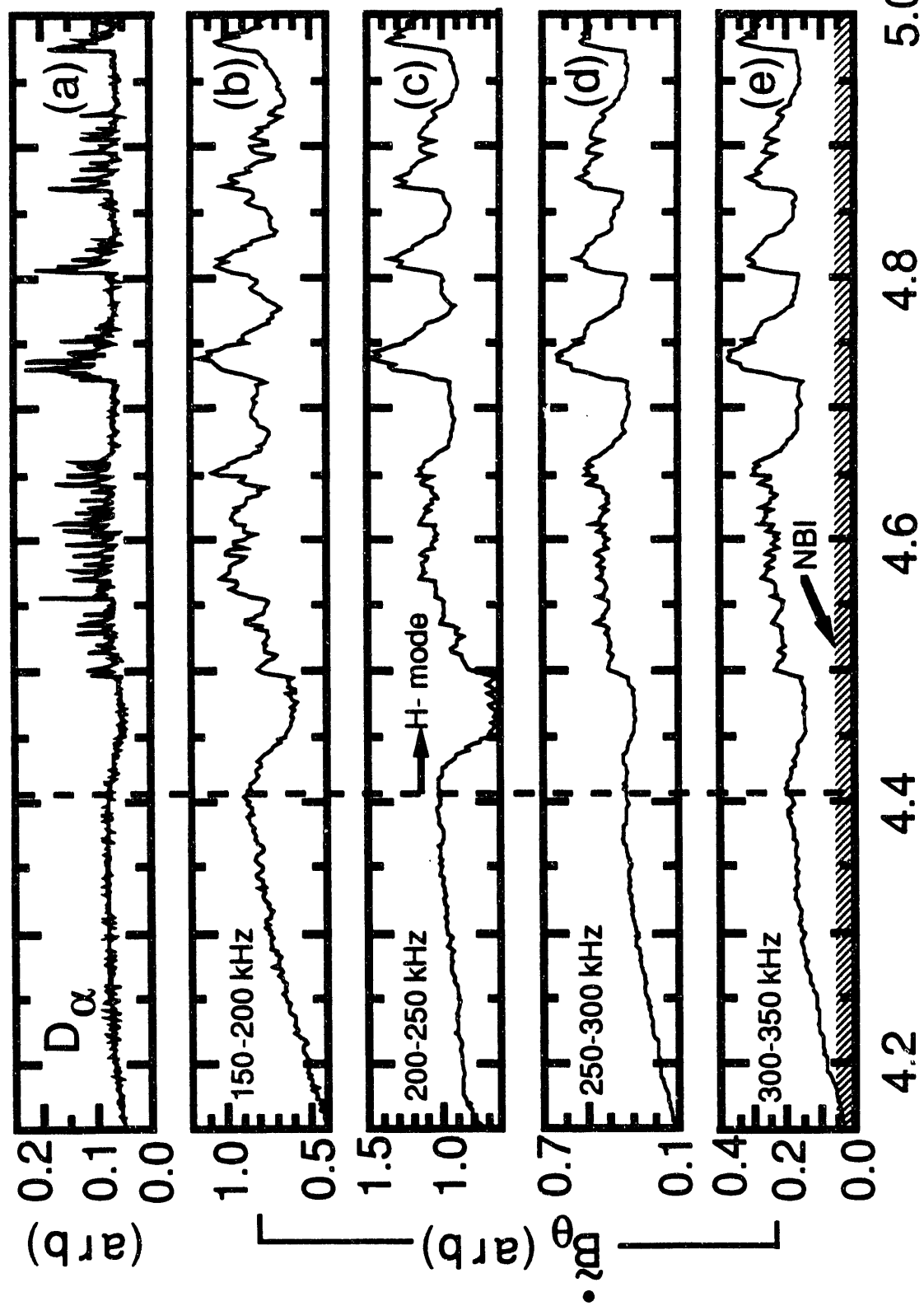
(a)
D_α
(b)
150-200 kHz
(c)
200-250 kHz
H- mode
(d)
250-300 kHz
(e)
300-350 kHz
NBI
(arb)
B_θ^2 (arb)
Time (sec)
4.2
4.4
4.6
4.8
5.0

Fig. 8

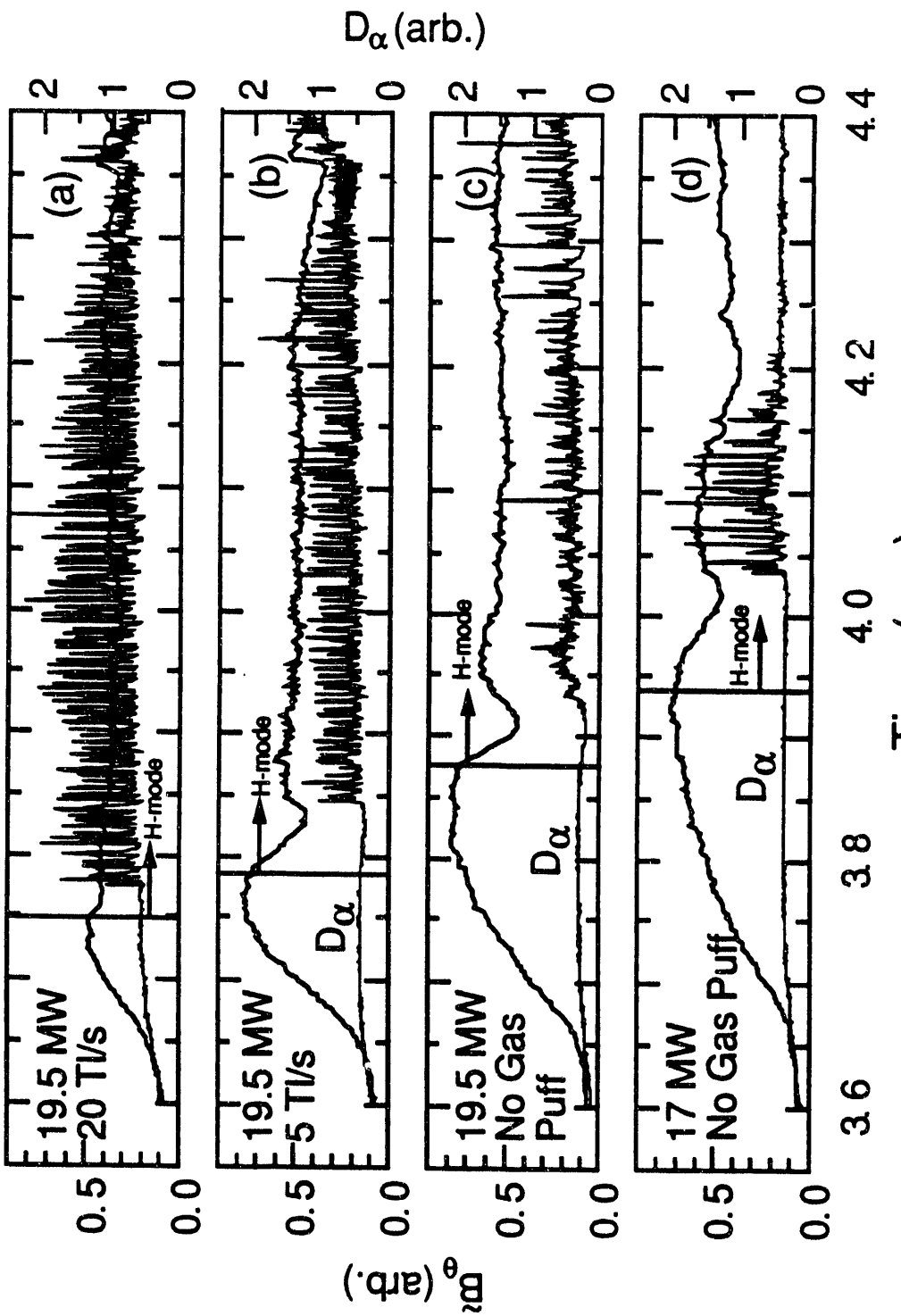
D_α (arb.)
(a)
19.5 MW
20 Tl/s
H-mode
(b)
19.5 MW
5 Tl/s
H-mode
D_α
(c)
19.5 MW
No Gas
Puff
H-mode
D_α
(d)
17 MW
No Gas Puff
H-mode
D_α
0.0
0.5
0
1
2
3.6
3.8
4.0
4.2
4.4
Time (sec)
B_θ (arb.)

Fig 9

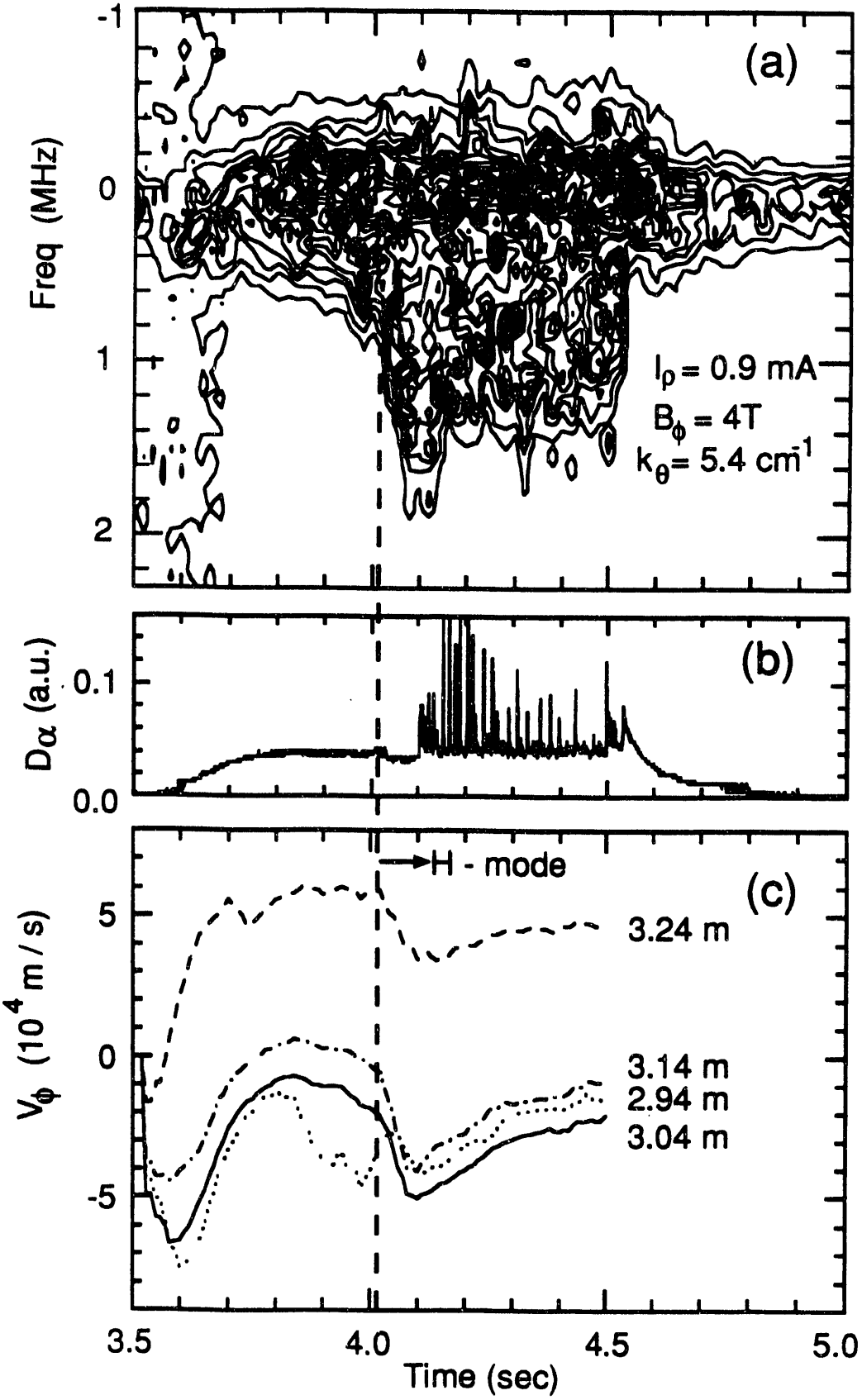
(a)
Freq (MHz)
-1
0
1
2
I_p = 0.9 mA
B_ϕ = 4T
k_θ= 5.4 cm^{-1}
(b)
Dα (a.u.)
0.1
0.0
(c)
H - mode
V_ϕ (10^4 m/s)
5
0
-5
3.24 m
3.14 m
2.94 m
3.04 m
3.5
4.0
4.5
5.0
Time (sec)

Fig. 10

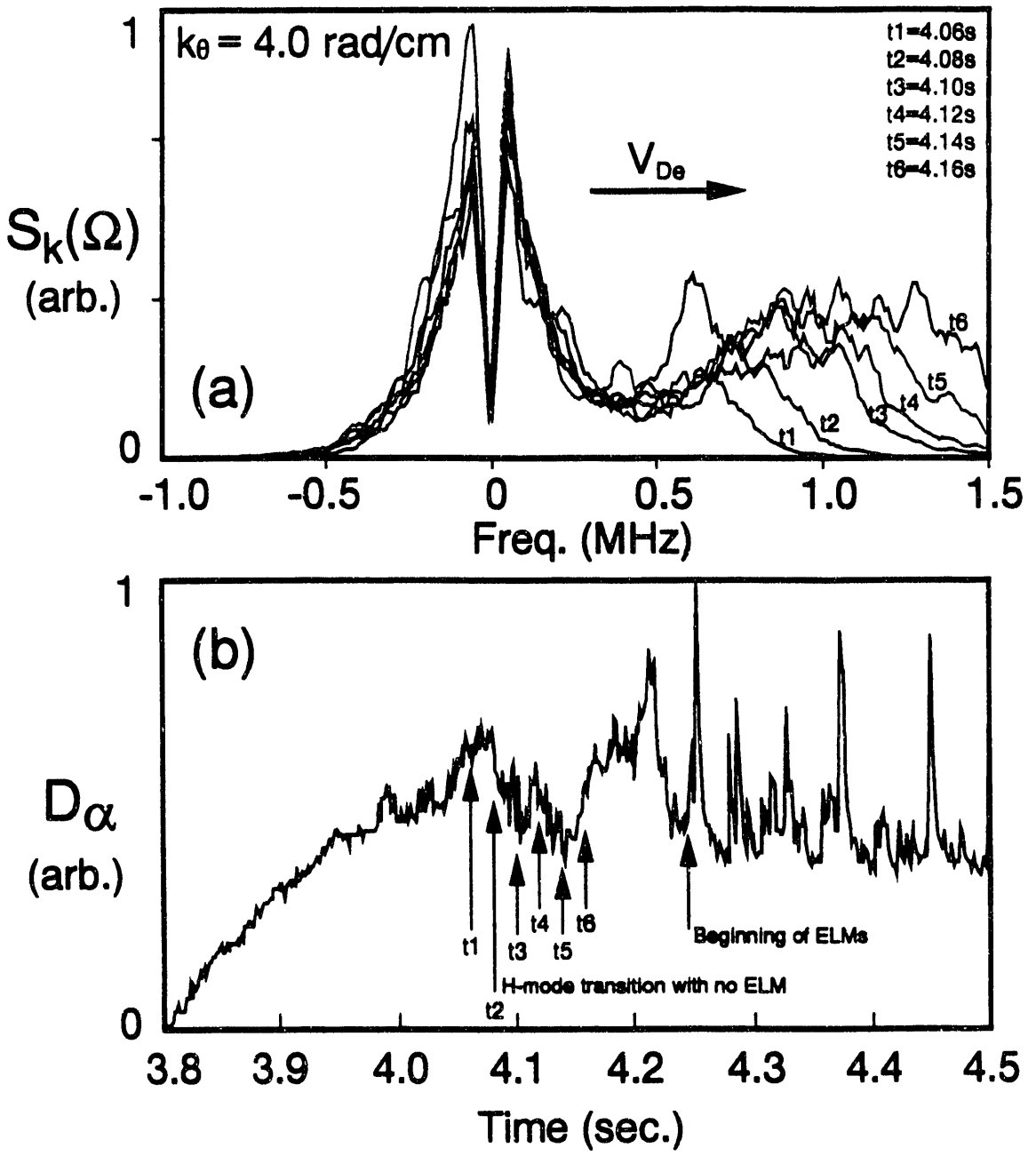
1
k_θ = 4.0 rad/cm
t1=4.06s
t2=4.08s
t3=4.10s
t4=4.12s
t5=4.14s
t6=4.16s
V_{De}
$S_k(\Omega)$
(arb.)
(a)
t6
t5
t4
t3
t2
t1
0
-1.0
-0.5
0
0.5
1.0
1.5
Freq. (MHz)
1
(b)
$D\alpha$
(arb.)
t1
t3
t4
t5
t6
Beginning of ELMs
H-mode transition with no ELM
t2
0
3.8
3.9
4.0
4.1
4.2
4.3
4.4
4.5
Time (sec.)

Fig. 11

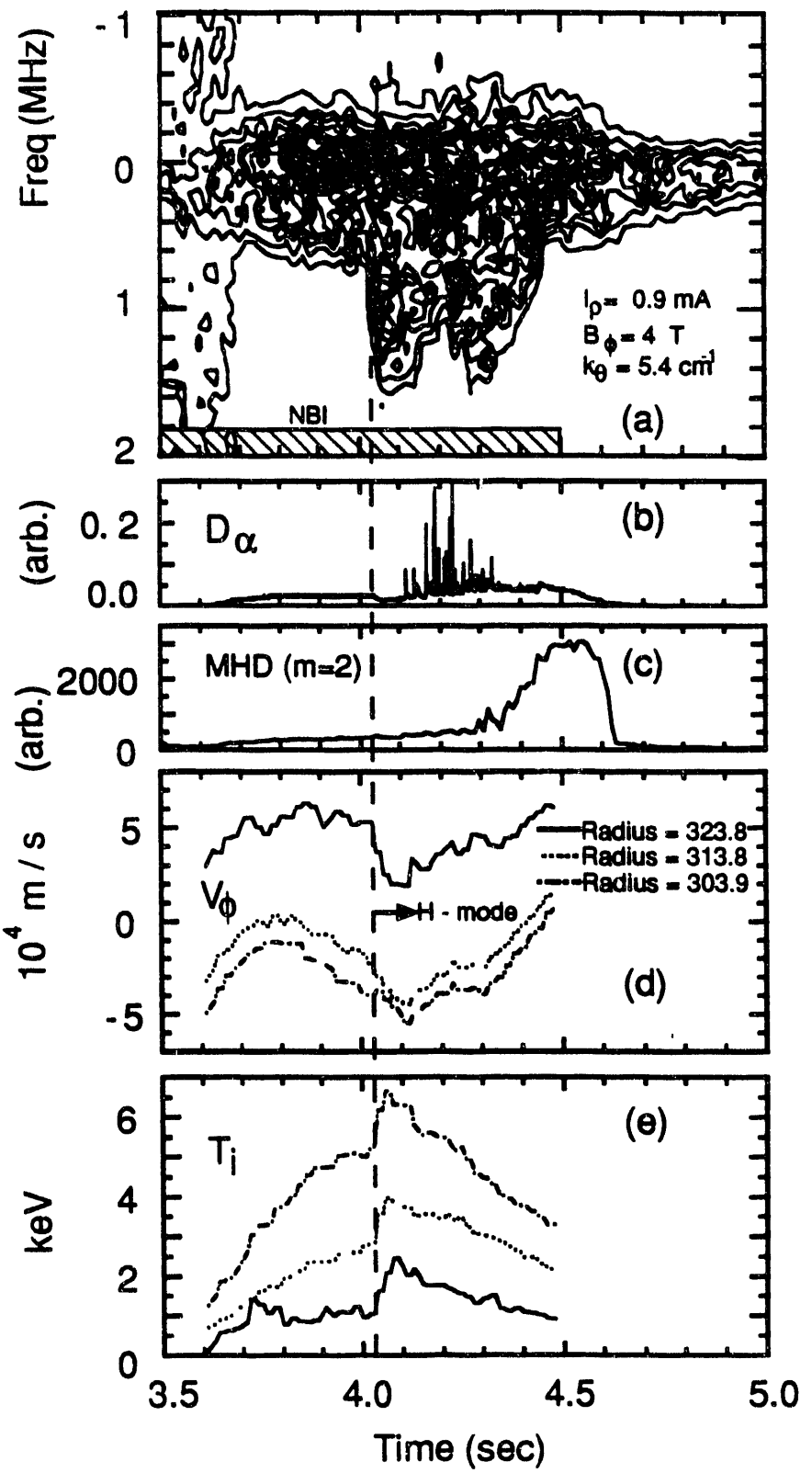
Freq (MHz)
-1
0
1
2
I_p= 0.9 mA
B_ϕ= 4 T
k_θ = 5.4 cm^{-1}
NBI
(a)
(arb.)
0.2
0.0
D_α
(b)
2000
0
MHD (m=2)
(c)
10^4 m / s
5
0
-5
V_ϕ
H - mode
Radius = 323.8
Radius = 313.8
Radius = 303.9
(d)
keV
6
4
2
0
T_i
(e)
3.5
4.0
4.5
5.0
Time (sec)

Fig. 12

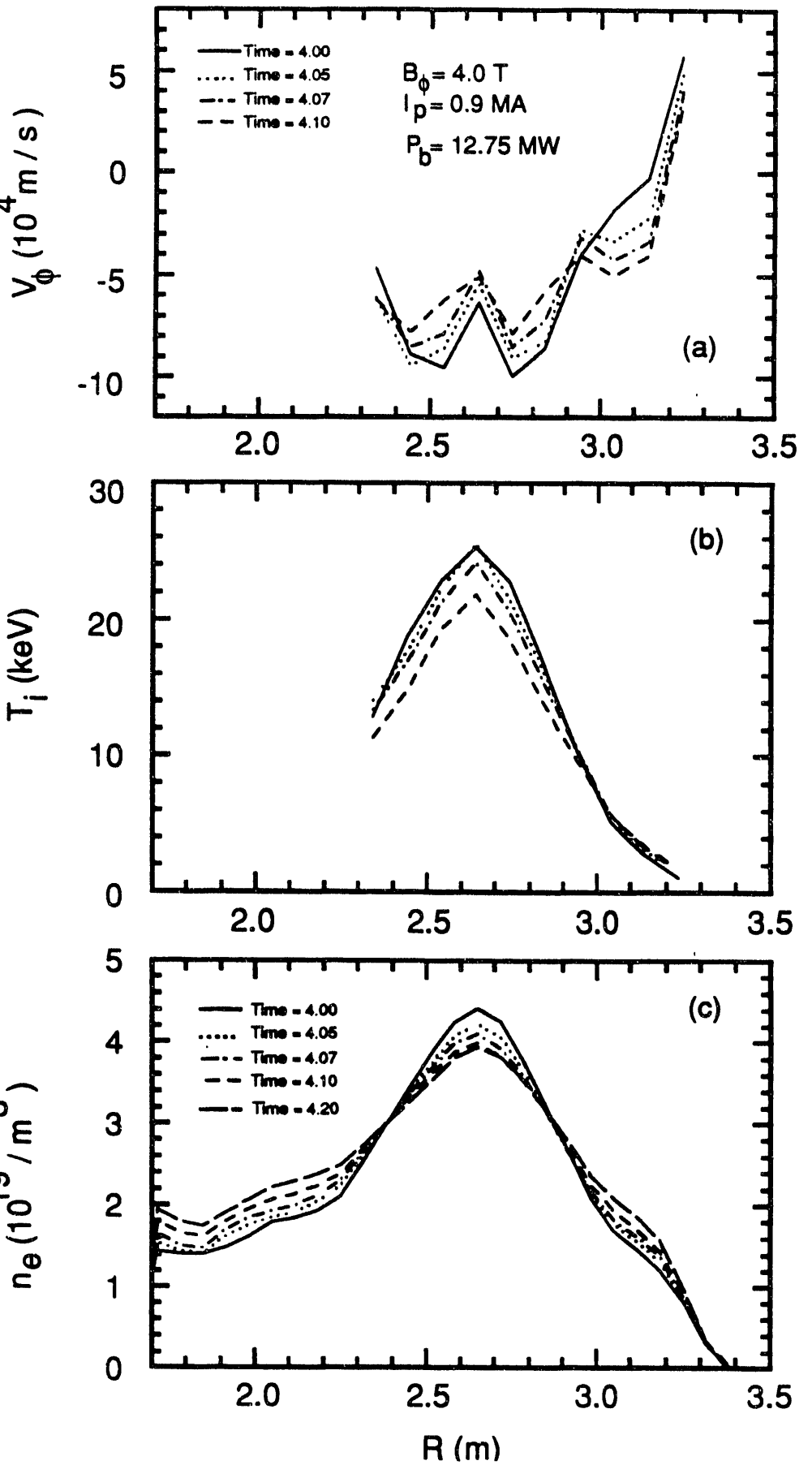
Time = 4.00
Time = 4.05
Time = 4.07
Time = 4.10
Time = 4.20
B_ϕ = 4.0 T
I_p = 0.9 MA
P_b = 12.75 MW
(a)
(b)
(c)
V_ϕ (10^4 m / s)
T_i (keV)
n_e (10^{19} / m^3)
R (m)

Fig. 13

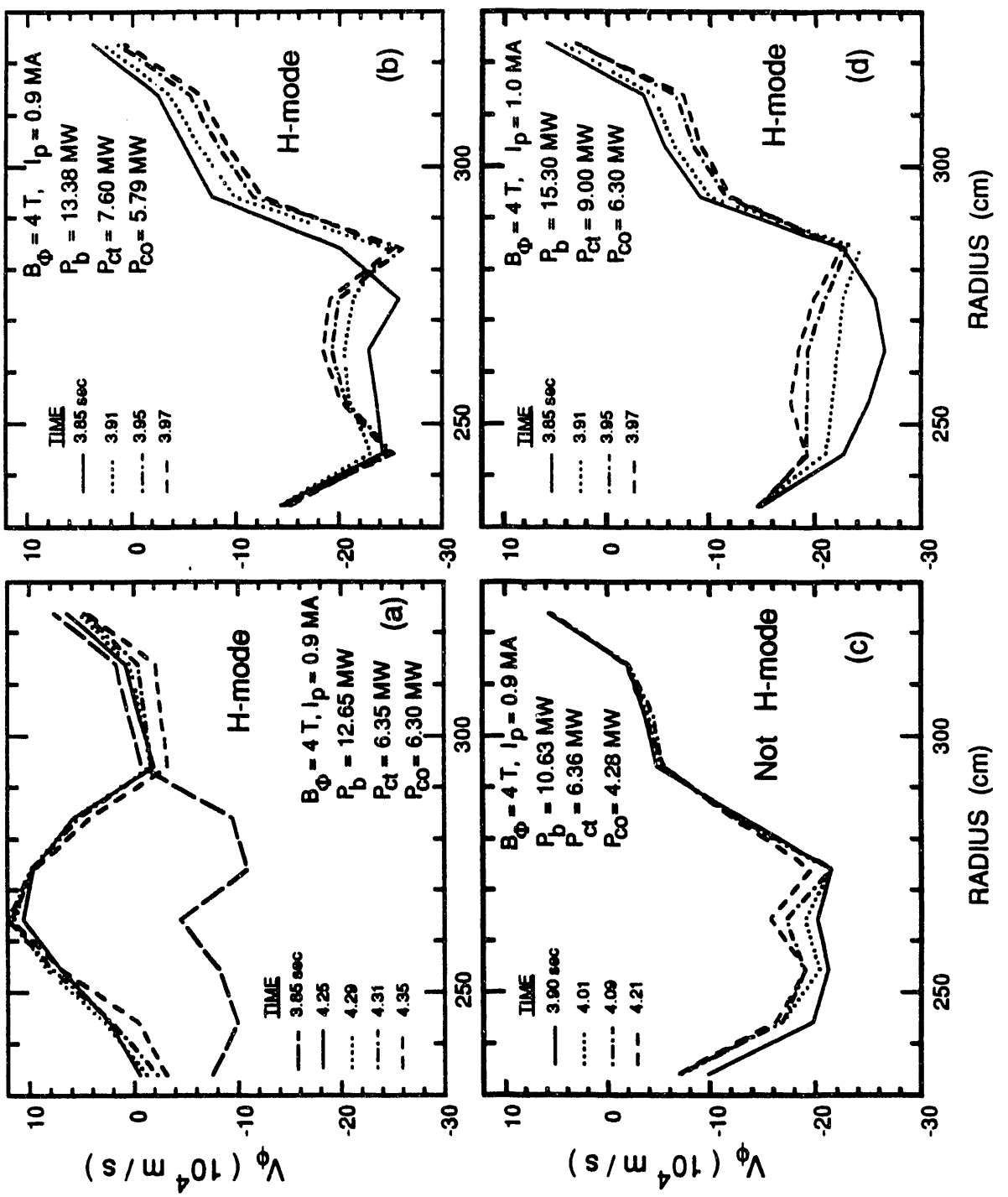
H-mode
(a)
B_Φ = 4 T, I_p = 0.9 MA
P_b = 12.65 MW
P_{ct} = 6.35 MW
P_{co} = 6.30 MW
TIME
3.85 sec
4.25
4.29
4.31
4.35
H-mode
(b)
B_Φ = 4 T, I_p = 0.9 MA
P_b = 13.38 MW
P_{ct} = 7.60 MW
P_{co} = 5.79 MW
TIME
3.85 sec
3.91
3.95
3.97
Not H-mode
(c)
B_Φ = 4 T, I_p = 0.9 MA
P_b = 10.63 MW
P_{ct} = 6.36 MW
P_{co} = 4.28 MW
TIME
3.90 sec
4.01
4.09
4.21
H-mode
(d)
B_Φ = 4 T, I_p = 1.0 MA
P_b = 15.30 MW
P_{ct} = 9.00 MW
P_{co} = 6.30 MW
TIME
3.85 sec
3.91
3.95
3.97
V_Φ (10^4 m/s)
RADIUS (cm)
10
0
-10
-20
-30
250
300

Fig. 14

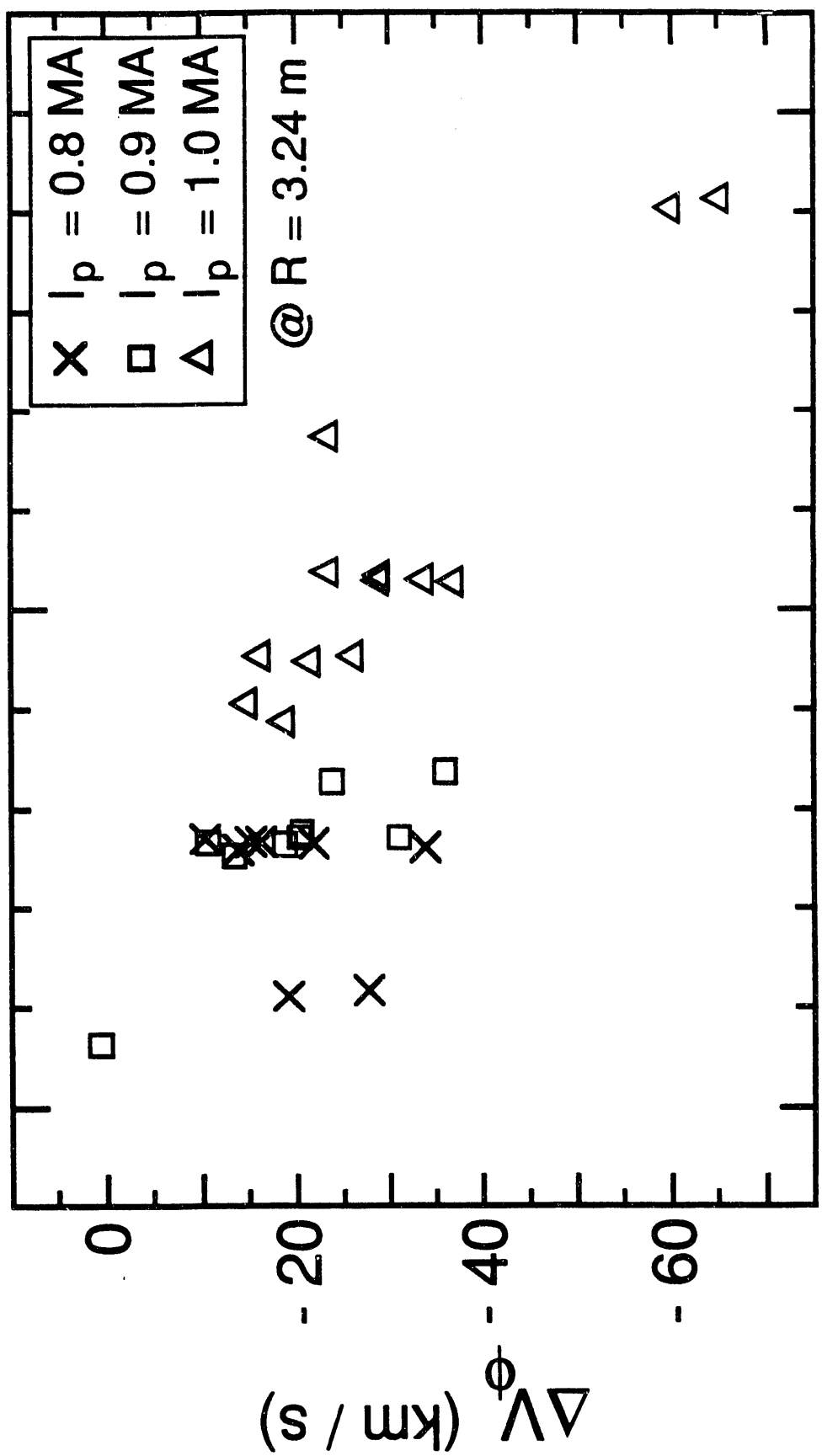
I_p = 0.8 MA
I_p = 0.9 MA
I_p = 1.0 MA
@ R = 3.24 m
0
-20
-40
-60
10
15
20
P_b (MW)
ΔV_ϕ (km / s)

Fig. 15

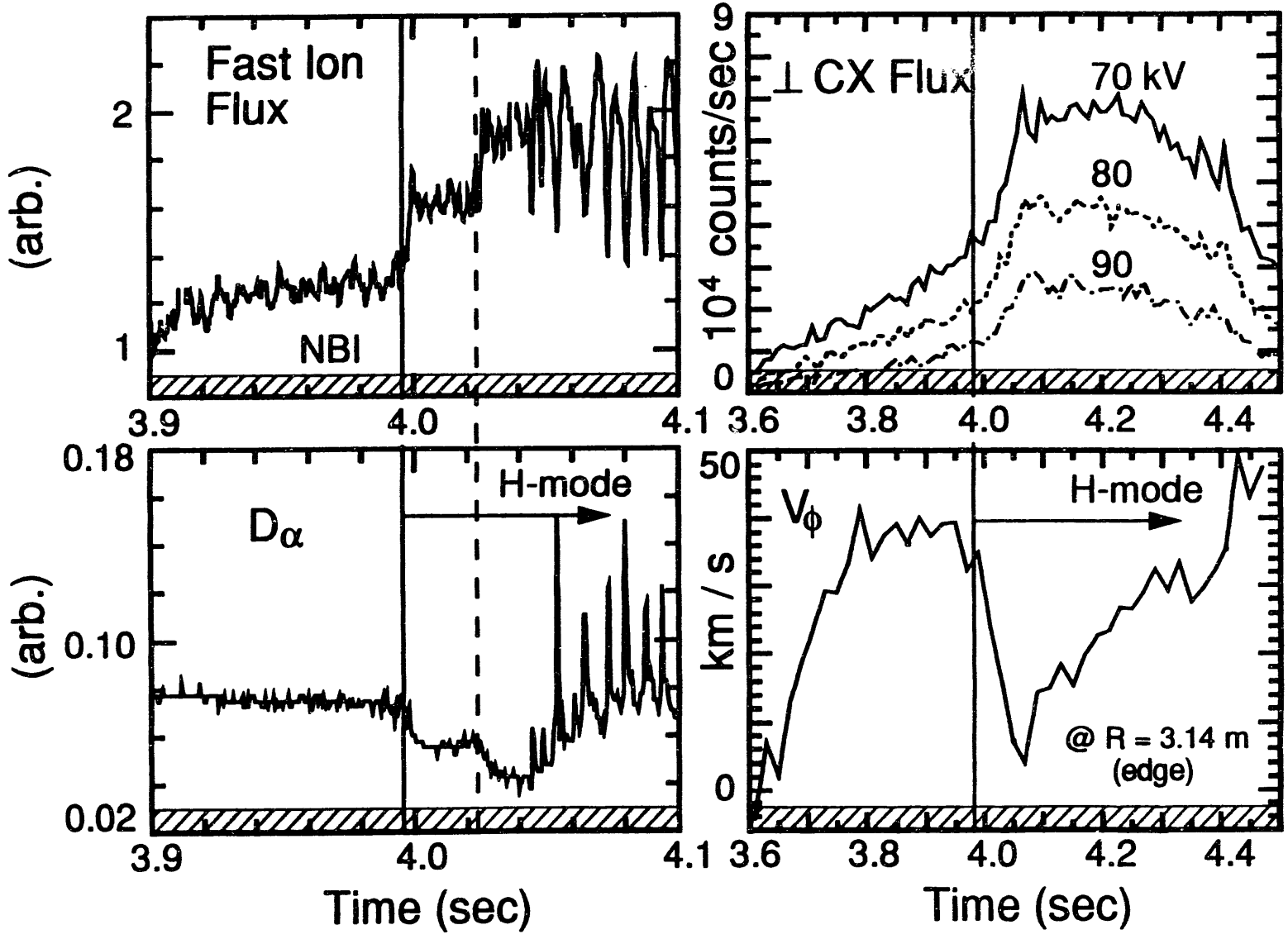
Fast Ion
Flux
(arb.)
2
1
NBI
3.9
4.0
4.1
⊥ CX Flux
70 kV
80
90
10^4 counts/sec
9
0
3.6
3.8
4.0
4.2
4.4
D_α
H-mode
(arb.)
0.18
0.10
0.02
V_ϕ
H-mode
km / s
50
0
@ R = 3.14 m
(edge)
Time (sec)
Time (sec)

Fig. 16

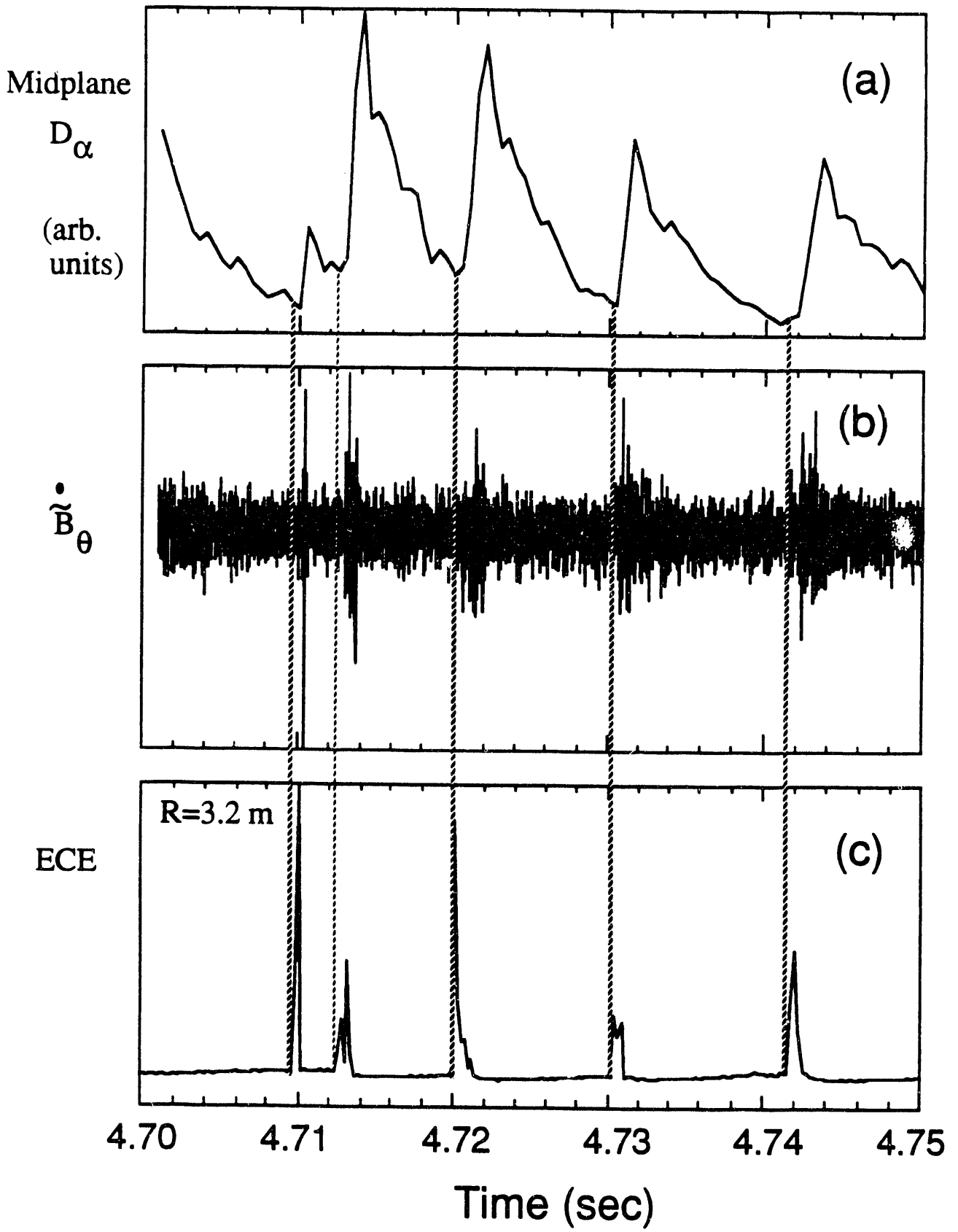
Midplane
D_α
(arb.
units)
(a)
(b)
$\tilde{B}_\theta$
R=3.2 m
ECE
(c)
4.70
4.71
4.72
4.73
4.74
4.75
Time (sec)

Fig. 17

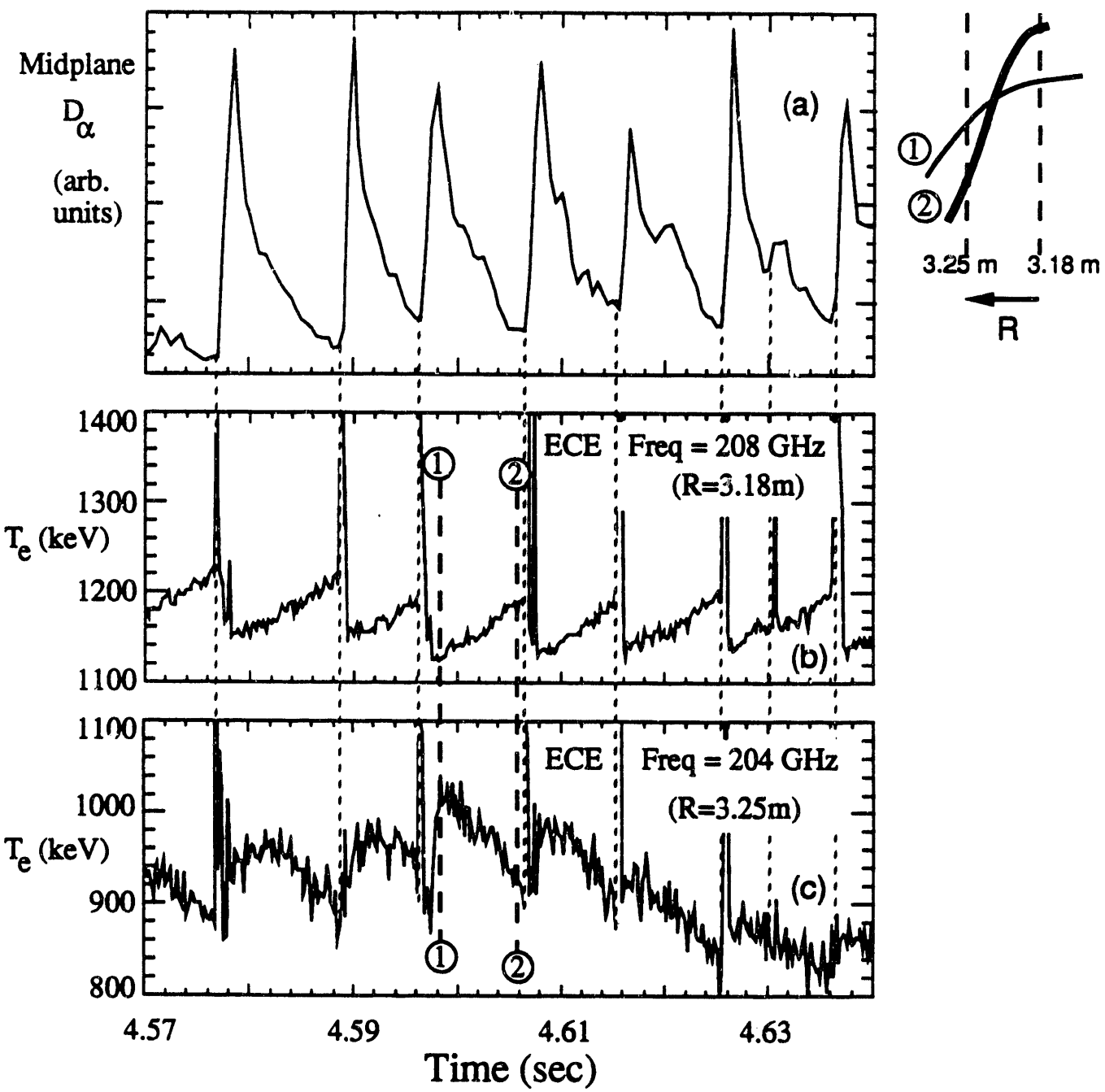
Midplane
D_α
(arb.
units)
(a)
1400
1300
T_e (keV)
1200
1100
ECE
Freq = 208 GHz
(R=3.18m)
(b)
1100
1000
T_e (keV)
900
800
ECE
Freq = 204 GHz
(R=3.25m)
(c)
4.57
4.59
4.61
4.63
Time (sec)
①
②
3.25 m
3.18 m
R

Fig. 18

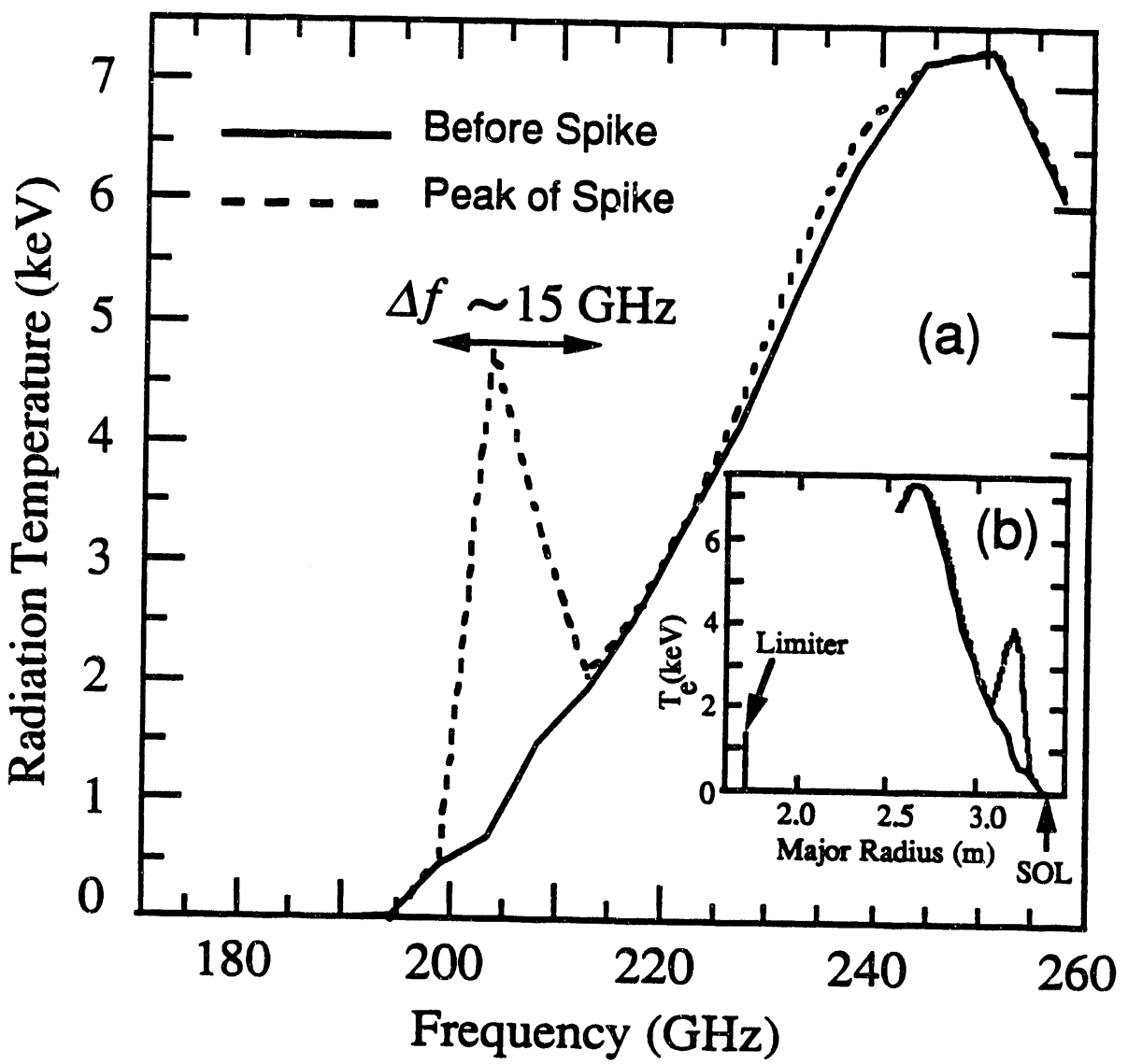
Radiation Temperature (keV)
Frequency (GHz)
Before Spike
Peak of Spike
Δf ~15 GHz
(a)
(b)
Limiter
SOL
Major Radius (m)
T_e(keV)

Fig. 19

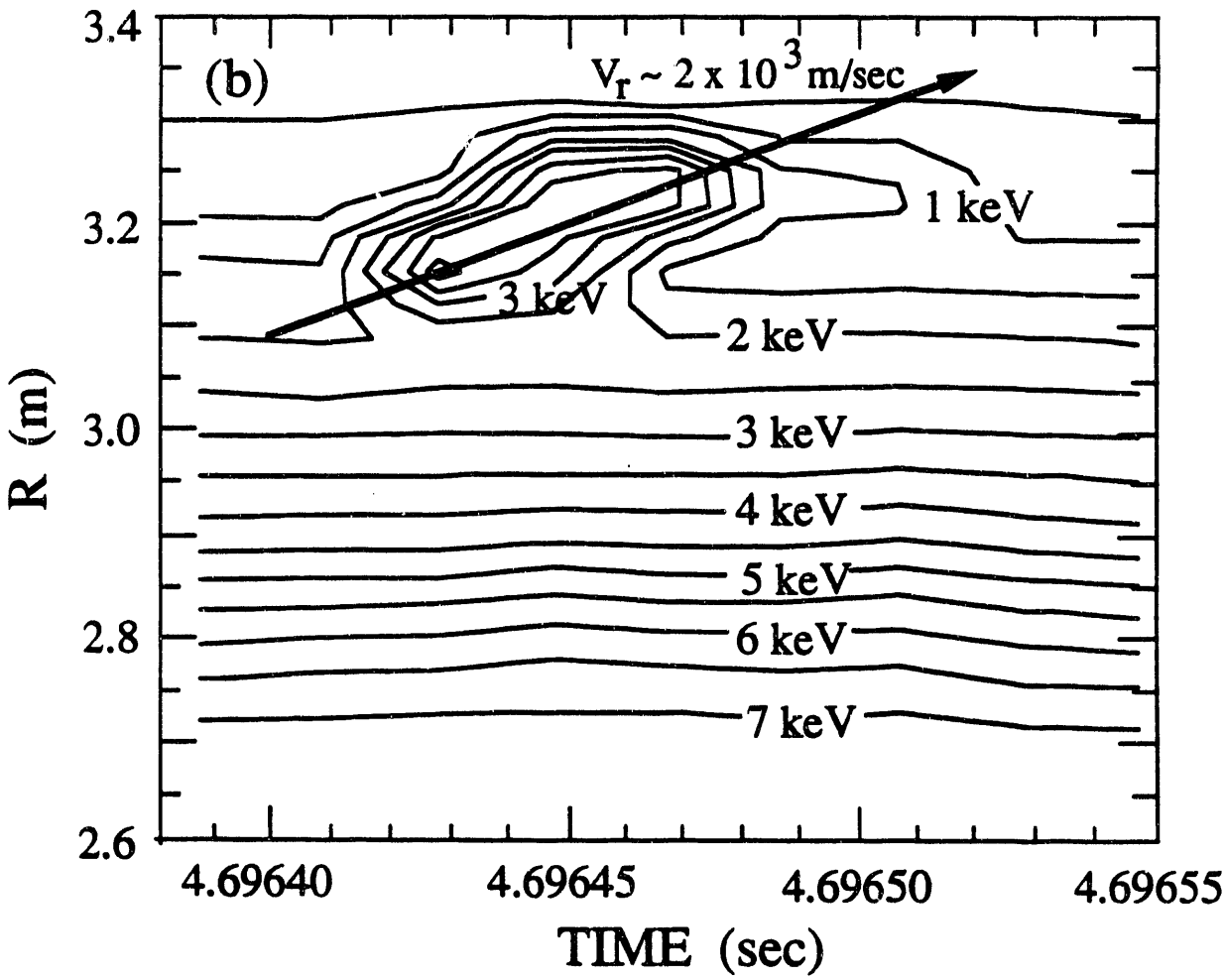
(b)
$V_r \sim 2 \times 10^3$ m/sec
1 keV
3 keV
2 keV
3 keV
4 keV
5 keV
6 keV
7 keV
3.4
3.2
3.0
2.8
2.6
R (m)
4.69640
4.69645
4.69650
4.69655
TIME (sec)

Fig. 20

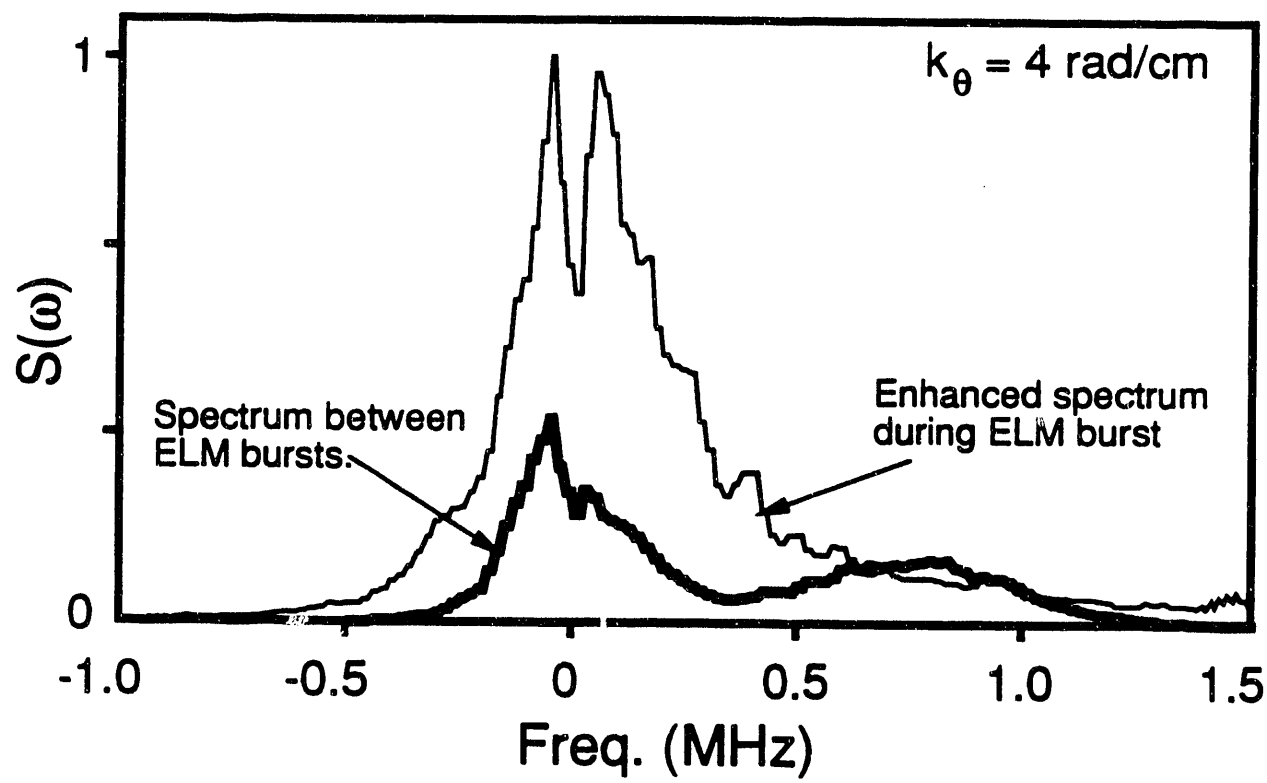
1
0
S(ω)
k_θ = 4 rad/cm
Spectrum between
ELM bursts.
Enhanced spectrum
during ELM burst
-1.0
-0.5
0
0.5
1.0
1.5
Freq. (MHz)

Fig. 21

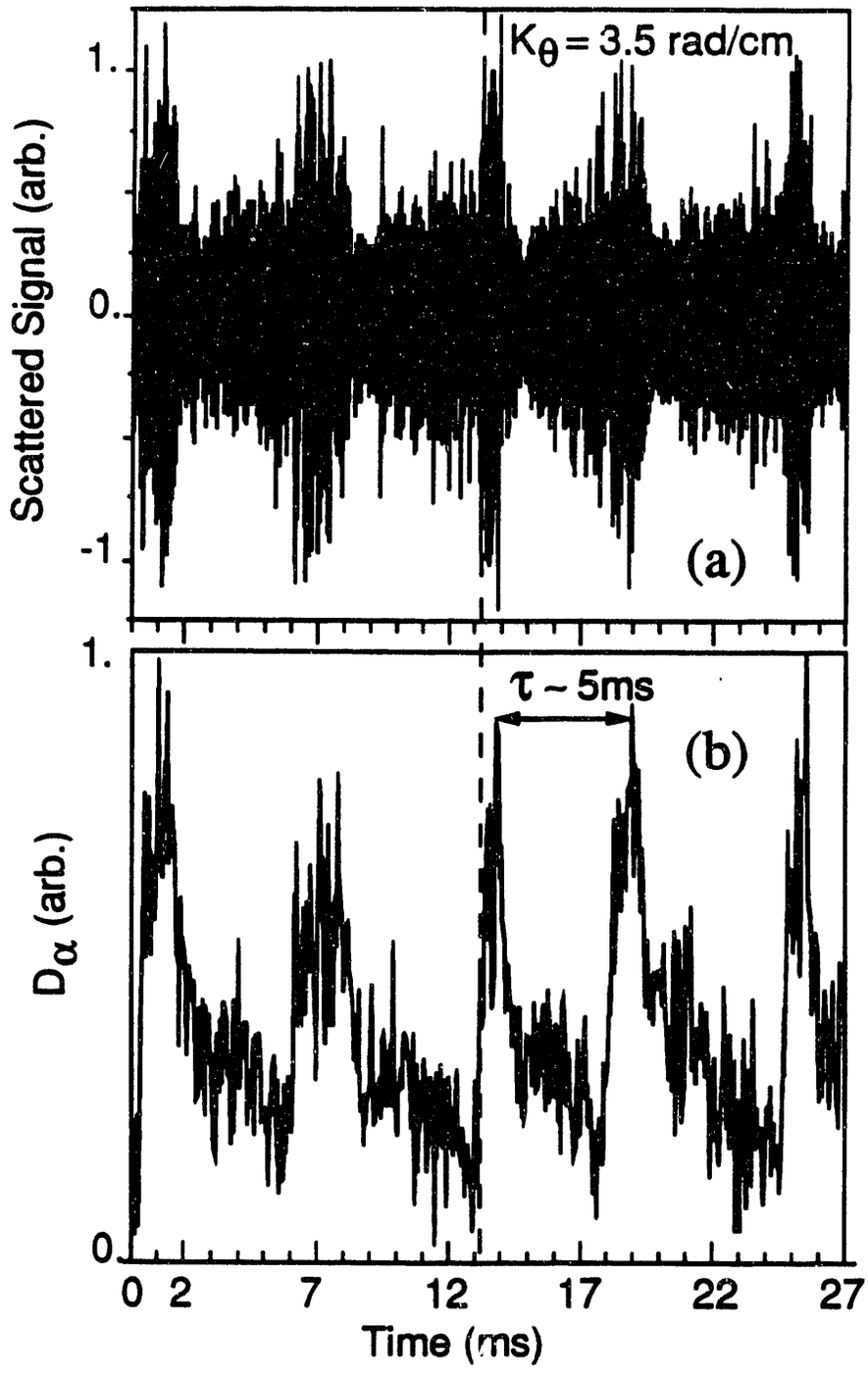
$K_\theta = 3.5$ rad/cm
Scattered Signal (arb.)
1.
0.
-1
(a)
1.
$\tau \sim 5$ms
(b)
D_α (arb.)
0
0 2 7 12 17 22 27
Time (ms)

Fig. 22

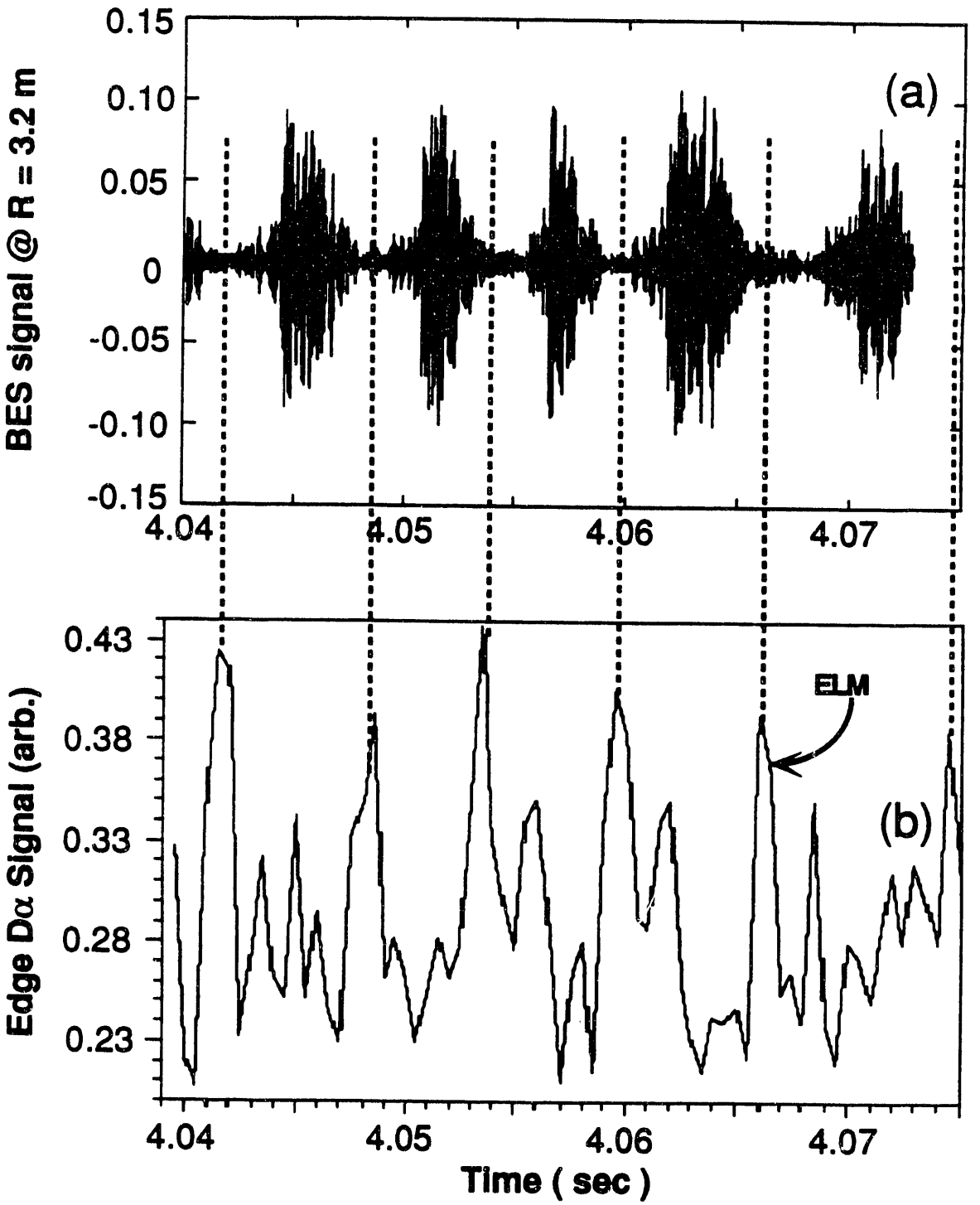
0.15
0.10
0.05
0
-0.05
-0.10
-0.15
BES signal @ R = 3.2 m
(a)
4.04
4.05
4.06
4.07
0.43
0.38
0.33
0.28
0.23
Edge Dα Signal (arb.)
ELM
(b)
4.04
4.05
4.06
4.07
Time (sec)

Fig. 23

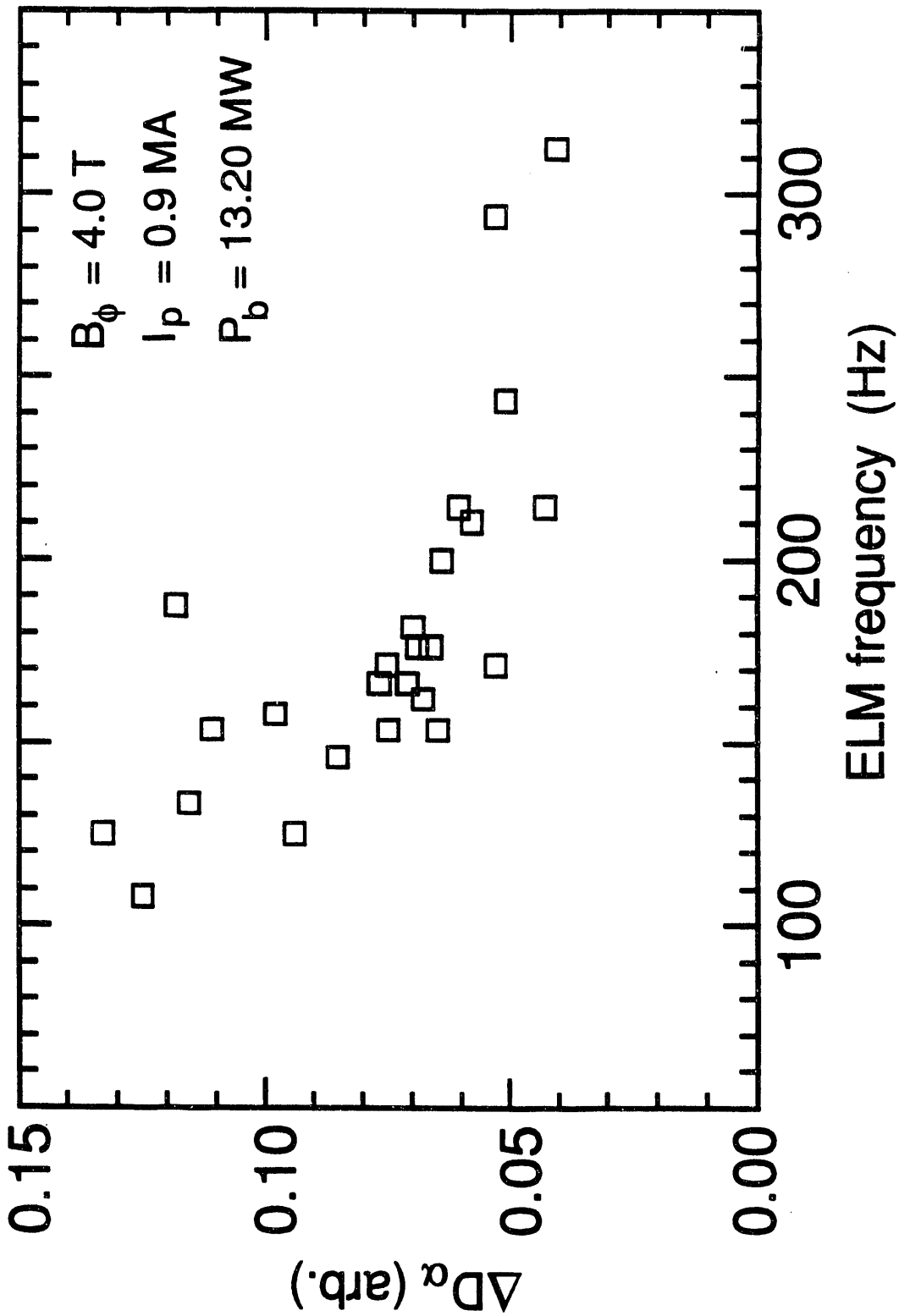
B_ϕ = 4.0 T
I_p = 0.9 MA
P_b = 13.20 MW
ΔD_α (arb.)
0.15
0.10
0.05
0.00
100
200
300
ELM frequency (Hz)

Fig. 24

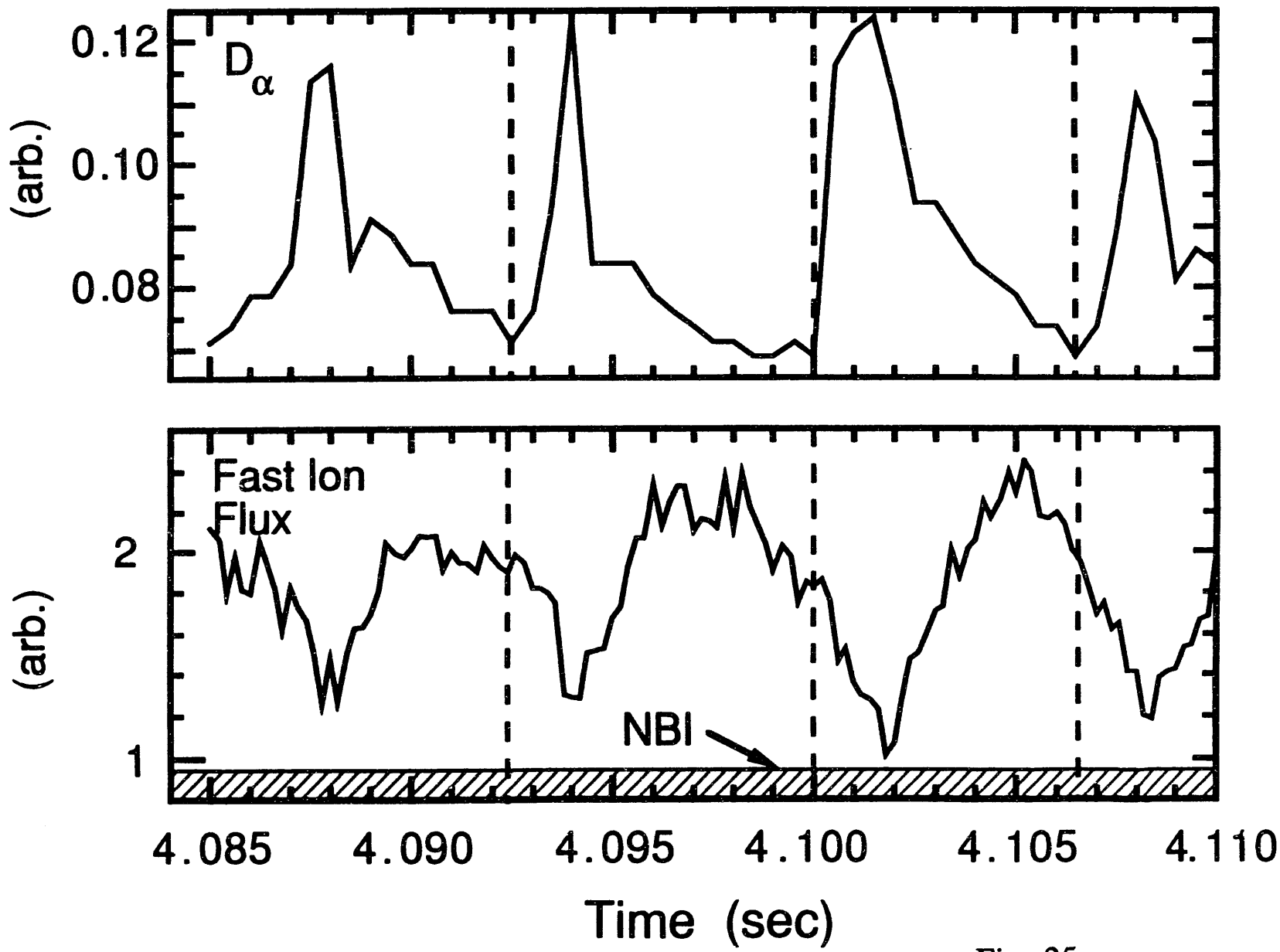
0.12
0.10
0.08
(arb.)
D_α
Fast Ion
Flux
2
1
(arb.)
NBI
4.085
4.090
4.095
4.100
4.105
4.110
Time (sec)

Fig. 25

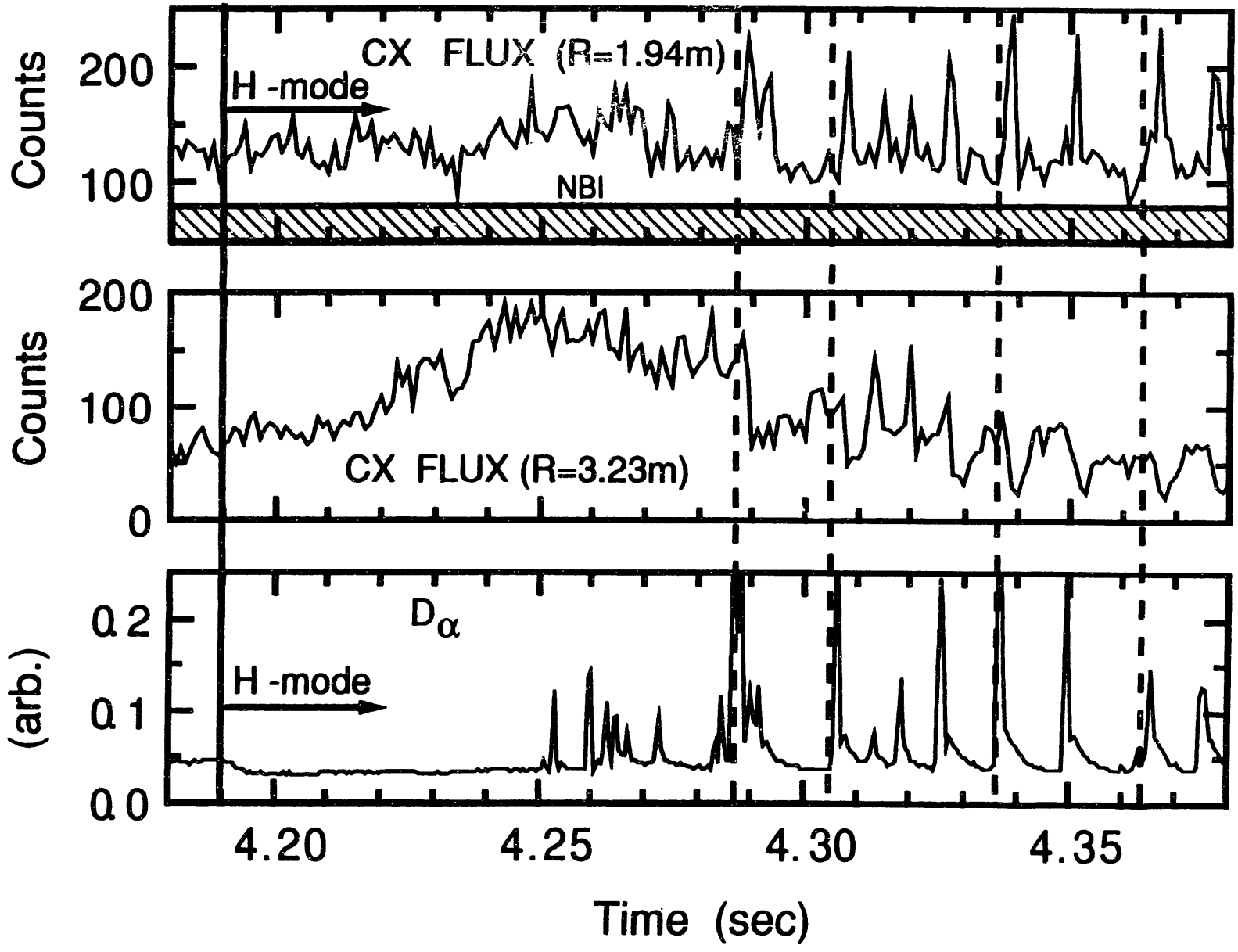
CX FLUX (R=1.94m)
H -mode
NBI
Counts
200
100
CX FLUX (R=3.23m)
Counts
200
100
0
D_α
H -mode
(arb.)
0.2
0.1
0.0
4.20
4.25
4.30
4.35
Time (sec)

Fig. 26

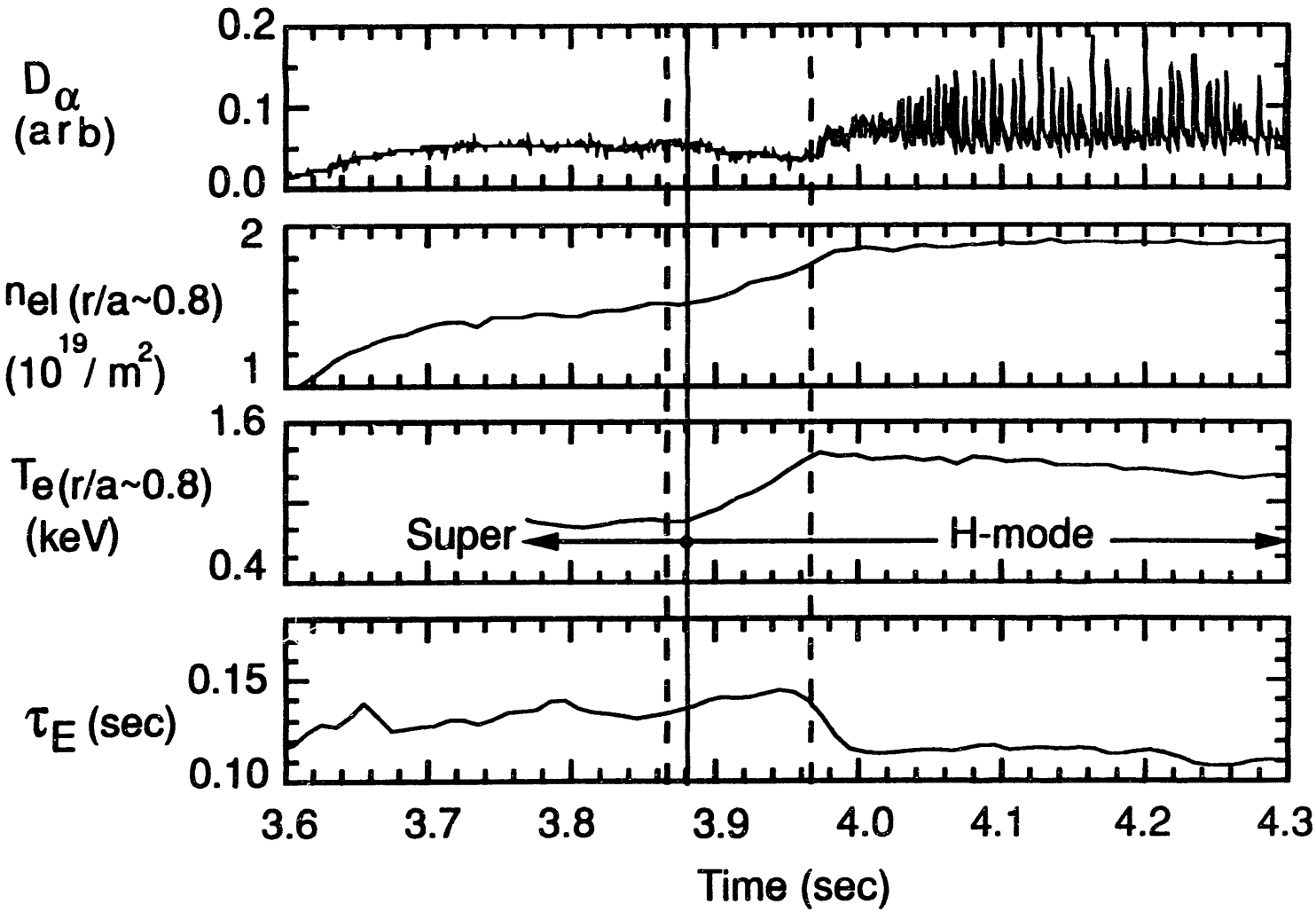
0.2
0.1
0.0
D_α (arb)
2
1
n_{el} (r/a~0.8)
(10^{19} / m^2)
1.6
0.4
T_e(r/a~0.8)
(keV)
Super
H-mode
0.15
0.10
τ_E (sec)
3.6
3.7
3.8
3.9
4.0
4.1
4.2
4.3
Time (sec)

Fig. 27

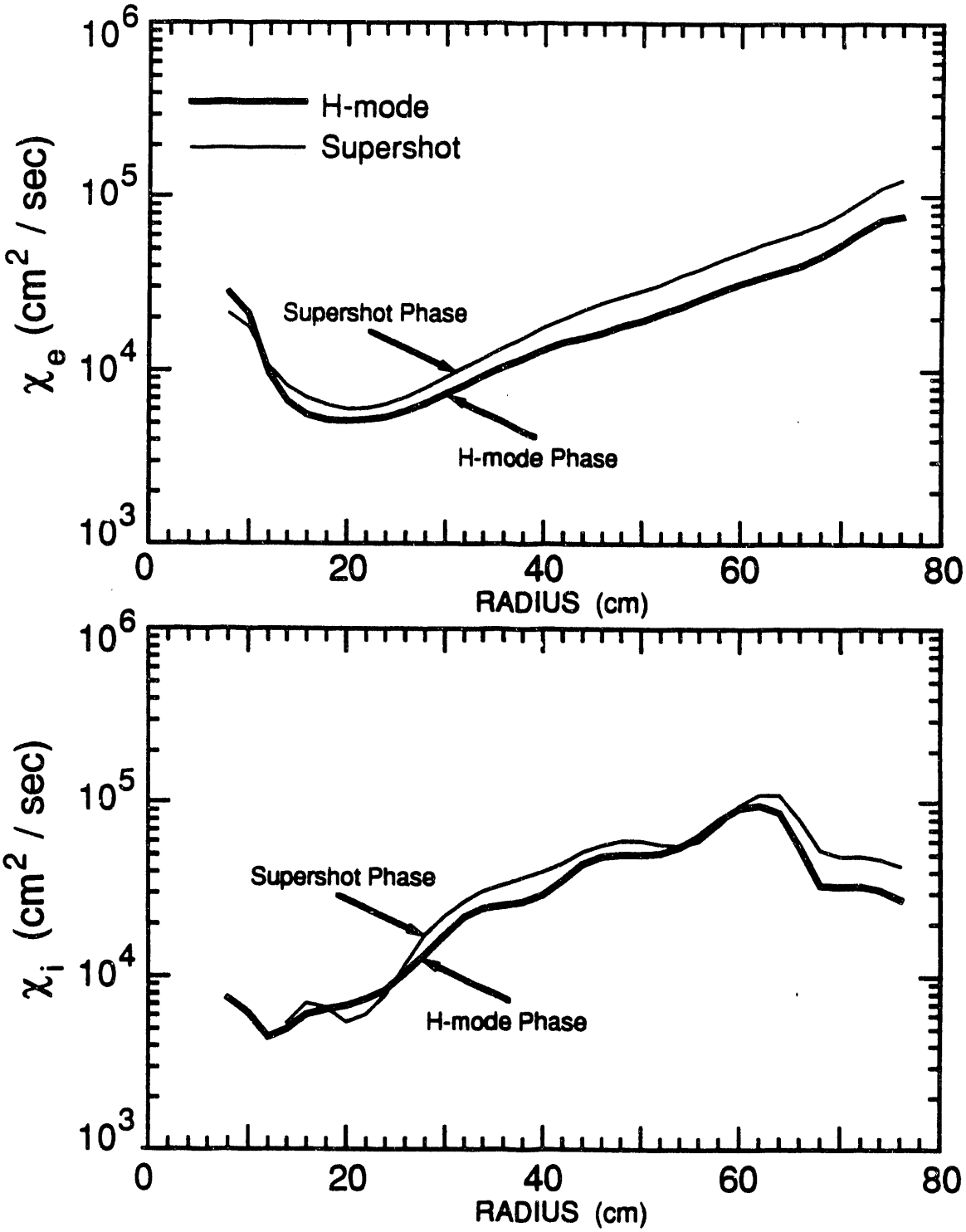
H-mode
Supershot
Supershot Phase
H-mode Phase
χ_e (cm^2 / sec)
10^6
10^5
10^4
10^3
0
20
40
60
80
RADIUS (cm)
Supershot Phase
H-mode Phase
χ_i (cm^2 / sec)
10^6
10^5
10^4
10^3
0
20
40
60
80
RADIUS (cm)

Fig. 28

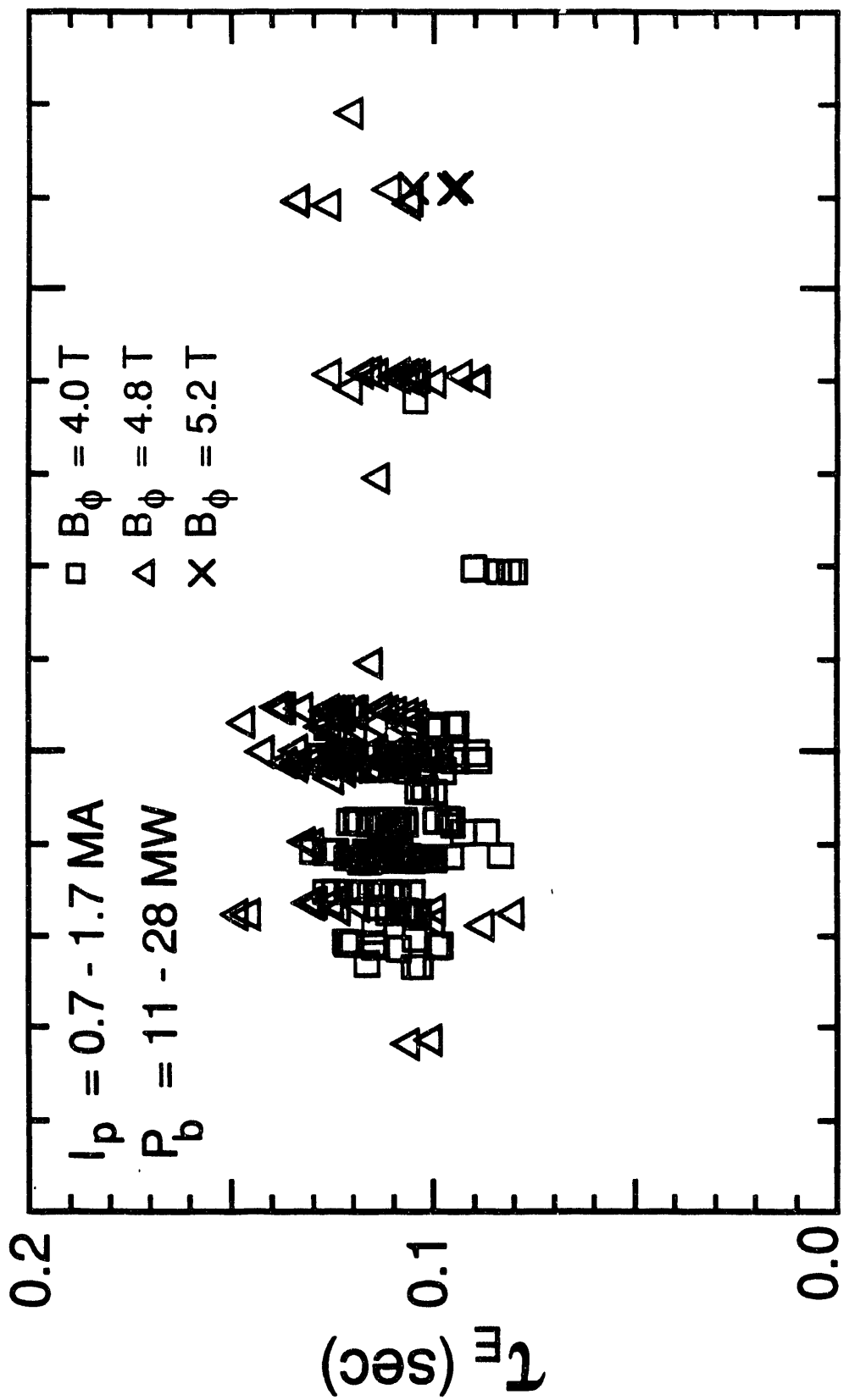
τ_E (sec)
0.2
0.1
0.0
0.5
1.0
1.5
I_p (MA)
I_p = 0.7 - 1.7 MA
P_b = 11 - 28 MW
□ B_ϕ = 4.0 T
△ B_ϕ = 4.8 T
× B_ϕ = 5.2 T

Fig. 29

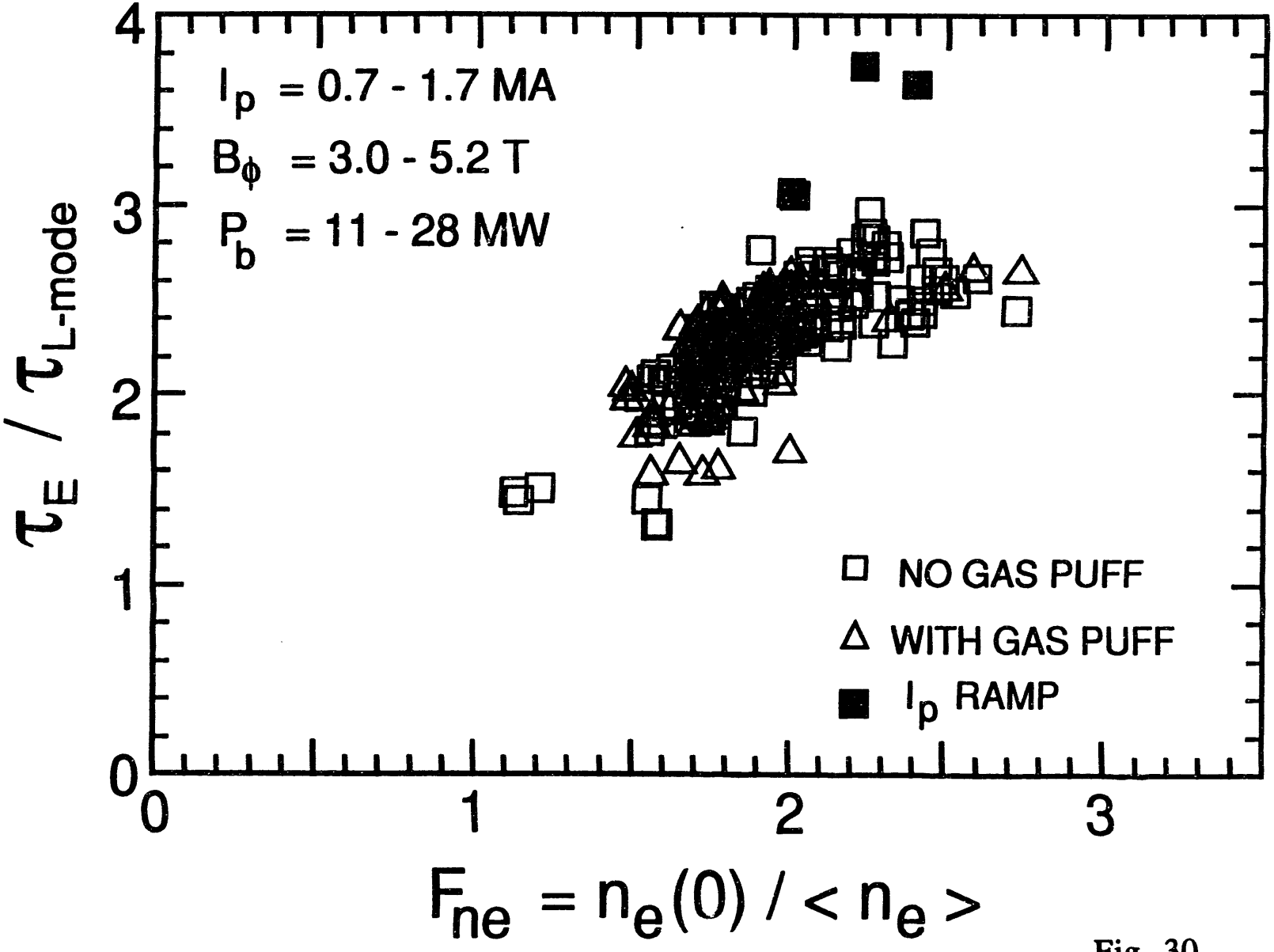
I_p = 0.7 - 1.7 MA
B_ϕ = 3.0 - 5.2 T
P_b = 11 - 28 MW
NO GAS PUFF
WITH GAS PUFF
I_p RAMP
τ_E / $\tau_{L\text{-}mode}$
$F_{ne} = n_e(0) / < n_e >$
0
1
2
3
4

Fig. 30

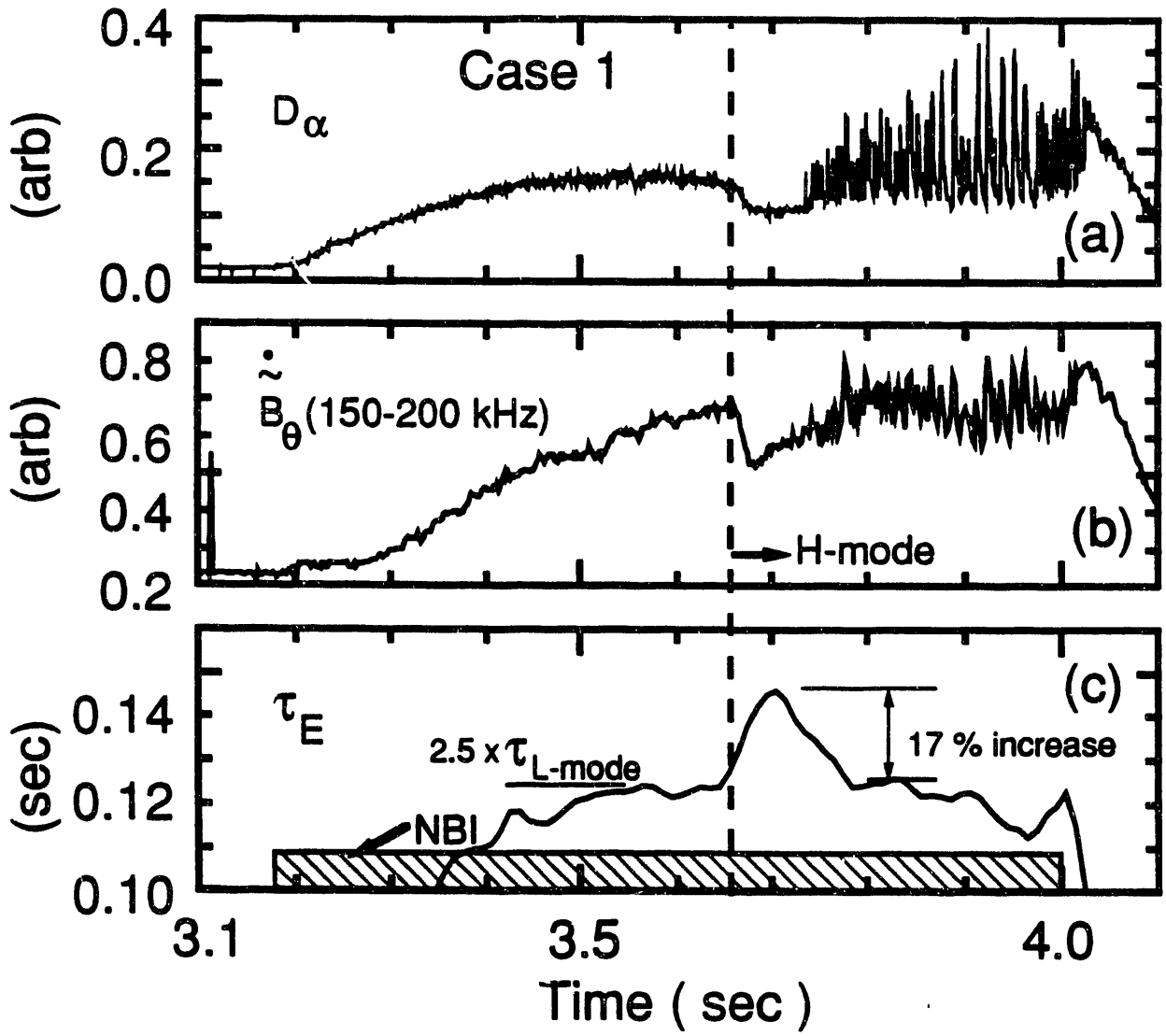
Case 1
D_α
(a)
(arb)
0.4
0.2
0.0
$\tilde{B}_\theta$(150-200 kHz)
(b)
H-mode
(arb)
0.8
0.6
0.4
0.2
τ_E
(c)
2.5 x $\tau_{L\text{-mode}}$
17 % increase
NBI
(sec)
0.14
0.12
0.10
3.1
3.5
4.0
Time (sec)

Fig. 31

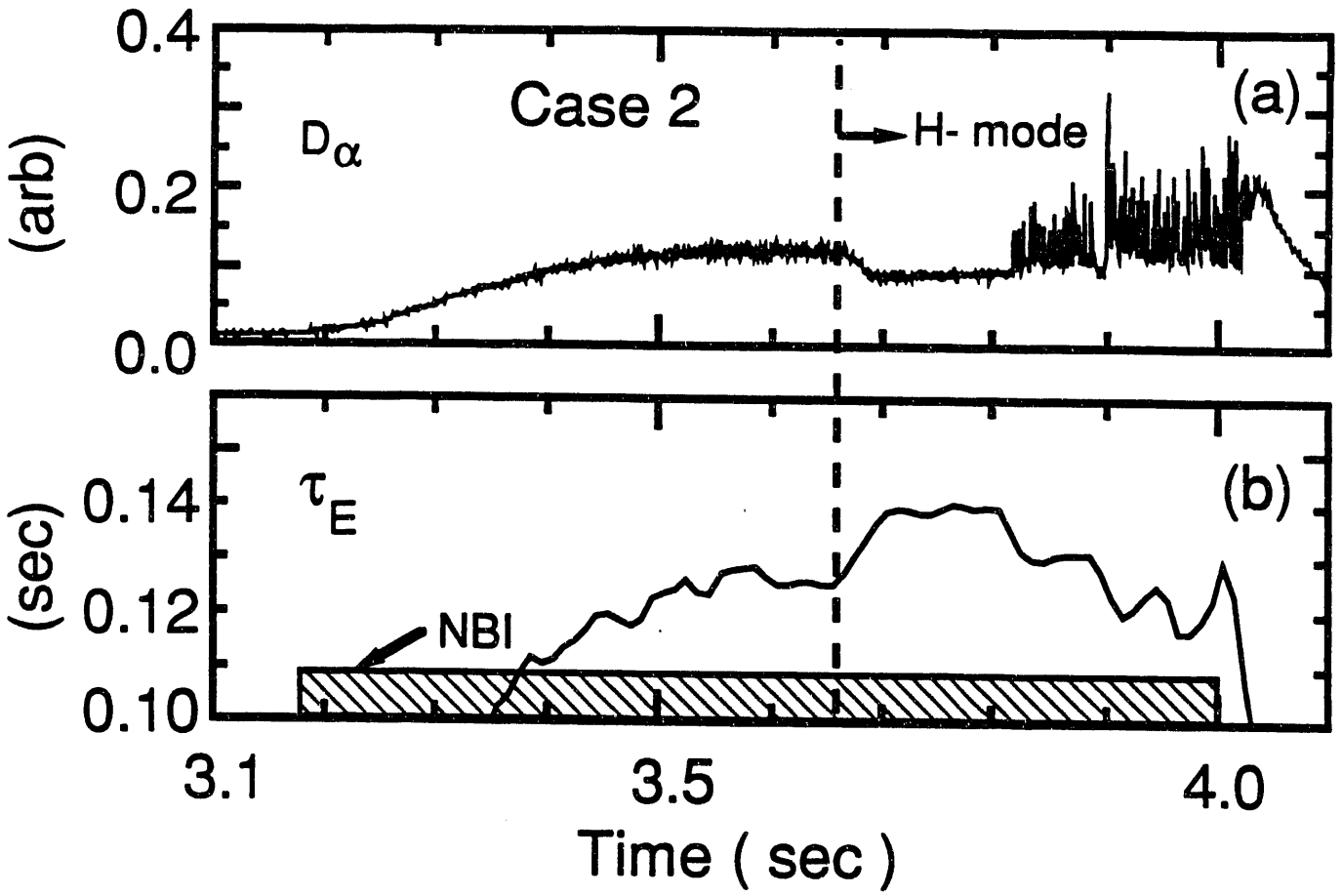
0.4
0.2
0.0
(arb)
Case 2
D_α
H- mode
(a)
0.14
0.12
0.10
(sec)
τ_E
NBI
(b)
3.1
3.5
4.0
Time (sec)

Fig. 32

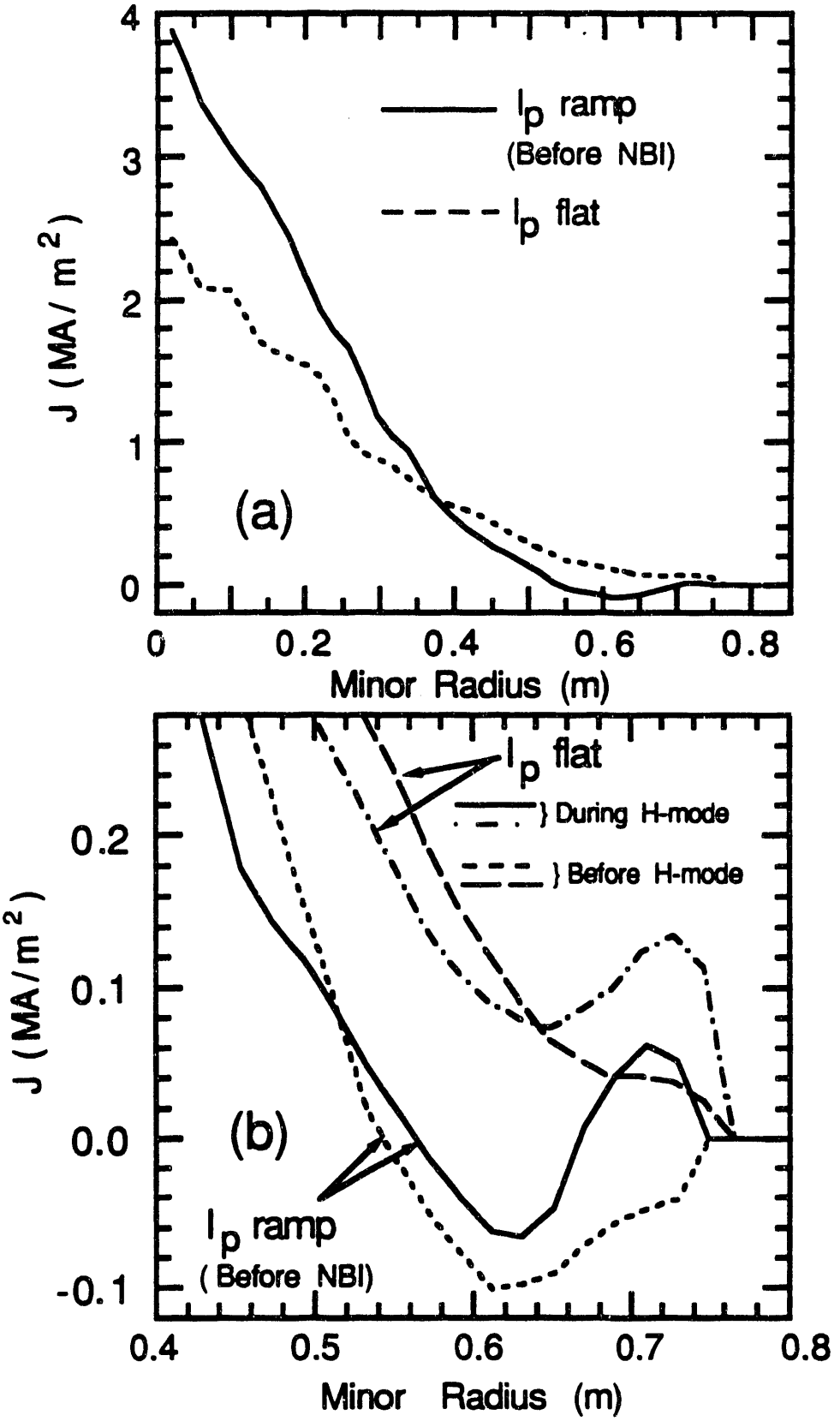
4
3
2
1
0
J (MA/ m²)
I_p ramp
(Before NBI)
I_p flat
(a)
0
0.2
0.4
0.6
0.8
Minor Radius (m)
I_p flat
} During H-mode
} Before H-mode
0.2
0.1
0.0
-0.1
J (MA/m²)
(b)
I_p ramp
(Before NBI)
0.4
0.5
0.6
0.7
0.8
Minor Radius (m)

Fig. 33

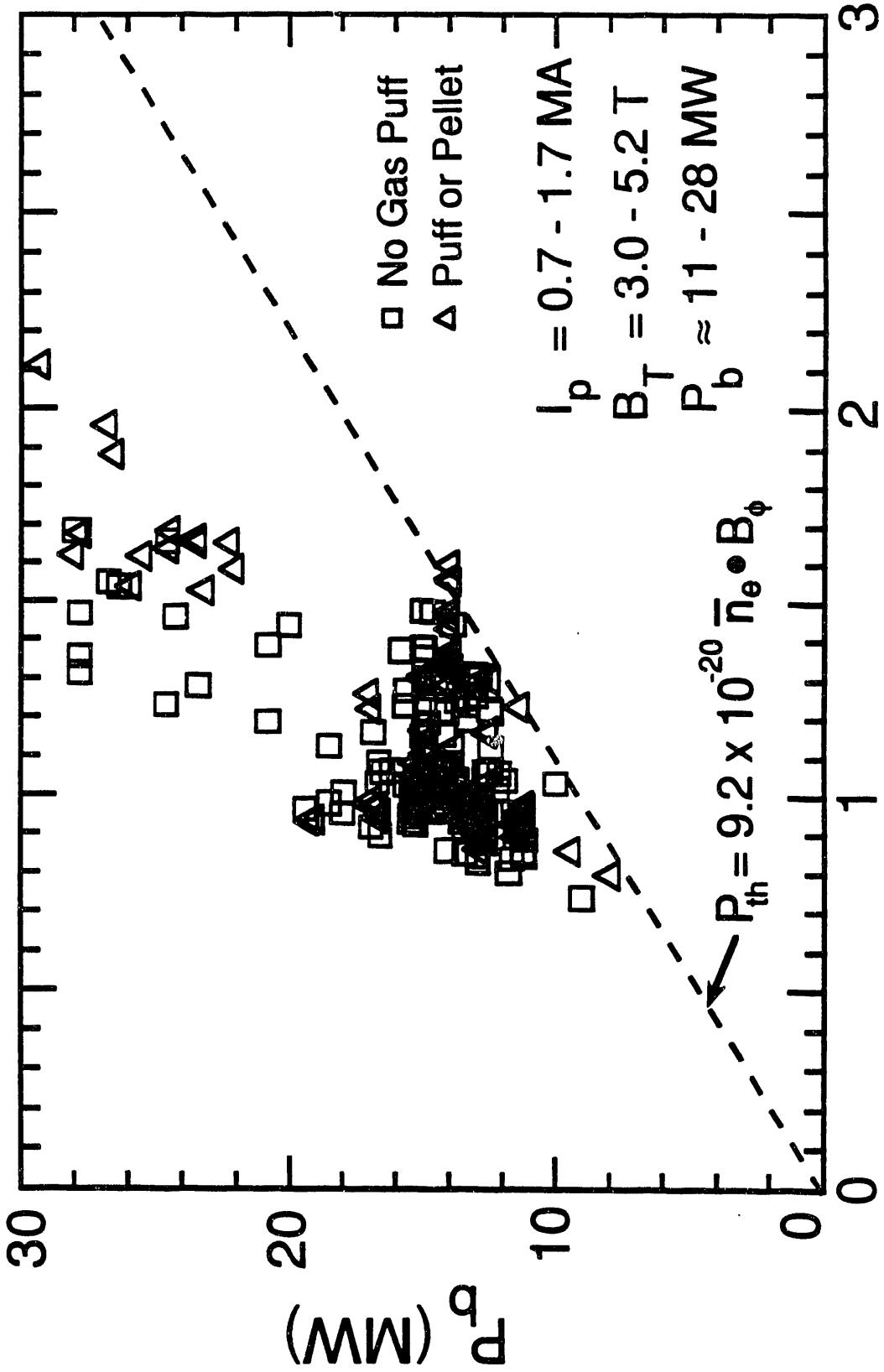
P_b (MW)
30
20
10
0
0
1
2
3
$\bar{n}_e \bullet B_\phi$ (10^{20} T m^{-3})
□ No Gas Puff
△ Puff or Pellet
I_p = 0.7 - 1.7 MA
B_T = 3.0 - 5.2 T
P_b ≈ 11 - 28 MW
$P_{th} = 9.2 \times 10^{-20} \bar{n}_e \bullet B_\phi$

Fig. 34

EXTERNAL DISTRIBUTION IN ADDITION TO UC-420

Dr. F. Paoloni, Univ. of Wollongong, AUSTRALIA
Prof. M.H. Brennan, Univ. of Sydney, AUSTRALIA
Plasma Research Lab., Australian Nat. Univ., AUSTRALIA
Prof. I.R. Jones, Flinders Univ, AUSTRALIA
Prof. F. Cap, Inst. for Theoretical Physics, AUSTRIA
Prof. M. Heindler, Institut für Theoretische Physik, AUSTRIA
Prof. M. Goossens, Astronomisch Instituut, BELGIUM
Ecole Royale Militaire, Lab. de Phy. Plasmas, BELGIUM
Commission-European, DG. XII-Fusion Prog., BELGIUM
Prof. R. Boucique, Rijksuniversiteit Gent, BELGIUM
Dr. P.H. Sakanaka, Instituto Fisica, BRAZIL
Instituto Nacional De Pesquisas Espaciais-INPE, BRAZIL
Documents Office, Atomic Energy of Canada Ltd., CANADA
Dr. M.P. Bachynski, MPB Technologies, Inc., CANADA
Dr. H.M. Skarsgard, Univ. of Saskatchewan, CANADA
Prof. J. Teichmann, Univ. of Montreal, CANADA
Prof. S.R. Sreenivasan, Univ. of Calgary, CANADA
Prof. T.W. Johnston, INRS-Energie, CANADA
Dr. R. Bolton, Centre canadien de fusion magnétique, CANADA
Dr. C.R. James,, Univ. of Alberta, CANADA
Dr. P. Lukác, Komenského Universzita, CZECHO-SLOVAKIA
The Librarian, Culham Laboratory, ENGLAND
Library, R61, Rutherford Appleton Laboratory, ENGLAND
Mrs. S.A. Hutchinson, JET Library, ENGLAND
Dr. S.C. Sharma, Univ. of South Pacific, FIJI ISLANDS
P. Mähönen, Univ. of Helsinki, FINLAND
Prof. M.N. Bussac, Ecole Polytechnique,, FRANCE
C. Mouttet, Lab. de Physique des Milieux Ionisés, FRANCE
J. Radet, CEN/CADARACHE - Bat 506, FRANCE
Prof. E. Economou, Univ. of Crete, GREECE
Ms. C. Rinni, Univ. of Ioannina, GREECE
Dr. T. Mual, Academy Bibliographic Ser., HONG KONG
Preprint Library, Hungarian Academy of Sci., HUNGARY
Dr. B. DasGupta, Saha Inst. of Nuclear Physics, INDIA
Dr. P. Kaw, Inst. for Plasma Research, INDIA
Dr. P. Rosenau, Israel Inst. of Technology, ISRAEL
Librarian, International Center for Theo Physics, ITALY
Miss C. De Palo, Associazione EURATOM-ENEA , ITALY
Dr. G. Grosso, Istituto di Fisica del Plasma, ITALY
Prof. G. Rostangni, Istituto Gas Ionizzati Del Cnr, ITALY
Dr. H. Yamato, Toshiba Res & Devel Center, JAPAN
Prof. I. Kawakami, Hiroshima Univ., JAPAN
Prof. K. Nishikawa, Hiroshima Univ., JAPAN
Director, Japan Atomic Energy Research Inst., JAPAN
Prof. S. Itoh, Kyushu Univ., JAPAN
Research Info. Ctr., National Instit. for Fusion Science, JAPAN
Prof. S. Tanaka, Kyoto Univ., JAPAN
Library, Kyoto Univ., JAPAN
Prof. N. Inoue, Univ. of Tokyo, JAPAN
Secretary, Plasma Section, Electrotechnical Lab., JAPAN
S. Mori, Technical Advisor, JAERI, JAPAN
Dr. O. Mitarai, Kumamoto Inst. of Technology, JAPAN
J. Hyeon-Sook, Korea Atomic Energy Research Inst., KOREA
D.I. Choi, The Korea Adv. Inst. of Sci. & Tech., KOREA
Prof. B.S. Liley, Univ. of Waikato, NEW ZEALAND
Inst of Physics, Chinese Acad Sci PEOPLE'S REP. OF CHINA
Library, Inst. of Plasma Physics, PEOPLE'S REP. OF CHINA
Tsinghua Univ. Library, PEOPLE'S REPUBLIC OF CHINA
Z. Li, S.W. Inst Physics, PEOPLE'S REPUBLIC OF CHINA
Prof. J.A.C. Cabral, Instituto Superior Tecnico, PORTUGAL
Dr. O. Petrus, AL I CUZA Univ., ROMANIA
Dr. J. de Villiers, Fusion Studies, AEC, S. AFRICA
Prof. M.A. Hellberg, Univ. of Natal, S. AFRICA
Prof. D.E. Kim, Pohang Inst. of Sci. & Tech., SO. KOREA
Prof. C.I.E.M.A.T, Fusion Division Library, SPAIN
Dr. L. Stenflo, Univ. of UMEA, SWEDEN
Library, Royal Inst. of Technology, SWEDEN
Prof. H. Wilhelmson, Chalmers Univ. of Tech., SWEDEN
Centre Phys. Des Plasmas, Ecole Polytech, SWITZERLAND
Bibliotheek, Inst. Voor Plasma-Fysica, THE NETHERLANDS
Asst. Prof. Dr. S. Cakir, Middle East Tech. Univ., TURKEY
Dr. V.A. Glukhikh,Sci. Res. Inst. Electrophys.I Apparatus, USSR
Dr. D.D. Ryutov, Siberian Branch of Academy of Sci., USSR
Dr. G.A. Eliseev, I.V. Kurchatov Inst., USSR
Librarian, The Ukr.SSR Academy of Sciences, USSR
Dr. L.M. Kovrizhnykh, Inst. of General Physics, USSR
Kernforschungsanlage GmbH, Zentralbibliothek, W. GERMANY
Bibliothek, Inst. Für Plasmaforschung, W. GERMANY
Prof. K. Schindler, Ruhr-Universität Bochum, W. GERMANY
Dr. F. Wagner, (ASDEX), Max-Planck-Institut, W. GERMANY
Librarian, Max-Planck-Institut, W. GERMANY
Prof. R.K. Janev, Inst. of Physics, YUGOSLAVIA

END

DATE
FILMED
2/19/93